THE PROCEEDINGS OF
THE PHYSICAL SOCIETY
Section A

VOL. 63, PART 2 1 February 1950 No. 362 A

Time Dependence of Electronic Processes in Dielectrics*

BY H. FRÖHLICH AND J. O'DWYER
Department of Theoretical Physics, The University, Liverpool

MS. received 22nd July 1949

ABSTRACT. In solid dielectrics electrons may be excited from low levels into conduction levels or into traps with energies slightly lower (shallow traps) by an ionizing radiation or by the action of strong fields. It is assumed that collisions amongst electrons in these levels are so frequent that an electronic temperature T is established which may be different from the lattice temperatures. Also the number of electrons in these levels need not correspond to equilibrium at temperature T, in which case transitions to or from lower levels (of lattice defects or foreign admixtures) will take place. Such transitions are either due to excitation by sufficiently fast moving electrons in the conduction levels, or to the inverse process. In this way it is possible to account for recombination within a reasonable time provided these lower levels (denoted as deep traps) are not much more than 1 electron volt below the lowest of the shallow traps. The difficulty of having to introduce recombination with simultaneous emission of very many vibrational quanta, an extremely unlikely process, is thus avoided. Other applications of this method, for example to the time dependence of electronic conductivity in strong fields, are indicated.

§ 1. INTRODUCTION

UNDER the influence of an ionizing radiation, or of a strong electric field, substances which are normally insulators will show some electronic conductivity. Some time will be required for the material to return to normal after the ionizing radiation (or the field) has been removed. Similarly time will be required for the conductivity to reach a stationary value on application of a strong field. It is the purpose of this paper to derive the basic formulae governing time dependent processes of the above and of a similar nature.

Closely connected with these time dependent processes is a question which has been a puzzle for some time; it is the question of how the energy absorbed by the material when ionization (by light, or by particles) takes place is ultimately transformed into heat. Excluding phosphors, where this transformation does not take place, one might think that an electron transfers its energy directly to the lattice vibrations when jumping from an excited to a lower level. This would involve, however, the simultaneous emission of a great number of vibrational quanta and thus be very unlikely.

Another possibility exists, however, if we consider the behaviour of all the electrons rather than a single process. An electron on returning from an excited to a lower level can transfer its energy to another excited electron which will thus acquire a high energy within the conduction levels of energy. It can then transfer its energy to the lattice vibrations by emission of single oscillation quanta. Alternatively, since collisions between excited electrons are rather frequent the electron may first share its energy with others. If in particular these collisions are much more frequent than collisions with lattice vibrations it will be possible to attribute an independent temperature T to the electrons. The above discussed process then implies an increase of electronic temperature T over the lattice temperature T_0. This in turn leads to an energy transfer from the electrons to the lattice.

---

* Based on report L/T 219 of the British Electrical and Allied Industries Research Association (E.R.A.).

§ 2. METHOD

The model used in the following is closely connected with that applied previously to dielectric breakdown (Fröhlich 1947, quoted as I). This model is based on a crystal lattice containing some defects or foreign admixtures. The electronic energy levels then consist of a continuum of conduction levels, below which there are a number of isolated energy levels. An electron can move freely through the conduction levels apart from frictional forces due to collisions with the lattice vibrations. In an isolated level, however, it is bound within a small region or trap. These traps are supposed to consist of two types: (i) shallow traps covering a range ΔV below the conduction levels; (ii) deep traps whose energy is an amount W below the energy of the lowest of the shallow traps. These two types of traps have previously been referred to as excited levels and ground levels respectively but the following work makes no special references to this particular representation.

It will now be assumed that collisions amongst electrons in conduction levels (let their number be N_C) and shallow traps (N_S) are frequent compared with other processes like collisions with the lattice vibrations and recombination to (or excitation from) lower levels. They are then always in equilibrium at an electronic temperature T, so that

$$N_C = N_{CS}\gamma \frac{\exp(-\Delta V/\boldsymbol{k}T)}{1+\gamma\exp(-\Delta V/\boldsymbol{k}T)}, \qquad \ldots\ldots(1)$$

$$N_S = \frac{N_{CS}}{1+\gamma\exp(-\Delta V/\boldsymbol{k}T)}, \qquad \ldots\ldots(2)$$

if

$$N_{CS} = N_C + N_S \qquad \ldots\ldots(3)$$

is the total number of electrons in conduction levels and shallow traps; γ is the ratio of the density of energy levels in a range $\boldsymbol{k}T$ near the bottom of the conduction levels to the corresponding quantity near the bottom of levels of shallow traps.

The electronic temperature may differ from the lattice temperature T_0. Energy will then be exchanged between the two systems tending to equalize the temperatures. The rate of this energy transfer per electron has been calculated in I as

$$b = \frac{\boldsymbol{h}\nu}{\tau_b} n(T_0)[\exp(\boldsymbol{h}\nu/\boldsymbol{k}T_0 - \boldsymbol{h}\nu/\boldsymbol{k}T) - 1], \qquad \ldots\ldots(4)$$

on the assumption that all lattice vibrations have the same frequency ν. Also

$$n(T_0) = \frac{1}{\exp(\boldsymbol{h}\nu/\boldsymbol{k}T_0) - 1}; \qquad \ldots\ldots(5)$$

$1/\tau_b$ is an average probability per second for the emission of a quantum $\boldsymbol{h}\nu$.

The above introduction of the electronic temperature T for C and S levels not only means that T may differ from the lattice temperature T_0, but also that the total number N_{CS} of electrons in these levels may differ from the equilibrium value at temperature T. This implies that both T and N_{CS} may depend on time. It is the purpose of the following section to derive this time dependence.

§ 3. THE FUNDAMENTAL EQUATIONS

Consider both the number $N_{\mathrm{CS}}(t)$ of electrons in C and S levels, and their temperature $T(t)$ as functions of the time t. Then the two conditions of conservation of particle number and of energy lead, as will be shown presently, to two simultaneous differential equations from which the two functions can be calculated. Assume that all transitions of electrons from C and S levels to lower levels, connected with the emission of light or of vibrational quanta, are negligible (which excludes phosphors). Then the number N_{CS} changes only through inelastic collisions connected with transitions to or from lower (D) levels. Either an electron with energy larger than W above the lowest C or S level excites a D electron into a C or S level, or the inverse process takes place, i.e. recombination of a C or S electron into an empty D level with transfer of the available energy to another C or S electron. The former process must be proportional to the number

$$N_{\mathrm{CS}}\gamma_W \exp(-W/\boldsymbol{k}T) \qquad \ldots\ldots(6)$$

of C or S electrons with sufficient energy. γ_W is the ratio of the density of energy levels in a range $\boldsymbol{k}T$ near the energy W above the lowest S level to the corresponding quantity at the bottom of S levels. The rate of change of N_{CS} is obtained from (6) by multiplication with the probability $1/\tau_{\mathrm{CD}}$ per second that an electron with sufficient energy will make the required transition.

The probability for the inverse process will be proportional to N_{CS}^{α}, where $\alpha=2$, if the number of D levels is much larger than the total number of available electrons; $\alpha=3$ when the latter two numbers are about equal. These two cases lead to equilibrium values for N_{CS} proportional to $\exp(-W/\boldsymbol{k}T)$ or to $\exp(-W/2\boldsymbol{k}T)$ respectively, as shown by Mott and Gurney (1948). Hence the rate of change of N_{CS} due to inverse processes must be equal to

$$-N(T)\left(\frac{N_{\mathrm{CS}}}{N(T)}\right)^{\alpha}\frac{\gamma_W}{\tau_{\mathrm{CD}}}\exp(-W/\boldsymbol{k}T), \qquad \ldots\ldots(7)$$

if $N(T)$ is the equilibrium number of N_{CS} at temperature T. For in equilibrium the rate of change due to the two processes must cancel.

We thus find the first fundamental equation,

$$\frac{\tau_c}{N_{\mathrm{CS}}}\frac{dN_{\mathrm{CS}}}{dt}=1-\left(\frac{N_{\mathrm{CS}}}{N(T)}\right)^{\alpha}, \quad \alpha=2 \text{ or } 3, \qquad \ldots\ldots(8)$$

where

$$\tau_c=\frac{\tau_{\mathrm{CD}}}{\gamma_W}\exp(W/\boldsymbol{k}T). \qquad \ldots\ldots(9)$$

To put into evidence the conservation of energy, three terms have to be considered:

(*a*) Transfer of energy from an external F to the electrons due to the establishment of an electronic current. This term is proportional to the number

N_{C} of conduction electrons. Per electron in the C and S levels, the rate of transfer is given by

$$a = \frac{\boldsymbol{e}^2 \tau_a F^2}{\boldsymbol{m}} \frac{N_{\mathrm{C}}}{N_{\mathrm{CS}}}, \qquad \ldots\ldots(10)$$

where τ_a is an average relaxation time.

(*b*) The rate of transfer of energy from the electrons to the lattice vibration is given by equation (4).

(*c*) With each inelastic collision with D electrons the energy of C and S electrons is decreased (increased) by at least W if N_{CS} changes by $+1(-1)$. The exact value differs from W by an amount of the order $\boldsymbol{k}T$. Hence if $\boldsymbol{k}T \ll W$ and $N_{\mathrm{CS}} \gg 1$,

$$c = -\frac{W}{N_{\mathrm{CS}}} \frac{dN_{\mathrm{CS}}}{dt}, \qquad \ldots\ldots(11)$$

is the average rate of change of energy per electron in C and S levels.

If now $U(T)$ is the average energy of an electron in C and S levels, conservation of energy requires that the rate of change of U is equal to $a-b+c$. Hence we find as second fundamental equation

$$\frac{dU}{dT}\frac{dT}{dt} = a - b + c = \frac{\boldsymbol{h}\nu}{\tau_b} n(T_0) \left[DF^2 \frac{\exp(-\Delta V/\boldsymbol{k}T)}{1+\gamma \exp(-\Delta V/\boldsymbol{k}T)} - \exp\left(\frac{\boldsymbol{h}\nu}{\boldsymbol{k}T_0} - \frac{\boldsymbol{h}\nu}{\boldsymbol{k}T}\right) + 1 \right] - \frac{W}{N_{\mathrm{CS}}} \frac{dN_{\mathrm{CS}}}{dt}, \qquad \ldots\ldots(12)$$

where

$$D = \frac{\boldsymbol{e}^2 \tau_a \tau_b \gamma}{\boldsymbol{m}\boldsymbol{h}\nu n(T_0)} \qquad \ldots\ldots(13)$$

can be considered to vary only slowly with T compared with the exponential terms.

§ 4. DISCUSSION

It is our intention here to give only a survey of some of the consequences from the two fundamental equations (8) and (12). Finer details depend of course on properties of the particular substance; an example of such a discussion is given by Simpson (1950) in the subsequent paper.

The assumption $\boldsymbol{k}T \ll W$ which we have already made above leads to considerable simplifications. For since the magnitudes of the times τ_b and τ_{CD} probably do not differ by more than a factor 100 it follows that T_c is very much larger than τ_b in view of the factor $\exp(W/\boldsymbol{k}T)$. This factor is of the order of 10^{10} if $W/\boldsymbol{k}T = 23$. This means that in (12) the c-term (last term on the right hand side) is very small. On this assumption Simpson (1947) has shown that the term on the left hand side ($\propto dT/dt$), concerning the specific heat dU/dT, involves delays of not more than 10^{-10} seconds in the establishment of the equilibrium temperature T. If we focus our interest to longer times dT/dt will vanish. Since also dN_{CS}/dt is very small equation (12) reduces to an ordinary equation,

$$DF^2 \frac{\exp(-\Delta V/\boldsymbol{k}T)}{1+\gamma \exp(-\Delta V/\boldsymbol{k}T)} = \exp\left(\frac{\boldsymbol{h}\nu}{\boldsymbol{k}T_0} - \frac{\boldsymbol{h}\nu}{\boldsymbol{k}T}\right) - 1. \qquad \ldots\ldots(14)$$

This equation which has already been derived and discussed in I permits a simple calculation of T which does not refer explicitly to the time. This means that the temperature T is entirely determined by the magnitude of the electric field F. The value obtained for $T(F)$ holds even for time dependent fields provided one is interested in times which are long compared with 10^{-10} second. In the absence of a field equation (14) would yield $T=T_0$. This should be a sufficiently good approximation for T to be inserted into (8) or (9). For a more exact calculation of $T-T_0$ the neglected c-term has to be used ($b=c$ in this case).

It follows from the above that for times larger than 10^{-10} second, time dependent processes are due mainly to the time dependence of the number of N_{CS} of electrons in C and S levels. The required function $N_{\mathrm{CS}}(t)$ can be derived from (8) and (9) where the temperature T can be considered as known from equation (14).

As an example consider the recombination of electrons after an ionizing radiation has excited some electrons into C and S levels. Some of these electrons may originally have been ejected from levels lower than D levels. These low levels may be expected to be rapidly refilled by Auger transitions from higher levels leading to the ejection of electrons into the conduction levels. Then after a very short time we need only consider recombination into D levels as all lower levels are occupied. This process is governed by equation (8) which can easily be integrated for either value of α, and $N_{\mathrm{CS}} \gg N(T)$ initially, since $T=T_0$ is time independent. The time involved is of the order $\tau_c(T_0)$. Using $\tau_{\mathrm{CD}} \simeq 10^{-15}$ second, $\gamma_W \simeq 10$, $\boldsymbol{k}T_0 \simeq 1/30$ ev., equation (9) leads to $\tau_c \simeq 10^{-6}$ second if $W=0{\cdot}8$ ev., $\tau_c \simeq 10^{-3}$ second if $W=1$ ev., and $\tau_c \simeq 10^4$ seconds if $W=1{\cdot}5$ ev. It follows then that our process leads to reasonable recombination times if W is not much larger than 1 ev. The energy transfer to the lattice will adjust itself automatically by the establishment of an electronic temperature T just slightly higher than the lattice temperature T_0.

Another example is found in the field dependence of electronic conductivity. On application of a strong field F an electronic temperature T will be established which can be calculated from (14). According to I, T is found from

$$\frac{\Delta V}{\boldsymbol{k}T_0} - \frac{\Delta V}{\boldsymbol{k}T} \simeq \frac{1}{2{\cdot}7}\frac{F^2}{F^{*2}} \qquad \ldots\ldots(15)$$

if F^* is the breakdown field. Within a very short time after application of the field the electronic temperature will rise from T_0 to T without an appreciable change in N_{CS} at first. The corresponding conductivity σ_1 is then given by

$$\log\frac{\sigma_1}{\sigma_0} = \frac{1}{2{\cdot}7}\frac{F^2}{F^{*2}} \qquad \ldots\ldots(16)$$

where σ_0 is the conductivity in weak fields.

After this initial rise the conductivity increases further towards a final value σ_2 given by

$$\log\frac{\sigma_2}{\sigma_0} = \frac{1}{2{\cdot}7}\frac{F^2}{F^{*2}}\frac{W}{2\Delta V}, \qquad \ldots\ldots(17)$$

as shown in I (this refers to $\alpha=3$; for $\alpha=2$ multiply the right hand side to two). The time increase of σ_2 is proportional to that of N_{CS} which is governed by equation (8). The time constant involved is thus the same as in the previous example.

For a detailed analysis of experiments on the time dependence of the conductivity of glass in strong fields the reader is referred to the subsequent paper by Simpson.

REFERENCES

Fröhlich, H., 1947, *Proc. Roy. Soc.* A, **188,** 521.

Mott, N. F., and Gurney, R. W., 1948, *Electronic Processes in Ionic Crystals*, 2nd edition (Oxford : Clarendon Press).

Simpson, J. H., 1947, *E.R.A. Technical Report* L/T 178 ; 1950, *Proc. Phys. Soc.* A, **63,** 86.

The Time Delay in Conduction and Breakdown Processes in Amorphous Solids

By J. H. SIMPSON
Radio and Electrical Engineering Division, National Research Council of Canada *

Communicated by H. Fröhlich ; MS. received 22nd July 1949

ABSTRACT. A method of estimating the time delay in changes of conductivity and in the breakdown process for amorphous materials, based on H. Fröhlich's high-temperature breakdown theory, is given. Numerical values of these times are obtained for the case of soda-lime glass, and it is estimated that the time constant of the conduction process is between 10^{-4} and 10^{-5} second, while that of the breakdown process may be considerably shorter. Experimental data obtained by Turner and Lewis indicate that the estimate for the conductivity process is of the correct order.

§ 1. INTRODUCTION

The theory of intrinsic dielectric breakdown in amorphous solids developed by H. Fröhlich (1945, 1947) predicts the temperature dependence of the breakdown field and the dependence of electrical conductivity on field strength. These results may be readily checked experimentally. However, in such experimental work care must be taken to distinguish between electronic processes and those due to other causes—ionic or thermal phenomena for example. Dielectric breakdown involving the latter is the well-known ' breakdown through thermal instability ', and in this case the dielectric strength does not depend upon the nature of the material alone but is a function of the size and shape of the specimen and of the length of time the electrical stress is applied. Similar considerations apply in the measurement of conductivity at field strengths below the thermal instability breakdown value. It is to be expected that an ' intrinsic ' process would take a much shorter time than one due to thermal causes, and it should be possible to distinguish between the two experimentally by applying the electric stress in short pulses, with sufficient time between them to allow for dissipation of the heat evolved. We may readily ascertain experimentally whether or not this attempt to separate the two processes is successful, since for intrinsic processes the dielectric strength or resistance should be a linear function of thickness, while for thermal processes this will not, in general, be the case. The pulses may be of many types, but the two most commonly used seem to be rectangular and saw-toothed (linearly rising) pulses, both of which are limited in duration to times of the order of a few hundred microseconds. It is necessary, however, to be sure that the duration of rectangular pulses, or the rate of rise of linear pulses, is such that any time delay which may occur in the electronic breakdown or conduction process will be negligible, as spuriously high values would otherwise be obtained. The purpose of this paper is to make a theoretical determination of the time delay in the conduction process, and to compare this with an experimental value obtainable from the results of Turner and Lewis (1947). A rough estimate of the time delay in the breakdown process is also made.

---

* Part of this work was done at H. H. Wills Physical Laboratory, University of Bristol.

§2. MODEL OF AN AMORPHOUS SOLID

Experimental difficulties have restricted efforts to obtain detailed pictures of the structure of ' amorphous ' materials, but there can be little doubt that the term covers a large number of different types of substance whose structures range from those in which there are volumes of almost macroscopic size whose nature is essentially crystalline, to those in which there is practically no long-range order and the criterion of structure as in a liquid is the ' co-ordination number ' which decides the approximate arrangement of nearest neighbours (see Warren 1942).

The picture of an amorphous solid used by Fröhlich is a very general one, in which it is assumed that the conduction levels of the electrons exist in a band structure similar to that of crystalline solids and that there are large numbers of defects and impurities in the lattice which act as electron trapping centres and lead to closely spaced discrete levels just below the conduction band. We should expect such a model to apply most accurately to materials at the near-crystalline end of the range mentioned above. In such materials we may expect electron trapping centres of the following types: (*a*) Those due to the absence of negative ions in an otherwise regular lattice. These are defects of the F-centre type, and the lowest levels of electrons trapped in such centres may be as much as 2 to 3 ev. below the conduction band for many materials. (*b*) Those due to interstitial ions of one of the lattice constituents or of foreign substances. (*c*) Those due to substitution of a foreign ion or atom for one of the constituents of the lattice. (*d*) Those due to discontinuities in lattice structure such as dislocations, boundaries between crystallites, etc. Calculations (Simpson 1949) have indicated that the energy levels of interstitial ions are quite close to the conduction band. The third type of trapping centre occurs in some semiconductors (see Pearson and Bardeen 1949) and also produces levels that are very close to the conduction band. It seems reasonable to suppose that the same is true of energy levels of the fourth type of trap, since, in general, the potential wells produced by lattice misfits will be rather shallow. From our physical ideas of the structure of these more regular amorphous materials we should also expect that the number of defects of type (*d*) will be considerably greater than those of the other types. We thus have a picture of a material in which there is a number of isolated energy levels some distance below the conduction band (up to 3 ev., depending on the material) and a much larger number in a range of energies much closer to the conduction band. Fröhlich has idealized this situation by assuming that the former are all at the same distance $2V$ below the conduction band and that the latter exist in a relatively narrow energy range ΔV immediately below the conduction band. The lower levels have been called the isolated ground levels and the upper ones the isolated excited levels. Many of these will not be 'excited' levels, in that they will not correspond to $2p$ or higher electronic states, and excitation of an electron to them from below will not be possible. This fact will have no bearing on the calculation of the breakdown field under steady conditions, since, in this case, the breakdown process is asssumed to be a quasi-equilibrium one and the number of electrons in any group of levels will be a function of the number of such levels, the temperature, and the total number of electrons only.

The effect of these independent levels just below the conduction band should also be negligible in the calculation of the time required for the conduction current to alter following a change of applied field, since the interchange of electrons between them and the conduction band will occur so rapidly, relative to the time required to raise electrons from the lower levels, that electrons in the two upper groups may be considered to be in equilibrium at all times. This is probably also the case for breakdown under rapidly changing conditions, although support for the argument is not then as powerful.

In view of the discussion of the previous paragraphs it seems desirable to use terminology that does not imply that the upper and lower levels belong to the same trapping centre. Fröhlich and O'Dwyer (1950) suggest that trapping centres leading to the upper levels be called 'shallow traps' and those leading to the lower levels 'deep traps'. These designations will be used in this paper and the associated levels referred to as S and D levels respectively. Some of the S levels will, of course, correspond to higher states of D levels but, as outlined above, the fraction of S levels in this category is probably quite small.

For materials at the other end of the range mentioned—those having very irregular structures—the existence of a band structure is not nearly so obvious. In this case an electron which is in the ionization continuum of one group of atoms may find, on motion through the substance, that it has insufficient energy to be ionized with respect to an adjacent group, and so may become trapped at a higher energy level. In this way an electron may go through several stages of excitation and retrapping in higher energy stages before it attains an energy which will enable it to move relatively freely through the substance. If it receives sufficient energy it will, however, eventually reach this stage, and may then be considered to exist in a sort of conduction band. It is thus seen that Fröhlich's picture may be considered to apply to these substances of highly irregular structure also, although, in this case, the two sets of levels (S and D) will be even more diffuse than in the preceding case, and the agreement between theoretical and experimental results may be correspondingly poorer.

In the derivation of his formulae Fröhlich assumes that the number of electrons in the conduction band is given by

$$N_1 = C_1(T) \exp(-V/\boldsymbol{k}T),$$

where the quantity $C_1(T)$ varies slowly with temperature compared with the exponential term and the energy gap between D level and conduction band is $2V$. The use of this formula implies that the number of D levels of trapping centres is approximately equal to the total number of (trapped and free) electrons. It is interesting to note, in view of later developments in this paper, that none of the formulae are changed if it is assumed that the number of deep trapping centres is very much greater than the total number of electrons, provided the gap between D level and conduction band is assumed to be V instead of $2V$.

§ 3. BASIC ASSUMPTIONS OF THE HIGH TEMPERATURE BREAKDOWN THEORY

Before proceeding to the calculation of the time to breakdown, it seems desirable to consider in detail the basic assumptions of Fröhlich's high-temperature theory. These may be classified as follows:

(*a*) The breakdown process as in the low-temperature breakdown case is an electronic one.

(*b*) The number of electrons in the conduction band of an amorphous material may be considerably greater than in a pure crystal, and the number of electrons in the isolated levels immediately below the conduction band (S levels) of an amorphous solid is much greater than the number in its conduction band.

(*c*) Hence collisions between conduction electrons and trapped electrons occur much more frequently than collisions between conduction electrons and lattice vibrations, and it is assumed that the electrons are in a state of thermal equilibrium under all conditions.

(*d*) When a field is applied to the substance it transfers energy to the conduction electrons, and through them to electrons in the isolated levels. Some of the latter will be raised from the levels which they occupy when no field is applied, and a few will reach the conduction band. The effect is similar to that which would occur if the temperature of all the electrons were raised above that of the remainder of the material, and, following Fröhlich, we may analyse the conduction or breakdown process in terms of this 'electron temperature'. Thus, when the field is applied we may consider that the temperature of all the electrons rises at a rate which is determined by the time taken for the conduction electrons to spread the energy received among them. The relation of this time to other delays in the process will be considered later.

(*e*) If equilibrium is to exist upon application of a field, the electrons must be able to transfer energy to the lattice vibrations. Fröhlich has assumed that this is accomplished chiefly by electrons in S levels. These transmit energy to the remainder of the material, which is at a lower temperature than the electrons.

(*f*) Breakdown occurs when the rate of energy transfer from field to electrons outlined under (*d*) is greater than that from electrons to lattice described in (*e*).

(*g*) The increase in the number of electrons in the conduction band may be considerable for very high fields. One of the important predictions of Fröhlich's theory indicates the way in which the conductivity should increase as breakdown is approached.

§4. MECHANISMS OF CONDUCTIVITY CHANGES AND BREAKDOWN

As implied above, the electrons are considered to be in equilibrium under the application of all fields less than the breakdown value, and their temperature is such that the rate of transfer of energy to the lattice is equal to the rate at which energy is received from the field. For the calculation of conductivity it is not necessary to consider how equilibrium is approached. Further, the criterion for breakdown is merely that the establishment of an equilibrium state shall be impossible, and the breakdown field strength is the minimum field strength at which this condition is satisfied. It is unnecessary to consider in detail what happens during the breakdown process. However, in the determination of the time (after a change of applied field) for a new conducting state to be reached—or for breakdown to take place if the field is greater than the critical value—it is necessary to make a detailed study of the processes involved. That is the purpose of this section.

The rate of increase of electronic conductivity is decided by the rate at which electrons from the isolated levels reach the conduction band, and it is assumed that the most important processes involved will be collisions between conduction electrons and those in isolated levels. These may be considered with reference to Figure 1. The energy diagram for excitation of an electron from an S level to the conduction band is shown at A. A collision between a conduction electron at 1 in the diagram and a trapped electron at 0 displaces them to 2 and 3 respectively, thus increasing the number of electrons in the conduction band by one. Transitions of the reverse type will also take place and the time constant of the whole process will depend on the collision cross sections and the number of electrons at 1, 0, 2 and 3. Another type of collision is shown at B. In this case, since the energy gap 4–7 is considerably greater than 0–3, the number of electrons in the conduction band at 5 will be very much smaller than at 1 and the time constant will be correspondingly increased. When the applied field is changed, but remains below the breakdown value, both these processes will play a part before the new equilibrium condition has been reached, and we may say that the delay before conditions have completely stabilized in the new state is of the order of the time constant involved in the excitation of electrons from the D levels to the conduction band. Transitions of this type thus decide the time delay in changes of electronic conductivity.

The time delay of the breakdown process * is also decided by the probability of collision excitation of electrons from the isolated levels to the conduction band. This delay will consist of two parts—that due to excitation of electrons from S levels to the conduction band, and that due to excitation of electrons from D levels. The former will occur at electron temperatures slightly higher than the lattice temperature, while, because of the catastrophic rise of conduction electron temperature, most processes of the latter type will take place when the electron temperature has reached a very high value. The two parts of the time delay may thus be of the same order, even though the energy steps involved are quite different in magnitude. The overall time delay should also be much shorter than that of conductivity changes.

For amorphous materials at low temperatures, the number of electrons in the conduction band and S levels may be so small that we may no longer consider that an electron temperature exists. Conditions are then intermediate between those treated by Fröhlich's low and high temperature theories, in that (in the early stages of the process at any rate) the behaviour of individual electrons must be considered, while the increase in the number of electrons in the conduction band comes, not from ionization of the lattice but from the collision excitation of electrons in deep traps. This case will not be considered in this paper.

§ 5. DETAILED CALCULATION OF CONDUCTIVITY CHANGES

5.1 *Rise in Temperature of the Electrons*

The attempt to estimate the time to reach new conductivity conditions can be simplified considerably if it can be shown that the changes of energy of the electrons in the S levels upon application of the field occur very rapidly compared with other steps in the process, i.e. if we can assume that the new electronic temperature is acquired almost instantaneously upon application of the field. The two factors which must be considered in deciding this are: (i) The delay in collision excitation processes of the type shown at C, Figure 1. These result in the transfer of an S electron to an adjacent level, and the time constant of such a process depends upon the number of electrons in the lowest levels of the conduction band, the number of S levels occupied by electrons and the collision cross section of these trapped electrons. (ii) The delay due to the specific heat of the trapped electrons. This is essentially due to the fact that energy is received from the field at a finite rate and there is accordingly some delay in the rise of temperature of the trapped electrons.

---

* This paragraph is based on a discussion by H. Fröhlich and J. O'Dwyer.

With regard to (i) we may say the following:

The ratio of the number of conduction electrons that can take part in transitions of the type C to the number that can raise other electrons from D levels to the conduction band is

$$\int_{\epsilon_1/\boldsymbol{k}T}^{\infty} \exp(-\epsilon/\boldsymbol{k}T)\sqrt{\epsilon}\,d\epsilon \bigg/ \int_{E/\boldsymbol{k}T}^{\infty} \exp(-\epsilon/\boldsymbol{k}T)\sqrt{\epsilon}\,d\epsilon,$$

where E is the distance of the D level from the conduction band. Thus $E \gg \boldsymbol{k}T$ and $\epsilon_1 \simeq \boldsymbol{k}T$. It can be readily shown that this ratio is of order $\exp(E/\boldsymbol{k}T)$. For the case in which the number of D levels N is greater than the number of electrons N_e, the number of trapped electrons taking part in C type transitions will be approximately $(N_eN_i/N)\exp(-E/\boldsymbol{k}T+\Delta V/\boldsymbol{k}T)$, where the number of electrons in D levels is taken to be approximately equal to N_e and the number of states in the S levels is N_i. If we take the collision cross sections of trapped electrons in S and D states to be equal, the ratio of the times taken in the two processes above becomes $N_1 \exp(\Delta V/\boldsymbol{k}T)/N$. Since $N_i > 10N$ and ΔV is probably not less than 0·1 ev., the ratio of the delay in the C type transition to that in raising an electron from a D level is 1:100 or less. A similar result will be obtained when the number of D levels is approximately equal to the number of electrons.

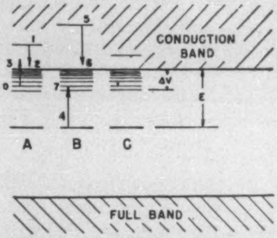

Figure 1. Types of transition which may accompany collisions between conduction electrons and those in isolated levels.

The effect (ii) of the specific heat of the trapped electrons during a change of conductivity has been considered in detail elsewhere (Simpson 1947) and it has been shown that the delay involved is of the order of 10^{-10} second.

Thus the total delay in the rise in temperature of the electrons, due chiefly to the delay in C type transitions, is at most 1% of the main delay in the process and the error introduced by assuming an instantaneous rise of electron temperature may, for the purpose of this paper, be neglected.

5.2 *Time Delay of Conductivity Changes*

In this calculation, since we are concerned with the longest delay in the process, the delay in lifting an electron from a D level to the conduction band, the model will be simplified by neglecting the effect of the S levels completely. Then, if the energy gap between D level and conduction band is E, the electrons in the conduction band responsible for collision excitation of other electrons from the D levels will be in a relatively narrow band whose energy is E above the bottom of the conduction band. The number of these electrons is $nC\exp(-E/\boldsymbol{k}T)$, where n is the total number of conduction electrons per unit volume and C is a quantity which varies slowly with temperature compared with the exponential term. For the most general case considered, in which the number of deep traps or D levels N is greater than the total number of electrons N_e, the number of transitions resulting in an increase in the number of conduction band electrons is $C_3 n(N_e - n)\phi_{01}\exp(-E/\boldsymbol{k}T)$, where C_3 includes C and also varies slowly with temperature, and ϕ_{01} is the probability of a transition of the type considered. Similarly the number of transitions in the reverse direction is $C_4 n^2(N - N_e + n)\phi_{10}$, where C_4 varies with temperature in a manner similar to C_3 and ϕ_{10}, the probability of a transition in this reverse direction, is equal to ϕ_{01}. The rate of change of the number of conduction electrons per unit volume is therefore given by

$$\frac{dn}{dt} = C_3 n(N_e - n)\exp(-E/\boldsymbol{k}T)\,\phi_{01} - C_4 n^2(N - N_e + n)\phi_{10},$$

where $C_3/C_4 = (2\pi \boldsymbol{mk}T/\boldsymbol{h}^2)^{3/2}$, as determined from conditions at equilibrium (Mott and Gurney 1940, p. 159). For amorphous materials at ordinary temperatures we may safely assume that $n \ll N_e$.

The first term on the right-hand side of this equation may be determined as follows: If E were zero, the number of transitions represented by this term would be given by $vQN_e n$ (assuming $N_e \gg n$), where Q is the collision cross section of a full trapping centre and v is the average velocity of essentially free electrons of thermal energy. The quantity vQN_e may also be put equal to $1/\tau$, where τ is the relaxation time for collisions between (low energy) conduction electrons and electrons in trapping centres. Hence we have

$$\frac{1}{\tau} = vQN_e = C_3 N_e \phi_{01} = C_4 N_e \phi_{01}\left(\frac{2\pi \boldsymbol{mk}T}{\boldsymbol{h}^2}\right)^{3/2}$$

and

$$\frac{dn}{dt} = \frac{1}{\tau} n \exp(-E/\boldsymbol{k}T) - \frac{1}{\tau}\left(\frac{\boldsymbol{h}^2}{2\pi \boldsymbol{mk}T}\right)^{3/2}\frac{n^2(N - N_e + n)}{N_e}, \qquad \ldots\ldots(1)$$

since $\phi_{10} = \phi_{01}$. This equation may be solved for two limiting cases as follows:

(*a*) $n \ll (N - N_e)$. In equilibrium $(dn/dt = 0)$

$$n_{0a} = \frac{N_e}{N - N_e}\left(\frac{2\pi \boldsymbol{mk}T_0}{\boldsymbol{h}^2}\right)^{3/2}\exp(-E_a/\boldsymbol{k}T_0),$$

where E_a is the value of E which is characteristic of this model, n_{0a} is the number of conduction electrons with no field applied, and T_0 is the temperature of both lattice and electrons under these conditions.

When the field is applied the electron temperature rises to a value T which, for fields appreciably less than the breakdown value, is only slightly greater than T_0 (Fröhlich 1945, 1947). In view of this we may express (1) as follows:

$$\frac{dn}{dt} = \frac{n}{\tau}\exp(-E_a/\boldsymbol{k}T) - \frac{n^2}{\tau n_{0a}}\exp(-E_a/\boldsymbol{k}T_0)$$

$$= \frac{n}{\tau_a{}^*} - \frac{n^2}{n_{0a}\tau_a{}^*}\exp(E_a/\boldsymbol{k}T - E_a/\boldsymbol{k}T_0), \qquad \ldots\ldots(2\,a)$$

where $\tau_a{}^* = \tau_a \exp(E_a/\boldsymbol{k}T)$. The solution of (2*a*), using the fact that $n = n_{0a}$ at $t = 0$, is

$$n = \frac{n_{0a}}{\exp(-t/\tau_a{}^*) + [\exp(-E_a/\boldsymbol{k}T_0 + E_a/\boldsymbol{k}T)][1 - \exp(-t/\tau_a{}^*)]}. \qquad \ldots\ldots(3\,a)$$

(*b*) For the other limiting case $n \gg (N - N_e)$ and

$$n_{0b} = N_e^{\frac{1}{2}}(2\pi \boldsymbol{mk} T_0/\boldsymbol{h}^2)^{3/2} \exp(-E_b/2\boldsymbol{k}T_0).$$

The equation corresponding to (2*a*) is

$$\frac{dn}{dt} = \frac{n}{\tau_b{}^*} - \frac{n^3}{n_{ob}^2 \tau_b{}^*} \exp(E_b/\boldsymbol{k}T - E_b/\boldsymbol{k}T_0), \qquad \ldots\ldots(2\,b)$$

where $\tau_b{}^* = \tau \exp(E_b/\boldsymbol{k}T)$. The solution of (2*b*) is

$$n^2 = \frac{n_{ob}^2}{\exp(-2t/\tau_b{}^*) + [\exp(-E_b/\boldsymbol{k}T_0 + E_b/\boldsymbol{k}T)][1 - \exp(-2t/\tau_b{}^*)]}. \qquad \ldots\ldots(3\,b)$$

The time constants of (3*a*) and (3*b*) are both of order τ^* but for a given material the value of E will depend on whether model (*a*) or (*b*) is chosen. If it were possible to make long time measurements, with experimental conditions such that the current flowing were primarily electronic, the value of E could be calculated from the temperature variation of n_0 (i.e. of conductivity). Using the formulae above we would obtain $E_b = 2E_a$, and since τ^* is an exponential function of E the values obtained for τ^* using the two models may be widely different. If it were possible to obtain the value of τ^* experimentally, in addition to the activation energy E, we could readily ascertain which of models (*a*) and (*b*) applies to the material considered. An attempt to do this for soda-lime glass will be made in the following paragraph.

5.3 *Determination of Time Delay from Experimental Results*

There is little information in the literature from which an estimate of the value of E can be obtained, since experimental conditions are usually such that the possibility of thermal effects and ionic conduction cannot be ignored, and indeed in many cases special attempts are made to obtain electrolytic conduction by the use of solutions as electrodes. In a report on one experiment of this type (see Quittner 1927), evidence that conduction in strong fields under steady conditions is entirely electrolytic has been given. However, if conditions are such that large numbers of electrons and few ions are available (metal electrodes) the current may be mainly electronic, although even in this case the motion of ions will produce an initial current (ionic displacement current) and a space charge in the material which may have some effect on the flow of electrons. Further, if the field is applied for short periods, the relatively long-time thermal effects should be minimized. Turner and Lewis (1947) have carried out measurements on soda-lime glass under these conditions and it will be the purpose of this section to interpret their results. They use a stress which rises linearly with time from zero to 4×10^5 volts/cm. in 150 microseconds. (An estimate of the thickness of the specimen (10^{-2} cm. at the thinnest part) was kindly furnished by Mr. C. H. M. Turner in a private communication to the writer.) The maximum stress is thus of the order of the breakdown value (see von Hippel and Maurer 1941). The currents flowing at different temperatures are shown in Figure 2. There is a small, rather sharp, rise at the beginning and a corresponding decay at the end of the record which is labelled 'displacement current'. A simple calculation shows that this is larger by a factor of order 10 than the expected charging current of the condenser (assuming a dielectric constant of 5), but it can readily be shown to correspond to an ionic displacement current due to the motion of roughly

10^{14} ions per cm^3. The field created in the material if this number of ions were concentrated on each electrode would be equivalent to an applied potential of 75 volts. Actually, however, the space charges in the material resulting from the motion of ions will be spread through it, the charge density increasing towards the electrodes, and the resultant field within the material will be quite a complicated function of the distance. For applied potentials of 1,000 volts and greater these space charges should have a relatively small effect on the measured current, however, and that range only will be considered in the following.

If the above interpretation is correct we may say that the currents shown in Figure 2 are predominantly electronic and we may discuss their magnitudes for applied potentials greater than 1,000 volts in the light of Fröhlich's theory. Such a conclusion, though apparently quite reasonable, must be tentative and a careful experimental and theoretical study of the 'displacement current' would be required to confirm it completely. A preliminary investigation using the results of the previous section is, however, quite useful in indicating the range over which this more complete study should be carried out, and such an investigation will therefore be made on the assumption that, in the range above 1,000 volts, the conduction process is electronic and the field essentially uniform.

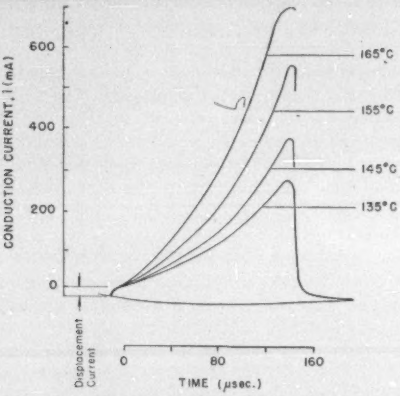

Figure 2. Variation of conduction current in glass with time when linearly rising voltage is applied.
(Taken from Turner and Lewis 1947.)

Using the results of the previous section it is possible to fit a theoretical curve to each of the experimental ones in Figure 2 and to obtain thereby an estimate of τ^*. This will be done in detail for case (*b*) of the previous section, in which the number of deep traps and electrons are approximately the same.

We must first express the first term on the right-hand side of (1) in terms of the applied field. To do this, we consider equation (15) of Fröhlich (1947):

$$HF^2+1=\exp(\boldsymbol{h}\nu/\boldsymbol{k}T_0-\boldsymbol{h}\nu/\boldsymbol{k}T), \qquad \ldots\ldots(4)$$

where

$$H=D\exp(-\Delta V/\boldsymbol{k}T)$$

and D, given by equation (16) of Fröhlich (1947), varies slowly with temperature compared to the exponential term. F is the field strength and ν the lattice vibration frequency, assumed for simplicity to be a single frequency only. As outlined above, it is assumed that equilibrium between electrons in conduction band and shallow levels is reached practically instantaneously.

Hence $\exp(-E/\boldsymbol{k}T)=(HF^2+1)^{E/\boldsymbol{h}\nu}\exp(-E/\boldsymbol{k}T_0)$ and from (1)

$$\frac{dn}{dt}=C_3nN_e\phi\exp(-E/\boldsymbol{k}T)-C_4\phi n^3$$

$$=\frac{\exp(-E/\boldsymbol{k}T_0)}{\tau}(HF^2+1)^{E/\boldsymbol{h}\nu}n-\frac{1}{\tau}\left(\frac{\boldsymbol{h}^2}{2\pi\boldsymbol{mk}T}\right)^{3/2}\frac{n^3}{N_e}, \quad \ldots\ldots(5)$$

where $N-N_e\ll n$.

Now from equation (17) of Fröhlich (1947):

$$\exp(\boldsymbol{h}\nu/\boldsymbol{k}T_0-\boldsymbol{h}\nu/\boldsymbol{k}T^*)=(\Delta V/\boldsymbol{h}\nu)DF^{*2}\exp(-\Delta V/\boldsymbol{k}T^*)=(\Delta V/\boldsymbol{h}\nu)H^*F^{*2}, \quad \ldots\ldots(6)$$

where F^* is the breakdown field, $H^*=D\exp(-\Delta V/\boldsymbol{k}T^*)$ and T^* is the electron temperature at breakdown. Since T^* is not much greater than T_0, the lattice temperature, D^* may be assumed to have the same value as D. From (4)

$$H^*F^{*2}+1=\exp(\boldsymbol{h}\nu/\boldsymbol{k}T_0-\boldsymbol{h}\nu/\boldsymbol{k}T^*) \quad \ldots\ldots(7)$$

and combining (6) and (7)

$$H^*F^{*2}=1/[(\Delta V/\boldsymbol{h}\nu)-1]\simeq\boldsymbol{h}\nu/\Delta V, \quad \ldots\ldots(8)$$

since $\Delta V/\boldsymbol{h}\nu\gg 1$. H^* may be expressed in terms of $H_0=D\exp(-\Delta V/\boldsymbol{k}T_0)$, since, from the above-mentioned paper, $(T^*-T_0)/T^*=\boldsymbol{k}T_0/\Delta V$ and hence $T^*=T_0/(1-\boldsymbol{k}T_0/\Delta V)$. Also $\boldsymbol{k}T_0/\Delta V\simeq 0{\cdot}1$ for glass, so that $T^*\simeq 1{\cdot}1\,T_0$. Hence $H_0\simeq(H^*)^{1{\cdot}1}$. The value of F^* at temperatures used by Turner and Lewis (408° – 438° K.) is 3,000 electrostatic volts per cm. approximately (see results of von Hippel and Maurer replotted by Fröhlich (1947)). Also, since $\boldsymbol{h}\nu$ is of order $\boldsymbol{k}T$, $\Delta V/\boldsymbol{h}\nu$ is of order 10, and hence from (8) $H^*\simeq 10^{-8}$ and $H_0\simeq 10^{-9}$. The applied stress has the form $F=Kt$, where $K\simeq 10^7$ electrostatic volts/cm/sec. The maximum value of HF^2, corresponding to an E.M.F. of 4,000 volts applied across a sample 10^{-2} cm. thick, is $10^{-8}(100\times 4{,}000/300)^2\simeq 10^{-2}$. Hence equation (5) may be expressed

$$\frac{dn}{dt}=\frac{\exp(-E/\boldsymbol{k}T_0)}{\tau}\left(1+\frac{E}{\boldsymbol{h}\nu}HK^2t^2\right)n-\frac{1}{\tau}\left(\frac{\boldsymbol{h}^2}{2\pi\boldsymbol{mk}T}\right)^{3/2}\frac{n^3}{N_e}. \quad \ldots\ldots(9)$$

The solution of this, when negligible factors are dropped, is

$$n\simeq n_0(1+\alpha t^3)\simeq n_0\exp(\alpha t^3), \quad \ldots\ldots(10)$$

where

$$\alpha=\frac{E}{3\tau\boldsymbol{h}\nu}HK^2\exp(-E/\boldsymbol{k}T_0)=\frac{EHK^2}{3\tau^*\boldsymbol{h}\nu} \quad \ldots\ldots(11)$$

and n_0 is the number of conduction electrons before the field is applied.

The graph of conductivity plotted against t^3 for small values of t should, according to (10), be a straight line. Two such graphs obtained, using Figures (1*a*) and (1*b*) of Turner and Lewis, are shown for two different temperatures in

Figure 3. Values of x calculated from these are 5×10^{11} at 165° c. and 4×10^{11} at 135° c. Hence, using (11),

$$\tau^{*}=\frac{EHK^{2}}{3h\nu x}\simeq\frac{E\times10^{-8}\times10^{14}}{h\nu\,.\,15\times10^{11}}\simeq\frac{E}{h\nu}\times10^{-6}.$$

Since $10\leqslant E/h\nu\leqslant100$, τ^{*} probably lies between 10^{-4} and 10^{-5} second at both temperatures (165° and 135° c.).

The value of E may be estimated since $\tau^{*}=\tau\exp(E/kT)$, where τ (Simpson 1947) is of order 10^{-14} second. The results obtained are 0·75 ev. for $T=135°$ c. and 0·80 ev. for $T=165°$ c. The slight increase in magnitude at the higher temperature may be an indication that the deep level group is rather diffuse, so that more electrons are excited from deeper traps at higher temperatures. It would indeed be surprising if this were not the case for a material of such irregular structure as glass. However, the degree of approximation in the above calculation is such that no definite conclusions can be drawn.

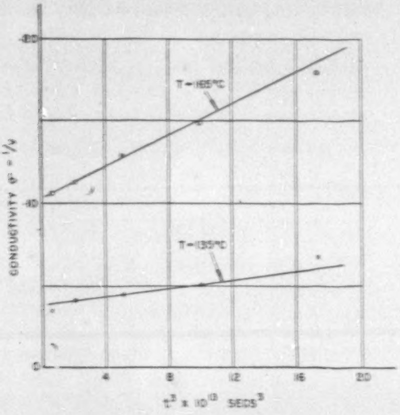

Figure 3. Variation of conductivity of glass with time when linearly rising voltage is applied.
(From the results of Turner and Lewis 1947.)

A similar analysis may be carried out when the number of deep traps is greater than the number of electrons. The value of τ^{*} obtained is, within the accuracy of the calculation, the same as that given above.

§6. DISCUSSION AND CONCLUSIONS

6.1 *Probable Model for Glass*

In view of the fact that the time delay of the conduction process is of the same order as the length of the applied pulse, we should not expect the temperature variation of the conductivity of glass obtained from the results of Turner and Lewis to be correct. We should, however, expect it to approach the correct value more closely at high than at low temperatures, since if the deep levels are widely distributed there will be more opportunity for the removal of electrons from the lower levels of the group. If the distribution of ground levels were a very narrow one, the time delay in the excitation process would become shorter as the temperature was raised. (This is not the case for glass, as seen above.) In either case the measured conductivity would, at higher temperatures, approach more closely to the true electronic conductivity obtainable under long-time conditions if other factors, such as motion of ions, could be taken into account.

Plots of ($\log\sigma$, $1/T$), again taken from Figure 2 of Turner and Lewis, are shown in Figure 4 for two different values of the applied field. (Actually this should be ($\log\sigma$, $1/T_0$), but since, for conduction processes, $T_0 < T < 1{\cdot}1T_0$, we may assume, with sufficient accuracy for the present purpose, that $T \simeq T_0$.) It will be noted that the slope of each curve is greater at high than at low temperatures. If delays in the conduction process were so short that the rate of rise of the applied voltage had a negligible effect, the curves should, according to the theory, be straight lines of slope E or $E/2$, depending upon which of the above models applies. Actually, for curve A the slopes at low and at high temperatures correspond to energies 0·43 ev. and 0·65 ev. respectively. For curve B the figures are 0·46 ev. and 0·80 ev., the increase being due to the effect of the field on the time constant. It thus appears that the limiting value of the slope is of the order of 0·80 ev., agreeing with the corresponding energy calculated from the time delay. This fact enables us to make a choice, for glass, between the two models described, since the energy terms in the expressions for τ^* and for the conductivity can only be equal if model (*a*) of §5.2 applies, i.e. if the number of deep trapping centres is much greater than the total number of electrons. If the number of deep traps and the number of electrons were approximately equal, the energy term in the expression for the conductivity would be one-half of that in the formula for τ^*.

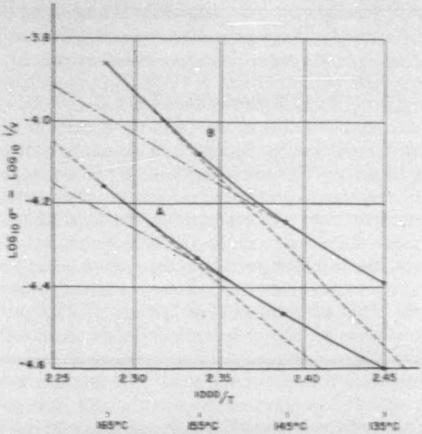

Figure 4. Variation of conductivity of glass with temperature when linearly rising voltage is applied.

Curve A: σ against $1{,}000/T$ when $V = 3{,}100$ volts.
Curve B: σ against $1{,}000/T$ when $V = 4{,}700$ volts.

It must be emphasized that this result is a tentative one based on rather scanty experimental evidence. To obtain the results required to put the above analysis on a firm foundation it would be necessary (in addition to the study of 'displacement current' mentioned previously) to extend the work of Turner and Lewis to higher temperature ranges and to use applied voltages having smaller rates of rise and possibly different wave forms (e.g. square waves).

The above analysis leads to a model different from that used by Fröhlich in his original papers on breakdown in amorphous dielectrics. However, as mentioned in §2, the distinction between the two models does not appear in processes of a quasi-equilibrium type such as those considered in the development of the theory; it becomes important only in calculations dealing with the approach to equilibrium. Further, the above result concerns a specific material, soda-lime glass, and may not apply to some other insulators. The present state of knowledge on most insulating materials of the amorphous type is such that the decision as to which model applies must be made on experimental evidence.

6.2 *Breakdown Time*

The time for the material to break down following application of a field greater than the critical value will not be discussed in detail, but the following general observations may be made: The first delay in this process, as discussed in §4, is due to the time $\tau_1{}^*$ required to raise the S electrons to the conduction band. For the same conduction electron temperature this can be readily shown to be less than the time to raise electrons from the D levels by a factor $N_{\mathrm{D}}/N_{\mathrm{S}}$, where N_{D} and N_{S} are the numbers of states per unit volume in the deep and shallow levels respectively. In view of previous discussions we should expect N_{S} to be larger than N_{D} possibly by a factor between 10 and 100 and the time constant due to this cause alone will be correspondingly less than that of the conductivity process. A further decrease will be produced by the catastrophic rise in temperature of the electrons under the influence of the field. As in the conductivity process this rise will have a shorter time constant than that to raise electrons from the lower excited levels to the conduction band and the factor involved will be of order $\exp(\Delta V/\boldsymbol{k}T)$, since in one case the electrons are being raised through an energy ΔV and in the other case through an energy of order $\boldsymbol{k}T$. Since

$$\tau_1{}^* = N_{\mathrm{D}}\tau \exp(E/\boldsymbol{k}T)/N_{\mathrm{S}}$$

with $E \simeq 0{\cdot}8$ ev. an increase of electron temperature by 10% will decrease $\tau_1{}^*$ by a factor of approximately 10. It is difficult to estimate the importance of this effect, but it is probably safe to say that because of it the initial breakdown delay is shortened in relation to the conductivity delay time by a factor of at least 100. The further delay due to excitation of the D electrons is probably also shorter than the conductivity by a factor of at least this magnitude because of the high electron temperature at this stage in the process. Thus if we take the time for changes of conductivity to be 10^{-4} second, the breakdown time will probably be less (and may be considerably less) than one microsecond.

6.3 *Experimental Data on Breakdown*

Three sets of experiments have recently given results which may be discussed in the light of the remarks in the preceding section. The first of these is the work of Plessner (1948) on the breakdown strength of thin films. Among the several materials tested by this worker, two—silica and polystyrene—were assumed to be amorphous. With an applied voltage rising linearly to the breakdown value in a minimum time of 10^{-4} to 10^{-5} second, a slight dependence of breakdown strength of silica on the rate of rise of voltage was found, although this was of the order of the scatter of the results. The time constant of the breakdown process for this material may be estimated using the value $\Delta V \simeq 0{\cdot}3$ ev. obtained from the results of von Hippel and Maurer (1941) and assuming that the delay due to excitation of S electrons is of the same order as the total delay in the breakdown process. The value thus obtained is of the order of 10^{-7} second instead of 10^{-5} second. The discrepancy may be due to a larger time delay in the excitation of electrons from D levels, or to the fact that the number of S and D levels is smaller than that in glass. The latter seems to be the more reasonable explanation, since the method of producing the film may result in a fairly regular structure.

Keller (1948) has determined the dielectric strength of Thuringian glass, using D.C., A.C. of power frequencies, and exponentially rising (condenser charging) voltages. He ascribes the different results obtained with these applied stresses and the effects of different electrodes to purely thermal effects, and estimates that pulses of 10^{-2} to 10^{-3} second duration are short enough to avoid them. He also expects, presumably as a result of preliminary experiments, that time-lag effects will become important for pulses of 10^{-4} second and shorter—a result which is in rough agreement with the calculations of this paper. The investigations now being undertaken by Keller to extend these results should make possible interesting comparisons with the results of this paper.

Macfadyen and Edwards (1949) have carried out dielectric breakdown experiments on liquids, using rectangular pulses. They find that the dielectric strength increases for pulses shorter than 2 microseconds, and they mention the possible application of Fröhlich's theory to breakdown in liquids. Whether the theory can be extended from amorphous materials to liquids is an open question, although it is possible that the model described previously for highly amorphous materials may be adapted to this purpose. The delay time is certainly of the order of that estimated above for amorphous materials, but in view of the present state of knowledge of these materials no definite conclusions can be drawn.

6.4 *Other Factors*

In the calculations and discussions of this paper it has been assumed, following Fröhlich, that the conductivity process is purely electronic. The possibility of ionic effects has been considered in detail and reasons given for believing that they are negligible. However, another type of conduction, common in semiconductors, is due to 'holes' (see, for example, Mott and Gurney 1940). Whether these play an important part in conduction processes in some insulators of the type considered in this paper is not known and will not be investigated here. It is sufficient, at the moment, to point out that there may be many amorphous materials to which the results of this paper do not apply. Further investigations, both experimental and theoretical, would be required to ascertain to what extent this is so.

Further important effects may be due to the energy step at the contact between the insulator and metal electrode (Mott and Gurney 1940, p. 169). There is no evidence concerning the importance of this for amorphous materials. For breakdown experiments in materials in which the number of conduction and trapped electrons is very small, the number of electrons getting into the conduction band from outside may become important in the initiation of the breakdown process, and in this case electrode effects might be very important. They might, for example, account for the delay obtained by Plessner for films of crystalline structure, although this could not be ascertained without further investigation. This delay may also, of course, be accounted for by the further development of Fröhlich's low-temperature theory.

6.5 *Conclusions*

From the results of this paper it seems reasonable to conclude that Fröhlich's theory is capable of explaining existing experimental data on the time for changes in conductivity (and probably for intrinsic breakdown) to take place in amorphous solids, if reasonable assumptions are made concerning the manner in which the energy received from the field is spread among the electrons. The amount of such data which may be considered applicable is at present very meagre, however, for, while there are many results of measurements on amorphous materials, especially conductivity measurements, very few of these can be interpreted on the basis of Fröhlich's theory, since conditions are usually such that non-electronic phenomena cannot be ignored.

One of the most promising experimental methods for work of this type is that used by Turner and Lewis (1947) and other workers mentioned in this paper. Extension of the work of these experimenters over a larger range of temperatures and materials with the use of applied voltage pulses of different types should furnish sufficient data to check the theory.

ACKNOWLEDGMENT

The writer wishes to express his appreciation of the interest and guidance of Professor H. Fröhlich who suggested the treatment of time dependent processes used in this paper and clarified the writer's ideas in many discussions.

REFERENCES

Fröhlich, H., 1945, *E.R.A. Technical Report*, ref. L/T 153; 1947, *Proc. Roy. Soc.* A, **188**, 521.

Fröhlich, H., and O'Dwyer, J., 1950, *Proc. Phys. Soc.* A, **63**, 81.

von Hippel, A., and Maurer, R. J., 1941, *Phys. Rev.*, **59**, 820.

Keller, K. J., 1948, *Physica*, **14**, 475.

Macfadyen, K. A., and Edwards, W. D., 1949, *Nature, Lond.*, **163**, 171.

Mott, N. F., and Gurney, R. W., 1940, *Electronic Processes in Ionic Crystals* (Oxford: Clarendon Press).

Pearson, G. L., and Bardeen, J., 1949, *Phys. Rev.*, **75**, 865.

Plessner, K. W., 1948, *Proc. Phys. Soc.*, **60**, 243.

Quittner, F., 1927, *Wien. Ber.*, **136** (IIa), 151.

Simpson, J. H., 1947, *E.R.A. Technical Report*, ref. L/T 178; 1949, *Proc. Roy. Soc.* A, **197**, 269.

Turner, C. H. M., and Lewis, W. E., 1947, *Nature, Lond.*, **159**, 334.

Warren, B. E., 1942, *J. Appl. Phys.*, **13**, 602.

Characteristics of Compound Barrier Layer Rectifiers

By E. BILLIG and P. T. LANDSBERG
Research Laboratory, Associated Electrical Industries Ltd., Aldermaston Court, Berks.

MS. received 6th July 1949

ABSTRACT. The assumptions involved in Mott's and Schottky's theories of rectification are analysed and a potential barrier at the metal–semiconductor interface is proposed which enables one to pass continuously from one theory to the other. The model is directly applicable to the practically important case of rectifiers possessing an additional insulating layer between semiconductor and counter-electrode. The current–voltage characteristic of such a compound barrier is obtained and contains Mott's and Schottky's results as special cases. In this connection, an expression for the volume distribution of current carriers is obtained and plotted for the case of a linear potential distribution in the barrier. A discussion of the distribution of charges throughout the rectifier leads naturally to the concept of a capacitance of the barrier, and to the derivation of the capacitance–voltage characteristic. In this connection, a definite experimental problem is suggested by the analysis.

---

§ 1. INTRODUCTION

RECTIFICATION is found to occur at the interface of certain semiconductors in contact with certain metals. An essential element of such a junction is a potential barrier which is believed to exist in a thin layer (thickness of the order of 10^{-4} to 10^{-6} cm.) of the semiconducting material adjacent to the rectifying metal electrode. In the main body of the semiconductor the potential is practically constant.

There exist at present two main variants of the diffusion theory of rectification, each of which seems to explain satisfactorily a certain number of experimental facts to the exclusion of the other. Thus Mott's theory (1939) is in agreement with the current–voltage characteristics obtained with copper-oxide rectifiers, whereas Schottky's theory (Schottky and Spenke 1939, Schottky 1942) is not so satisfactory in this case. On the other hand, Schottky's theory, unlike Mott's, accounts for the variation of the capacitance of selenium rectifiers with applied voltage.

In view of these considerations, it seems desirable to have available a treatment of rectifier characteristics which enables one to pass continuously from Mott's theory to Schottky's. Such a treatment, which is here attempted, contains the former two theories as special cases and is also directly applicable to rectifiers with an artificial barrier layer at the metal–semiconductor interface, provided the space charge due to the current carriers is neglected. We obtain below the current–voltage and capacitance–voltage relations for such a barrier, and a general equation for the distribution of the current carriers, which is evaluated for the case of our insulating barrier.

§ 2. THE ASSUMPTIONS MADE BY MOTT AND SCHOTTKY

In both theories the assumption * is made that

(MS 1) Practically the whole potential drop across the rectifier takes place in the barrier layer.

This becomes inapplicable when the potential applied in the forward direction approaches the height of the barrier ($U \sim V_D$ in Figures 1 to 4). In this case the series resistance of the body of the semiconductor must be taken into account.

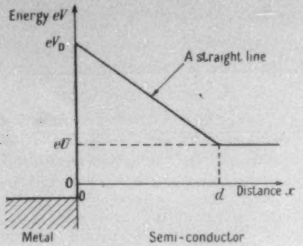
Energy eV
eV_D
A straight line
eU
0
0
d
Distance x
Metal
Semi-conductor

Figure 1. Mott's barrier.
The volume density of ionized impurity centres is zero throughout.

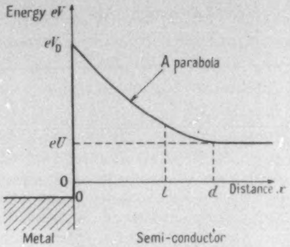
Energy eV
eV_D
A parabola
eU
0
0
l
d
Distance x
Metal
Semi-conductor

Figure 2. Schottky's barrier.
The volume density of ionized impurity centres has a constant (non-zero) value, n, between $x=0$ and $x=l$.

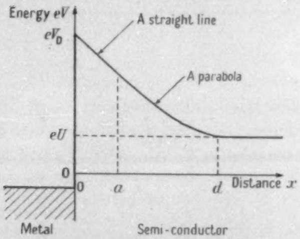
Energy eV
eV_D
A straight line
A parabola
eU
0
0
a
d
Distance x
Metal
Semi-conductor

Figure 3. Bethe's barrier.
The volume density of ionized impurity centres is zero between $x=0$ and $x=a$, and has a constant value, n, between $x=a$ and $x=d$.

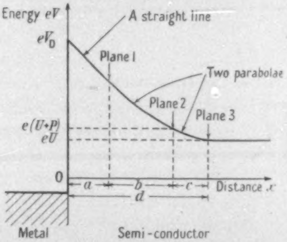
Energy eV
eV_D
A straight line
Plane 1
Two parabolae
Plane 2
Plane 3
$e(U+P)$
eU
0
a
b
c
d
Distance x
Metal
Semi-conductor

Figure 4. The barrier used in this paper.
The volume density of ionized impurity centres is zero in the layer of thickness a, and has two constant values, n and m, in the layers of thickness b and c respectively.

The second common assumption may be stated thus:

(MS 2) The barrier is such that

(*a*) its thickness d † is too great for the quantum-mechanical tunnel effect to become important;

(*b*) the electrical field $\mathbf{E}$ in the barrier is so weak that on the average the energy lost by a current carrier over the mean free path (l) when running up against the barrier (i.e. the energy $e\mathbf{E}\cdot\mathbf{l}$) is small compared with its kinetic energy ($3kT/2$).

---

* Assumptions made by Mott or Schottky are denoted by ' M ' or ' S ' respectively, assumptions made by both authors are denoted by ' MS '.

† We denote by *d* the distance—measured from the metal–semiconductor interface—over which the potential in the semiconductor exhibits a significant variation.

The effect of (*b*) is that the number of electrons stopped by the potential barrier is small compared with the number stopped by collisions. It follows that an electron will suffer many collisions as it passes over the barrier, so that the electron migration is in the nature of a diffusion process. The Table gives experimental values of l and calculated values of a critical field strength E_0 for various semiconductors used in practical rectifiers. The field in the barrier must then be small compared with the corresponding value of E_0 (defined as $3kT/2el$) for the diffusion theory to hold.

Semiconductor	Si	Ge	Se	Cu_2O
Mean free path l (A.)	200 (1)	750 (2)	0·7 (3)	50 (4)
Critical field strength E_0 (v/cm.)	18,750	5,000	5,350,000	75,000

(1) Torrey and Whitmer 1948, p. 64; (2) Torrey and Whitmer 1948, p. 63; (3) the value for the mean free path of holes in selenium has been calculated from the expression $l=(3v/4e)\sqrt{(2\pi mkT)}$, where the mobility has been taken as $v=1$ cm^2/volt. sec. (Eckart and Kittel 1941); (4) Mott and Gurney 1940, p. 182.

On the average the field in the barrier is of the order of 10,000 to 100, 000 v/cm. This suggests that diffusion theory can certainly be applied to the case of Se and probably of Cu_2O, but not to the case of Si or Ge.

Lastly,

(MS 3) The potential difference ($2Z$) corresponding to work necessary to excite an electron from an impurity level of the semiconductor into its conduction band is small compared with the height (V_D) of the barrier.

This assumption ($Z \ll V_D$) implies that the potential in the interior of the semiconductor, with no current flowing, is not greatly different from that in the metal counter-electrode.

The theories diverge in the assumptions made for the distribution of the space charge and for the width of the barrier:

(M 4) The space charges in the barrier may be neglected.	(S 4) The space charges in the barrier layer are due to a uniform distribution of fixed, singly-charged centres.
(M 5) d is independent of the applied voltage.	(S 5) d is determined by the boundary conditions for the potential distribution.

It follows from assumptions (4) and (5) that the shape of the potential barrier is a straight line in Mott's and a parabola in Schottky's theory. Figures 1 and 2 show these barriers for an applied potential difference U.

§ 3. THE PRESENT ASSUMPTIONS

In the present discussion assumptions (MS 1) to (MS 3), together with (S 5), are adopted. The shape of the barrier assumed here (Figure 4) is governed by our purpose to cover Mott's theory as well as Schottky's. The barrier may be specified by the following requirements:

(i) The potential distribution is continuous in the semiconductor and assumes a constant value in its interior.

(ii) In contact with the metal electrode there is an insulating layer of thickness a, and free of ionized impurity centres.

(iii) In the layer of thickness b there are n ionized impurity centres per unit volume. The layer extends to a plane 2 where the field strength and the potential have (for given U) the prescribed values E and $U+P$ respectively, U being the applied potential, P a constant (small) potential difference and E a constant (small) field strength.

(iv) In the layer of thickness c there are m ionized impurity centres per unit volume. This layer extends to a plane 3 at which the potential has become constant ($=U$).

(v) The height (V_D+Z) of the barrier above the Fermi level of the metal is independent of the applied potential U.

The impurity centres in the bulk of the semiconductor are ionized to a degree depending on their activation energy ($2Ze$) and on the temperature. In the barrier region the potential distribution is an additional factor, and complete ionization exists in most of the barrier if $V_D \gg Z$. Near the end of the barrier, however, the fraction of ionized impurity centres drops to zero. This effect is taken into account by our assumption of an insulating layer. The ions which are practically immobile create a stationary space charge in the barrier. They are here treated as fixed charges of constant volume density (n in layer b, and m in layer c). The much more mobile current carriers—electrons or positive holes—also contribute to the space charge. In the absence of a current their volume density decreases exponentially as one passes from the interior of the semiconductor towards the metal electrode (see equation (15)). This suggests that in the case of substances with readily ionizable impurity centres (e.g. Ge or Se) the contribution of the current carriers to the space charge in the barrier layer is negligible.

For a current to pass across the rectifier, the current carriers require, after activation, an additional energy to take them over the barrier into the metal. The amount of energy required to do this is lowered if (for positive carriers) the applied voltage U acts from the semiconductor to the metal, i.e. with the semiconductor positive and the metal negative. This direction of U is here taken as positive.*

Our model, therefore, generalizes that used by Bethe (1942) (see Figure 3) who considered an artificial barrier layer, corresponding to our first layer, in series with another one which corresponds to our second layer. In order to pass from our model to those of the previous authors, we may use the following scheme:

$$\left.\begin{array}{ll} \text{Mott} & : n=0,\ P \text{ small}; \\ \text{Schottky} & : a=0,\ E \text{ and } P \text{ small}; \\ \text{Bethe} & : n=m,\ P=E=0. \end{array}\right\} \qquad \ldots\ldots(1)$$

Mott's theory has been applied to the current–voltage characteristic, Schottky's to the current–voltage and to the capacitance–voltage characteristic. Bethe has obtained the capacitance–voltage and the current–voltage relationship, the latter on the assumption that (MS 2*b*) does not apply. Since we shall adopt assumption (MS 2), the present treatment of the current–voltage characteristic bears no simple relation to Bethe's. The image force effect (Mott 1939, Bethe 1942, Schottky 1942) will not be considered.

---

* U is thus positive if it acts in the forward direction for positive carriers, i.e. for deficit semiconductors such as selenium.

§4. THE POTENTIAL DISTRIBUTION IN THE BARRIER LAYER

To determine the potential $V(x)$ of a current carrier in the barrier layer, we integrate the three Poisson equations

$$\frac{\partial^2 V_j}{\partial x_j^2} = \frac{4\pi}{\kappa}\rho_j(x)$$

which, for $j = 1, 2, 3$, hold respectively in the layers of thickness a, b and c, where $\rho_1 = 0$, $\rho_2 = en$, $\rho_3 = em$ are the space-charge densities and κ is the dielectric constant of the semiconductor. Hence, six constants A_j, B_j are obtained in the solutions

$$V_j = 2\pi\rho_j x_j^2 + A_j x_j + B_j,$$

and four of these may be found by the continuity conditions for the potentials and gradients at planes 1 and 2 (Figure 4). The remaining two are fixed by the stipulated values E and $U+P$ of field and potential respectively at plane 2. In this argument we regard a, n, V_{D}, U, P, E as given, while we determine b, c, d and m

The thickness (c) and space-charge density (em) in the last layer are determined by

$$V_3 = U, \quad \text{and} \quad \partial V_3/\partial x_3 = 0 \qquad \text{for } x_3 = d. \qquad \ldots\ldots(2)$$

This gives

$$c = 2P/E, \qquad m = \kappa E^2/8\pi e P. \qquad \ldots\ldots(3)$$

The potential for $x = 0$ is equal to V_{D}, and this yields an equation for b. On solving, the two cases $n \neq 0$, $n = 0$ must be treated separately, and we find

$$b = \left\{a^2 + \left(\frac{\kappa E}{4\pi n e}\right)^2 + (V_{\mathrm{D}} - U - P)\frac{\kappa}{2\pi n e}\right\}^{\frac{1}{2}} - a - \frac{\kappa E}{4\pi n e} \qquad (n \neq 0), \quad \ldots\ldots(4)$$

$$b = \frac{V_{\mathrm{D}} - U - P}{E} - a \qquad (n = 0) \quad \ldots\ldots(5)$$

The field in the first layer is given by

$$-\frac{dV_1}{dx_1} = \frac{4\pi n e}{\kappa} b + E. \qquad \ldots\ldots(6)$$

If the constants E and P are chosen to be zero, the third layer disappears

$$\lim_{E,P \to 0} c = \lim \frac{2P}{E} = 0. \qquad \ldots\ldots(7)$$

§5. THE CURRENT-VOLTAGE CHARACTERISTIC

The current in the barrier is made up of one component flowing in the direction of the field E, and another component due to the carriers diffusing from the region of high concentration. This gives (Wagner 1931) for the total current density (in the positive x direction)

$$-evN\frac{\partial V}{\partial x} - eD\frac{\partial N}{\partial x},$$

where e, v, N are, respectively, the (algebraic) charge, mobility and number per unit volume of the current carriers and D the diffusion coefficient which satisfies Einstein's relation

$$D = vW, \qquad W = kT/e, \qquad \ldots\ldots(8)$$

where k is Boltzmann's constant, T the absolute temperature, and W the 'temperature potential' (1/40 electron volt at room temperatures). As explained in §3, however, the positive x direction is the 'reverse' direction of rectification (for positive current carriers). Having taken U as positive if acting in the 'forward' direction (i.e. in the negative x direction), we wish to take the current density j as positive if acting in the same direction, whence

$$j = ev\left(N\frac{\partial V}{\partial x} + W\frac{\partial N}{\partial x}\right). \qquad \ldots\ldots(9)$$

By (8) and (9),

$$\frac{\partial N}{\partial x} = \frac{j}{evW} - \frac{N}{W}\frac{\partial V}{\partial x}. \qquad \ldots\ldots(10)$$

j being independent of x, the solution of this equation is

$$j(U) = evWN(0, U)\exp(V_{\mathrm{D}}/W)\,\frac{\dfrac{N(x, U)}{N(0, U)}\exp\left([V(x, U) - V_{\mathrm{D}}]/W\right) - 1}{\displaystyle\int_0^x \exp[V(y, U)/W]dy}, \qquad \ldots\ldots(11)$$

as may be verified by direct differentiation. The dependence of N and V on both x and U has been indicated explicitly. As $j(U)$ and the first part of equation (11) do not depend on x, the second part must also be independent of x, and can only be a function D of U:

$$j(U) = evWN(0, U)\exp(V_{\mathrm{D}}/W)\,.\,D(U). \qquad \ldots\ldots(12)$$

The current must, of course, disappear with the applied voltage:

$$j(0) = 0. \qquad \text{Hence } D(0) = 0. \qquad \ldots\ldots(13)$$

From the definition of D, the charge distribution is then

$$\frac{N(x, U)}{N(0, U)} = \left[1 + D(U)\int_0^x \exp[V(y, U)/W]dy\right].\exp\left([V_{\mathrm{D}} - V(x, U)]/W\right). \qquad \ldots\ldots(14)$$

Without applied voltage ($U = 0$), this gives the well-known exponential distribution

$$N(x, 0) = N(0, 0)\exp\left([V_{\mathrm{D}} - V(x, 0)]/W\right). \qquad \ldots\ldots(15)$$

Equations (12) to (15) indicate the dependence of the distribution of the current carriers on the magnitude of the current through the barrier.

The density of carriers at the boundaries of the barrier can be taken as independent of the applied voltage: for electrical neutrality, the density of carriers in the bulk of the semiconductor must be equal to that of the impurity centres, which does not, of course, depend on the applied voltage. At plane 3 the carrier density begins to drop gradually as the potential rises in the barrier:

$$N(d, U) = N(d, 0) = n. \qquad \ldots\ldots(16)$$

Since the potential at the metal–semiconductor interface is always the same (V_D), it is reasonable to assume* that the carrier density there is also constant:

$$N(0, U) = N(0, 0). \qquad \ldots\ldots(17)$$

Substitution into (15) and (11) gives

$$j(U) = evWn \frac{\exp(U/W) - 1}{\int_0^d \exp[V(x, U)/W]\, dx}. \qquad \ldots\ldots(18)$$

The main contribution to the integral derives from those parts of the barrier where V is large, i.e. for the type of barrier considered in Figure 4 and for small U, from small values of x. For a quantitative evaluation of the integral, we may, in first approximation, replace the actual potential distribution by a linear one,

$$V(x, U) \sim V_D - \overline{F}x, \qquad \ldots\ldots(19)$$

fitting it closely at the metal–semiconductor interface (broken line in Figure 5).

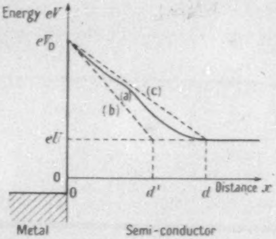

Figure 5. Linear approximations applied to an arbitrary potential barrier.
(a) An actual barrier.
(b) An approximation to the corresponding Schottky barrier.
(c) An alternative approximation.

In this equation, V_D is constant and $\overline{F}$ depends only on U and not on x. The meaning of the approximation (19) is that the actual barrier extending over a distance d has been replaced by an approximate one of constant field strength $\overline{F}$ extending for a distance d' such that $\overline{F}d' = V_D - U$. Hence (18) reduces to

$$j = nev\,\overline{F} \frac{\exp(U/W) - 1}{\exp(V_D/W) - \exp(U/W)}. \qquad \ldots\ldots(20)$$

To ensure that the approximation be best for small x, the correct and the approximate potential distributions should have a common tangent at $x = 0$. For $\overline{F}$ we therefore use the expression (6) for the field between the plane $x = 0$ and $x = a$. For Schottky's case ($a = 0$; P, E negligibly small), substitution for b from (4) yields

$$j \simeq nev \left\{\frac{8\pi ne}{\kappa}(V_D - U)\right\}^{\frac{1}{2}} \frac{\exp(U/W) - 1}{\exp(V_D/W) - \exp(U/W)}. \qquad \ldots\ldots(21)$$

---

* Schottky (1942, equation (9)) and Mott (1939, p. 34); assumptions (16) and (17) have only been made implicitly by these authors.

This derivation of the current–voltage relation is somewhat simpler than that given by Schottky (1942, equation (17)). The above approximation is good for very small x, but over-estimates the field for larger x (up to $x=d'$). For $d'<x<d$, the approximation implies zero field, so that in this less important region the field is under-estimated. We now replace (6) by an approximation which under-estimates for small x, while over-estimating for larger x (barrier (c) in Figure 5):

$$\overline{F}=(V_{\mathrm{D}}-U)/d. \qquad \ldots\ldots(22)$$

As, however, the region of small x is more important, this approximation would be expected to give an under-estimate for j. In Schottky's case, using (4) and (20), this gives just half the previous value for j (equation (21)).

Collecting results, j is given by (20) where $\overline{F}$ satisfies

$$\frac{4\pi ne}{\kappa}b+E\gtrsim\overline{F}\gtrsim\frac{V_{\mathrm{D}}-U}{d}.$$

The current–voltage characteristic can be somewhat simplified: The second term in the denominator of equation (21) may be neglected over the whole range of the characteristic, except for $U\rightarrow V_{\mathrm{D}}$ when the forward current would become excessive anyhow. Equation (21) may then be written in a dimensionless form

$$\frac{j}{j_0}=\left(\frac{V_{\mathrm{D}}-U}{W}\right)^{\frac{1}{2}}(\exp(U/W)-1), \qquad \ldots\ldots(23)$$

where

$$j_0=nev\left[\frac{8\pi neW}{\kappa}\right]^{\frac{1}{2}}\exp(-V_{\mathrm{D}}/W). \qquad \ldots\ldots(24)$$

For Se, for example, we may take $\kappa=6{\cdot}3$, $n=10^{16}\,\mathrm{cm}^{-3}$, $v=1\,\mathrm{cm}^2/\mathrm{v.\,sec.}$, $V_{\mathrm{D}}=0{\cdot}5$ v., so that at room temperature ($W=0{\cdot}025$ v.) the specific current density becomes $j_0=0{\cdot}04\,\mu\mathrm{a/cm}^2$. For reverse voltages of any but the smallest magnitudes the exponential term in equation (23) disappears, and the current varies only slowly—with the square root of the voltage. Whilst this is borne out by experiment at small and medium voltages, it does not apply to the larger reverse voltages where the image force comes into play, effectively reducing the height of the barrier and increasing the leakage current. The effect of the image has not been allowed for in this paper but will be the subject of a future publication.

§ 6. THE DISTRIBUTION OF CURRENT CARRIERS IN THE PRESENCE OF AN APPLIED POTENTIAL

In § 5 our purpose was to obtain the D.C. characteristic for the general potential barrier and obtain Mott's and Schottky's cases by specialization. We now wish to determine the form of the distribution function $N(x, U)$. This has recently been investigated by Fan (1948) for a layer without fixed space charge. For this purpose we combine (12), (14) and (18) giving

$$\frac{N(x,U)}{N(0,U)}=\left[(\exp(U/W)-1)\frac{\int_0^x \exp\,[V(y,U)/W]\,dy}{\int_0^d \exp\,[V(y,U)/W]\,dy}+1\right]\times\exp([V_{\mathrm{D}}-V(x,U)]/W). \qquad \ldots\ldots(25)$$

In the case of a constant field

$$V(x, U) = V_D - \frac{V_D - U}{d}x,$$

one obtains

$$\frac{N(x, U)}{N(0, U)} = \left\{1 + \exp\left(\left[U + \frac{x}{d}(V_D - U)\right]\Big/ W\right) - \exp(U/W) - \exp\left[-\frac{V_D - U}{W}\left(1 - \frac{x}{d}\right)\right]\right\}\left\{1 - \exp[-(V_D - U)/W]\right\}^{-1}. \quad \ldots\ldots(26)$$

For $U = 0$, this reduces to

$$\frac{N(x, 0)}{N(0, 0)} = \exp(xV_D/dW). \quad \ldots\ldots(26a)$$

The expression (26) is plotted in Figure 6 for various values of U, assuming

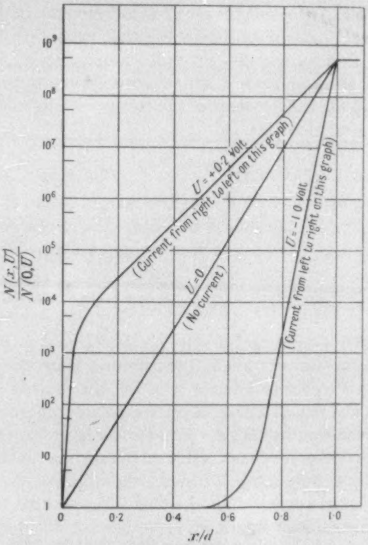

Figure 6. Volume distribution of positive current carriers in a constant-field boundary layer of a contact rectifier. $V_D = 0{\cdot}5$ v. $kT/e = 0{\cdot}025$ v.

$V_D = 0{\cdot}5$ v. and $W = 0{\cdot}025$ v. These curves demonstrate clearly the tendency of the mobile current carriers to accumulate at the regions of lowest potential V, i.e. at the end of the barrier. Thus the assumption of a constant field in the barrier, i.e. neglecting the space charge due to the current carriers within the barrier, does not lead to any serious inconsistency. It is also in general agreement with the results obtained by Fan.

In order to maintain electrical neutrality the number of current carriers in the interior of the semiconductor beyond the end of the barrier must be equal to the number of ionized impurity centres,* $N(x, U) = n$ for $x \geqslant d$. For zero applied voltage one obtains from (26*a*)

$$N(0,0) = N(d,0)\exp(-V_D/W) = n\exp(-V_D/W).$$

We shall now estimate the number of current carriers which pass from the semiconductor into the metal when contact is made. The total charge on the semiconductor is due to the space charge in the barrier layer only. The ionized impurity centres contribute a negative charge $q_1 = ned$ per unit area, whilst the current carriers contribute a positive charge of only

$$q_2 = e\int_0^d N(x,0)\,dx = N(0,0)ed\frac{W}{V_D}\{\exp(V_D/W)-1\} \simeq ned\,W/V_D,$$

as usually $V_D \gg W$. The net (negative) charge in the barrier per unit area is therefore

$$q = q_2 - q_1 \simeq ned(1 - W/V_D). \qquad \ldots\ldots(27)$$

With the values for V_D, W, κ and n as assumed for selenium in the previous section, we obtain $d \sim b \sim \{V_D\kappa/2\pi ne\}^{\frac{1}{2}} \sim 1{\cdot}87 \times 10^{-5}$ cm., hence $N(0,0) = 2{\cdot}06 \times 10^7\,\text{cm}^{-3}$ or $q = 1{\cdot}78 \times 10^{11}$ electron charges per cm². Inspection of (27) shows that the net charge on the semiconductor is almost entirely due to the immobile ionized impurity centres in the barrier, most of the corresponding mobile carriers having passed into the metal electrode.

§7. THE CAPACITANCE-VOLTAGE CHARACTERISTIC

The separation of positive and negative charges (each of value q) which has been discussed above, is analogous to the separation of charges, on application of an external voltage $V_D - U$, in a capacitor having a voltage-dependent capacitance

$$C = \frac{dq}{d(V_D - U)} = \left(\frac{ne\kappa}{8\pi(V_D - U)}\right)^{\frac{1}{2}} \text{(per unit area)}. \qquad \ldots\ldots(28)$$

We have here used $q \simeq ned$ and $d \sim \{(V_D - U)\kappa/2\pi ne\}^{\frac{1}{2}}$ as before, i.e. we have neglected the—comparatively small—contribution from the carriers which are crowded towards the semiconductor end of the barrier. The capacitance (equation (28)) is just that of a parallel-plate capacitor whose plates are separated by the voltage-dependent distance d. In a barrier layer, however, corresponding positive and negative charges do not reside on the surfaces of two opposite metallic plates separated by a definite gap. Instead, the negative charges are distributed throughout the barrier space, whilst the balancing positive charges are residing on the metal–semiconductor interface.

In the more complete calculation, again neglecting the contribution of the current carriers to the space charge, we obtain for the charge per unit area of the barrier $q = e(nb + mc)$ and, from this, the capacitance $dq/d(V_D - U)$.

Treating P and E in equations (3) and (4) as small quantities one obtains

$$\frac{1}{C^2} = \frac{8\pi}{ne\kappa}\left[\frac{2\pi ne}{\kappa}a^2 + V_D - U\right] \quad (n \neq 0), \qquad \ldots\ldots(29a)$$

$$\frac{1}{C^2} = \left(\frac{4\pi d}{\kappa}\right)^2 \quad (n = 0). \qquad \ldots\ldots(29b)$$

---

* The discontinuity in the gradient of N at $x = d$ is of no great importance and is connected with a corresponding discontinuity in the potential distribution assumed for Mott's barrier.

Equation (29 *a*) first derived by Bethe reduces, with $a=0$, to Schottky's expression (29 *b*) in agreement with our scheme. The plot of $1/C^2$ against U should make the intercept

$$V_D + \frac{2\pi ne}{\kappa} a^2 \qquad \ldots\ldots(30)$$

on the line $1/C^2=0$, which agrees with Schottky's theory for $a=0$. It is to be noted that the occurrence of a in (30) offers a new interpretation of the different intercepts obtained by A. Schmidt (cf. Schottky (1942, Figure 5)) in her plots of $1/C^2$ against U.

Experimental work to decide between Schottky's and the present explanation of the various intercepts obtained with different rectifiers would be of interest and is in progress here. The result (29 *b*) for Mott's theory is at variance with the experimental results on selenium rectifiers which exhibit a variation of C with U. Hence, in such rectifiers (29 *a*) should be used in the analysis of capacitance characteristics to determine the component a in d.

ACKNOWLEDGMENT

Our thanks are due to Dr. T. E. Allibone for permission to publish this paper.

REFERENCES

Bethe, H. A., 1942, *Theory of the Boundary Layer of Crystal Rectifiers*, M.I.T. Report 43–12.

Eckart, F., and Kittel, A., 1941, *Naturwissenschaften*, **29**, 371.

Fan, H. Y., 1948, *Phys. Rev.*, **74**, 1505.

Mott, N. F., 1939, *Proc. Roy. Soc.* A, **171**, 27.

Mott, N. F., and Gurney, R. W., 1940, *Electronic Processes in Ionic Crystals* (Oxford: University Press).

Schottky, W., 1942, *Z. Phys.*, **118**, 539.

Schottky, W., and Spenke, E., 1939, *Wiss. Veröff. Siemens-Werk.*, **18**, 225.

Torrey, M. C., and Whitmer, C. A., 1948, *Crystal Rectifiers* (New York: McGraw-Hill).

Wagner, C., 1931, *Phys. Z.*, **32**, 641.

Fast Neutron Reactions with Fluorine and Sodium

BY J. V. JELLEY AND E. B. PAUL
Cavendish Laboratory, Cambridge

Communicated by O. R. Frisch; MS. received 24th November 1948, *and in amended form 24th June* 1949

ABSTRACT. The yields of the (np) and (nα) reactions in fluorine and sodium have been measured by observations on the radioactivity produced by bombardment with neutrons from the (dn) reactions in Li, B, Be and D. Cross sections have been estimated and methods of deriving the absolute disintegration rates and the neutron flux are described.

The reaction energies have also been derived, by assuming a particular form for the excitation function, and using published data on the energy distribution of the neutrons used.

---

§1. INTRODUCTION: SURVEY OF PREVIOUS WORK

WHEN fluorine is bombarded by fast neutrons the following reactions may take place:

$$^{19}F + {}^{1}n \rightarrow {}^{19}O + {}^{1}H, \qquad \ldots\ldots(1)$$

$$^{19}F + {}^{1}n \rightarrow {}^{16}N + {}^{4}He. \qquad \ldots\ldots(2)$$

Reaction (1) was reported by Bjerge and Westcott (1934), by Amaldi and his co-workers (1935) and by Nahmias and Walen (1936), who identified the activity of 31 second half-life as ^{19}O and showed that fast neutrons were required to produce it. Polessitsky (1937) identified the ^{19}O chemically. Scherrer, Huber and Rossel (1941) studied the energy distribution of pulses in an ionization chamber containing a fluorine compound which was irradiated by fast neutrons. They identified a proton group which they attributed to reaction (1) and derived a reaction energy of $+0{\cdot}45$ MeV. Later work on the maximum β-energy of ^{19}O by Huber, Lienhard, Scherrer and Wäffler (1945) suggested however that the reaction energy was negative, being less than $-2{\cdot}44$ MeV. A more recent value for the half-life of ^{19}O has been obtained by Bleuler and Zünti (1947) who measured it to be $27{\cdot}0 \pm 0{\cdot}5$ seconds.

Reaction (2) was reported by Fermi and his collaborators (1934), by Nahmias and Walen (1936) who concluded that fast neutrons were required, by Harkins, Gans and Newson (1935) who studied the α-particle energy distribution in a cloud chamber, and by Chang, Goldhaber and Sagane (1937) who observed that the reaction occurred with the neutrons from the reaction $^{11}B(dn)^{12}C$ but not with those from the reaction $^{9}Be(dn)^{10}B$.

Wilhelmy (1937) investigated the α-groups in an ionization chamber and found energies corresponding to a positive energy release in reaction (2) in disagreement with the results of Harkins and of Chang, Goldhaber and Sagane (1937). The measurements of the maximum β-ray energy from ^{16}N made by Fowler *et al.* (1936) and by Naidu and Siday (1936) seemed to confirm the mass value for ^{16}N found by Wilhelmy. However, the later work of Holloway (1940) on the reaction $^{15}N(dp)^{16}N$, of Bleuler, Scherrer and Zünti (1945) and of Somers and Scherr (1946) on the $(\beta\text{–}\gamma)$ disintegration scheme of ^{16}N led to a mass value making (2) a fast neutron reaction (negative energy release). Scherrer, Huber and Rossel (1941) also found α-particle groups from this reaction by an ionization chamber method which confirmed this and they reported a reaction energy of $-1{\cdot}3$ Mev. The accepted half-life of ^{16}N is $7{\cdot}35 \pm 0{\cdot}05$ seconds (Bleuler *et al.* 1947).

The following reactions have been observed when sodium is bombarded by fast neutrons:

$$^{23}\mathrm{Na} + {}^{1}\mathrm{n} \rightarrow {}^{23}\mathrm{Ne} + {}^{1}\mathrm{H}, \qquad \ldots\ldots(3)$$

$$^{23}\mathrm{Na} + {}^{1}\mathrm{n} \rightarrow {}^{20}\mathrm{F} + {}^{4}\mathrm{He}. \qquad \ldots\ldots(4)$$

The first reaction was reported by Amaldi *et al.* (1935) and by Nahmias and Walen (1936). Polessitsky (1937) observed a 40 second activity when sodium was irradiated by fast neutrons and identified it as an inert gas. The mass of ^{23}Ne quoted by Elder, Motz and Davidson (1947) requires the energy release in reaction (3) to be $-3{\cdot}9$ Mev. The accepted half-life of ^{23}Ne is $40{\cdot}7 \pm 0{\cdot}8$ seconds (Huber *et al.* 1944).

Reaction (4) was reported by Nahmias and Walen (1936) who observed an 8 second activity as well as the ^{23}Ne activity when sodium was bombarded by fast neutrons. This was identified with ^{20}F. From the reaction energy for the $^{19}F(dp)^{20}F$ reaction reported by Bower and Burcham (1939) the mass of ^{20}F is 20·00654. This would make the reaction energy of (4) equal to $-4{\cdot}0$ Mev., again using the masses published by Elder, Motz and Davidson (1947). The accepted half-life of ^{20}F is 12 seconds (Mattauch and Flügge 1947).

§ 2. METHODS OF DETERMINING REACTION ENERGIES

A direct method for determining a negative reaction energy would be to measure the reaction yield from bombardment of the target under investigation by monokinetic neutrons of different energies. This requires a source of monokinetic neutrons of variable energy, such as the neutrons from the reactions $^{12}C(dn)^{13}N$, $D(dn)^{3}He$ or $^{7}Li(pn)^{7}Be$. Then the threshold neutron energy E_T at which the reaction just begins to occur can be determined. The reaction energy, Q, is given by

$$Q = -E_T M_0/(M_0 + M_1), \qquad \ldots\ldots(5)$$

where M_0, M_1 are the masses of the initial nucleus and incident particle (neutron) respectively. The remaining kinetic energy of the incident particle is taken up as kinetic energy of the centre of mass of the system. Since, however, at the threshold the energy available for the emergent particle and hence the penetrability of the potential barrier are zero, the observed threshold will depend on the sensitivity of the detecting apparatus and in general will give a Q-value which is too negative. This error may be almost as large as the barrier height.

Alternatively, the energies of the emergent charged particles when the target nucleus is bombarded by monokinetic neutrons whose energy is in excess of the threshold may be observed in an ionization chamber or cloud chamber. It is, however, often difficult to distinguish the proton or α-particle group of maximum range due to the reaction in question from groups arising from other reactions and from recoils arising from collisions of the neutrons with the chamber gas. Sometimes the group corresponding to the ground state transition is less intense than groups corresponding to transitions to excited states and the former may thus be missed.

If the masses of the nuclei involved are known the Q-value may be calculated. The mass of an unstable product nucleus may be derived from the maximum

β-disintegration energy of this nucleus and the mass of its stable isobar. If there are no γ-rays involved in the disintegration scheme this is definite, but careful coincidence experiments are necessary to determine whether the maximum energy β-particles lead to the ground state or to an excited state of the isobar.

Monokinetic neutrons with energy variable over a large range were not available for the experiments to be described. Neutron sources for which the energy distribution is known were therefore used and the reaction energies have been estimated by making certain assumptions about the form of the excitation function for the reaction (see Appendix). This method is very much less definite than a direct determination of the excitation function using monokinetic neutrons, as in the work of Klema and Hanson (1948) on the reaction $^{32}S(np)^{32}P$, since it depends on the accuracy of the neutron spectra and on the particular form of excitation function adopted. It may, however, yield more information than the statement that this reaction does or does not occur with a certain neutron source.

§ 3. EXPERIMENTAL DETAILS

(i) *Apparatus and Method*

The sodium sample consisted of 100 gm. of NaCl and the fluorine sample of 49 gm. of CaF_2. These salts were enclosed in holders in the shape of a cylindrical shell 3·5 cm. inside diameter, 5 cm. outside diameter and 5 cm. length (Figure 1), the inner wall being made of transparent cellulose tape. The neutron sources were targets of LiOH, B, Be or heavy phosphoric acid ($D_2O + P_2O_5$), bombarded by 0·75 MeV. deuterons. Irradiation was carried out for 2 minutes; during the second minute the neutron flux was monitored by a method to be discussed below. The deuteron beam was then interrupted by a shutter and the sample carried to counting equipment about twenty feet from the irradiation position to avoid the strong radioactivity of the target. The sample was placed around a cylindrical steel Geiger counter 2·5 cm. diameter, 5 cm. length and 0·025 cm. wall thickness. The whole arrangement was surrounded by $1\frac{1}{2}$ inches of lead. The amplified pulses from the counter were displayed on an oscilloscope together with timing

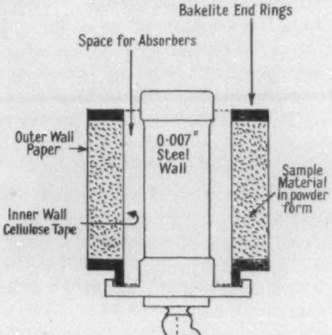

Figure 1.

pulses derived from a pendulum. The time-base was supplied by a saw-tooth generator whose frequency was about 3 c/s. The oscilloscope screen was photographed on recording paper moving at right angles to the time-base at a rate such that the ⅓ second traces were well separated. Recording was begun about ten seconds after the end of irradiation and carried on for 2 minutes. The background with the unirradiated sample in place was determined immediately before each run. The pulses photographed in individual seconds after the end of irradiation were counted visually, the background subtracted and decay curves constructed. The maximum counting rate convenient for subsequent analysis was about 100 per second, and a distance from the source of neutrons was chosen for irradiation such that the initial recorded rate did not exceed this value.

(ii) *Estimation of Absolute Disintegration Rates*

The efficiency of the counting arrangement is the product of two factors, (*a*) the fraction ϵ_A of β-particles having sufficient energy to emerge from the sample and penetrate the counter wall, and (*b*) a geometrical factor ϵ_B. The second factor is the same for all samples since they were the same shape and size, while the first factor depends on the β-particle energy distribution, on the sample density and on the counter wall thickness.

Table 1

Irradiated material	Active nucleus	Radiation energy (MeV.)	Relative intensity	ϵ_A
NaCl	^{20}F	5·0	1·0	0·41
NaCl	^{23}Ne	4·1	1·0	0·31
CaF$_2$	^{16}N	10·5	0·2	0·62
		4·3	0·4	
		3·8	0·4	
CaF$_2$	^{19}O	4·5	0·3	0·46
		2·9	0·7	

The transmission factor ϵ_A was calculated for each sample and for each β-particle spectrum. The sample thickness was divided into ten equal intervals and the fraction of the β-particles starting from each shell which could enter the counter was estimated from experimental absorption curves. The contributions from each shell were then summed. If ϵ_i is the fraction from the *i*th shell, of radius R_i, which reaches the counter when entering it radially, and if it is assumed that the total number of radioactive atoms in the *i*th shell is proportional to R_i then ϵ_A may be written:

$$\epsilon_A = \sum_{i=1}^{10} \epsilon_i \left(\frac{R_i}{R_0}\right) \Big/ \sum_{i=1}^{10} \left(\frac{R_i}{R_0}\right), \qquad \ldots\ldots(6)$$

where R_0 is the radius of the inner wall of the sample. The counter wall thickness is negligible if the beta ray end-point energy E_{max} exceeds 3 MeV.

In this method no correction was made for the increased absorption due to those β-particles passing obliquely through the sample. However since this is predominantly a geometrical effect and there is likely to be almost the same correction to ϵ_A for each sample it can be considered as included in the geometry factor which has been determined as described below. The values of ϵ_A derived for each of the radiations and samples are shown in Table 1.

In deriving the values of ϵ_A in Table 1 from equation (6) the following data were used: for ^{20}F the experimental absorption curve published by Curran and Strothers (1940) was employed; for ^{23}Ne an absorption curve was constructed from curves by Bleuler and Zünti (1946) using the accepted value of 4·1 MeV. for the beta-spectrum end-point obtained by Pollard and Watson (1940). For ^{16}N and ^{19}O experimental absorption curves were used, by Bleuler, Scherrer and Zünti (1947), and by Bleuler and Zünti (1947) respectively.

In order to determine the geometry factor ϵ_B, a sample of sulphur was cast in the same geometrical form as the sample holders and was irradiated for a few hours together with a quantity of powdered sulphur in a fast neutron flux produced by bombarding beryllium with 8 MeV. deuterons in the Cavendish cyclotron. The specific activity of ^{32}P produced by the ^{32}S(np)^{32}P reaction was determined by counting 6·5 mg. of the powder with an end-window β-counter of known solid angle. The total disintegration rate of ^{32}P in the large cylindrical sample (114 gm.) being then known, the overall counting efficiency could be measured. The transmission factor ϵ_A was calculated for the ^{32}P radiation in the sulphur sample by the method described above and ϵ_B, the geometry factor, could thus be determined. Several other measurements of the ^{32}P activity were made with absorbers round the counter in order to estimate the wall absorption, which was not negligible in this case. For each of these the effective counter wall thickness was different and a different value of ϵ_A was calculated. The derived values of ϵ_B varied from 0·04 to 0·02, the mean value being 0·031. There is likely to be a large probable error associated with this value of ϵ_B on account of the fact that the energy of the ^{32}P radiation, 1·7 MeV., is considerably less than the energies encountered in the main experiments, with the result that the effects of beta-rays passing obliquely through the sulphur sample may not be predominantly geometrical. From the various values for ϵ_B obtained above an error of up to $\pm 50\%$ has been roughly estimated. As will be seen later this error, if it exists, enters into the final errors estimated in deriving the absolute values of the cross sections but does not affect the determinations of the errors in the reaction thresholds.

(iii) *Neutron Flux Measurements*

The calculation of the cross section and threshold energy from the observed activities requires knowledge of the flux of fast neutrons from each source used and of their distribution in energy. For the determination of the fluxes with inhomogeneous neutron sources it is desirable to use a method which is as far as possible insensitive to the energy of the neutrons: according to the results of Ageno and his co-workers (1941), a uranium fission chamber, screened by cadmium to exclude slow neutrons, is suitable since the cross section for fission is approximately constant above the fast-fission threshold of 0·7 MeV. The different neutron fluxes used were therefore standardized to an arbitrary level by means of such a fission chamber; in the individual irradiations during the experiments a BF$_3$ proportional counter, operated so as to discriminate against γ-radiation and encased in a paraffin cylinder, was used since it had a higher sensitivity. This neutron monitor was compared with the fission chamber in a separate experiment for each neutron source used.

The arbitrary level of neutron flux was made absolute by comparing the counting rates with the BF$_3$ counter with that in a standard hydrogen-filled ionization chamber when both were placed in a flux of neutrons from the reaction D(dn)^{3}He.

This ionization chamber was developed in this laboratory by K. W. Allen (1947), and consisted of a cylinder of accurately known dimensions filled with three atmospheres of argon and 0·5 atmosphere of hydrogen. An analysis of the bias curve of the recoil proton pulses enabled the absolute flux to be determined. The comparison between the BF_3 and the hydrogen chamber with the d–d neutrons was carried out at 135° to a 0·9 Mev. deuteron beam and yielded a figure for the flux of 330 neutrons/cm^2/μa. at a distance of 26 cm. at 0° to the beam.

As a result of these measurements and intercalibrations, the number of neutrons of energies above the fast fission threshold passing per second through each sample, with the different neutron sources used, was known.

Table 2 shows the relative sensitivity of the neutron monitoring counter, as determined by standardization with the fission chamber, to the various neutron sources used.

Table 2

Neutron source	D(dn)	Be(dn)	B(dn)	Li(dn)
Relative sensitivity	1·00	0·76	0·78	0·64

The neutron fluxes were always measured at 135° to the deuteron beam and the flux through the sample was derived from the measured flux by correcting for the angular distribution of the neutrons from the target. This was determined by means of the fission chamber in a separate experiment.

§ 4. ANALYSIS OF RESULTS AND ESTIMATION OF CROSS SECTIONS

The decay curves obtained from each irradiation of each sample were analysed, assuming that the two activities resulting from the (np) and (nα) reactions were the only ones present, and that their half-lives had the accepted values. The slow neutron (nγ) reaction in fluorine leading to 12 second ^{20}F was excluded by irradiating the fluorine sample holder in a cadmium box. The slow neutron capture in sodium leads to 14 hour ^{24}Na which is too long a period to interfere. A typical decay curve (for Na bombarded by Li(dn) neutrons) is shown in Figure 2 together with the 12 and 40·7 second components into which it has been analysed.

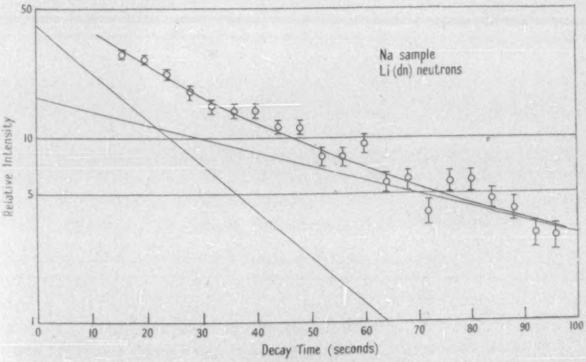

Figure 2.

The counting rates due to each product at the end of irradiation were derived and were then corrected (*a*) to a standard neutron flux as measured by the calibrated long counter, (*b*) to a standard distance from the neutron source during irradiation, and (*c*) to an infinite irradiation time, i.e. divided by $(1-e^{-\lambda T})$ where T is the irradiation time. Each counting rate so corrected was converted to an absolute yield by the counting efficiency factor, $\epsilon_A \epsilon_B$, described above. The cross sections were calculated by the equation

$$\sigma = n/N_0 \nu \epsilon_A \epsilon_B, \qquad \ldots\ldots(7)$$

where n is the corrected counting rate, N_0 the number of atoms in the sample, ν the neutron flux (corrected as described above) and ϵ_A and ϵ_B are the transmission and geometrical factors already discussed.

The cross sections thus calculated are presented in Table 3 together with values of σ_0, the cross sections without barrier, estimated by a method described in the next section. The irradiations were carried out at 0° to the 0·75 MEV. deuteron beam.

Table 3

Reaction	Source	$\sigma \times 10^{26}$ cm^2	$\sigma_0 \times 10^{26}$ cm^2
$F(np)^{19}O$	Li(dn)	7·81	12
	B(dn)	3·56	
	Be(dn)	1·45	
	D(dn)	0·60	
$F(n\alpha)^{16}N$	Li(dn)	12·64	19
	B(dn)	5·64	
	Be(dn)	8·26	
	D(dn)	3·68	
$Na(np)^{23}Ne$	Li(dn)	8·02	12
	B(dn)	3·64	
	Be(dn)	0·108	
	D(dn)	(0·002)	
$Na(n\alpha)^{20}F$	Li(dn)	11·87	31
	B(dn)	0·951	
	Be(dn)	0·112	
	D(dn)	(0·033)	

Estimation of Errors in determining Absolute Cross Sections

It is seen from equation (7) that five factors are involved in estimating the probable errors to be assigned to the derived cross sections. The largest source of error lies in the uncertainties of the values of $\epsilon_A \epsilon_B$ owing to the fact that no straightforward method existed for computing the effects of (*a*) obliquity in the paths of beta-rays entering the counter, or (*b*) scattering; the former has been discussed above in an earlier section and is thought to be the larger of the two effects. In the derivation of absolute values of the cross sections, it seems reasonable to assign a probable error of ±50% to $\epsilon_A \epsilon_B$ in each case, for the error in ϵ_B is likely to be considerably greater than the errors in the other factors; this error then gives the order of magnitude of precision attainable in the absolute value of a cross section by this method.

The figures in Table 3 are quoted to three significant figures for reasons which will be discussed in the section below on the determination of errors in the measurements of reaction thresholds.

§ 5. DETERMINATION OF REACTION THRESHOLDS

In order to use the yields of the reactions with inhomogeneous neutron sources for the determination of the threshold energy, it is necessary to make an assumption about the form of the excitation function. Let us assume it has the form:

$$\sigma_E = \sigma_0 P_{qQ}, \qquad \sigma_E = 0 \text{ for } E < E_T, \qquad \ldots\ldots(8)$$

where σ_E is the cross section for neutrons of energy E, σ_0 is the cross section without barrier, P_{qQ} is the penetrability of the barrier for the particle q escaping from the residual nucleus Q, and E_T is the threshold energy. An excitation function of this form is shown in Figure 3.

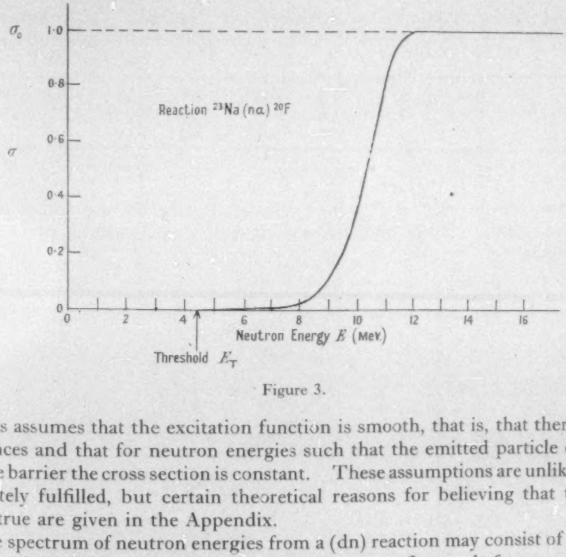

Figure 3.

This assumes that the excitation function is smooth, that is, that there are no resonances and that for neutron energies such that the emitted particle can pass over the barrier the cross section is constant. These assumptions are unlikely to be completely fulfilled, but certain theoretical reasons for believing that they are nearly true are given in the Appendix.

The spectrum of neutron energies from a (dn) reaction may consist of n peaks, the ith peak containing a fraction f_i of the total neutron flux, and of mean energy E_i. Then the effective cross section for a flux of neutrons distributed in energy in this way is given by

$$\sigma_{(dn)} = \sigma_0 \sum_{i=1}^{n} (P_{qQ})_{E_i} f_i. \qquad \ldots\ldots(9)$$

It is assumed that all the neutrons in a peak have the same energy. The variation of P_{qQ} with neutron energy will depend on the kinetic energy available to the emitted particle q at the given neutron energy, which is in turn determined by the neutron energy and the reaction energy (Q-value). By comparing the ratio of the calculated cross sections for two different neutron distributions with the observed ratios of the values in Table 3 a threshold energy may be found for which the agreement is best, and hence the Q-value, using equation (5).

The factors f_i for the different energy distributions have been estimated from the published spectra. Only those neutron groups with energies in excess of the uranium fast fission threshold were used in these calculations. In Table 4 are shown the values of E_i and f_i at 0° for a deuteron energy of 0·75 Mev. for each of the (dn) reactions. The data for Li(dn) are from Richards' work (1941), while the remainder are from Powell's determinations (1942). Since the published determinations were made at 90° to the deuteron beam, and at other deuteron energies, the neutron energies were corrected for these factors. It was assumed that f_i did not change with angle. This is certainly true for D(dn) and recently Green (private communication) has shown that it is true for Li(dn) to about 10%.

Table 4

Source	Li(dn)		B(dn)		Be(dn)		D(dn)	
i	E_i	f_i	E_i	f_i	E_i	f_i	E_i	f_i
1	4·6	0·35	3·1	0·46	1·4	0·23	3·8	1·00
2	6·8	0·07	4·6	0·24	2·6	0·22		
3	9·1	0·14	6·6	0·05	3·2	0·08		
4	12·4	0·33	9·6	0·23	3·9	0·32		
5	15·7	0·11	13·8	0·02	4·8	0·15		

The penetrability factors P_{qQ} were calculated using the expression given by Bethe (1937) and a nuclear radius $R = 1{\cdot}5A^{\frac{1}{3}} \times 10^{-13}$ cm. where A is the nuclear mass number.

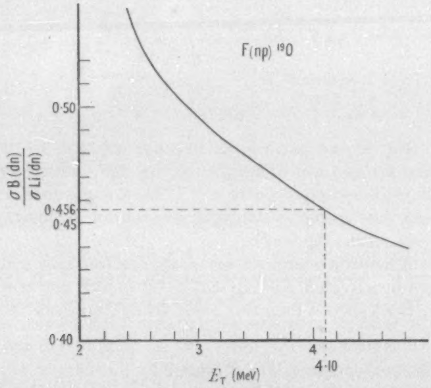

Figure 4.

The ratio of σ for B(dn) neutrons to σ for Li(dn) neutrons calculated from equation (9) was plotted against values of the neutron threshold energy E_T. The graphs for the four reactions are shown in Figures 4, 5, 6 and 7. The dotted coordinates represent the observed ratio taken from the figures in Table 3 and the corresponding threshold value.

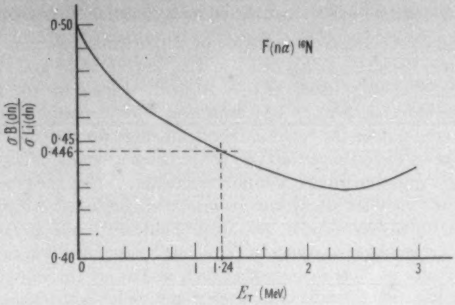

Figure 5.

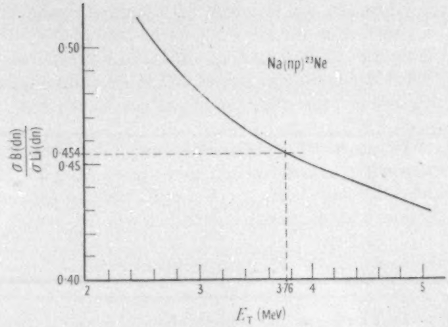

Figure 6.

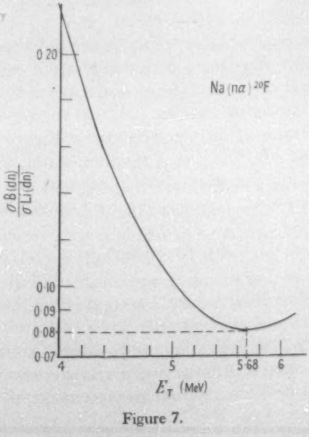

Figure 7.

Estimation of Errors in determining Reaction Thresholds

In obtaining ratios of cross sections for a particular reaction with different neutron sources the same values of ϵ_A and ϵ_B are involved and the large error quoted earlier, of $\pm 50\%$,which is present in the values for the absolute cross sections, is therefore irrelevant. This is fortunate for it enables more trustworthy figures to be obtained for the reaction thresholds than for the cross sections.

An estimate of the error in the ratio of the cross sections, in a given reaction, with B(dn) and Li(dn) neutrons, will now be made. From the graphical method of analysing the complex decay curves into their separate components it was estimated that it was reasonable to assign a probable error of approximately $\pm 3\%$ to the individual values of n (equation (7)) in each case, or $\pm 4\%$ in a ratio of two values. The value of N_0 is a constant in each case as are the values of ϵ_A and ϵ_B. Furthermore, it is only the ratio of neutron fluxes which is involved, and since the relative sensitivity of the BF_3 monitor counter was measured for B(dn) and Li(dn) neutrons, and the monitor is used here only for relative flux determinations, the errors in the two values of ν will be small. It appeared reasonable to assign an error of $\pm 2\%$ to either value of ν, or $\pm 3\%$ to the ratio of the two values. The resultant error in the ratio of cross sections $\sigma B(dn)/\sigma Li(dn)$ is then of the order of $\pm 5\%$. It is justifiable then to quote figures in Table 3 to three significant figures even though it is realized that the absolute values of the cross sections have associated errors of $\pm 50\%$.

Use is made of Figures 4 to 7 in obtaining values of the errors in the threshold energies E_T corresponding, in each reaction, to the errors of $\pm 5\%$ assigned to the cross section ratios; the errors in E_T are then converted, through equation (5), to errors in the Q-values and the masses quoted below.

§ 6. DISCUSSION

(i) *Masses*

In Table 5 are shown the reaction energies derived from the threshold energies by equation (5) and the corresponding masses of the product nuclei. The standard masses for the stable elements used in this calculation were: ^{23}Na—22·99715, ^{19}F—19·00452, ^{4}He—4·00386, ^{1}H—1·00813, and ^{1}n—1·00895. The product nucleus masses determined by other methods are included for comparison.

The agreement with other mass determinations is on the whole satisfactory within the limits of error except in the case of the last reaction. The deviation in this case is probably associated with the fact that the experimental cross section ratio occurs at the minimum of the calculated curve (Figure 7) where the sensitivity of the method is low. In this case a rigorous assignment of the error is not possible. The error in Q quoted in Table 5 assumes that the unknown negative error was equal in magnitude to the positive error, which latter was obtained as in the other cases.

(ii) *Cross Sections*

In Table 6, columns 2 and 3, are shown values of the cross section without barrier, derived from the observed cross sections for Li(dn) and B(dn) neutrons by equation (9) for the four reactions.

The assumption made in evaluating the Q-values (Appendix), namely that the (nn) process is more probable than the (np) or (nα) processes cannot unfortunately be directly justified by these cross section measurements, since both the magnitude of the elastic (potential) scattering, and the average value of the sticking probability for compound nucleus formation are unknown. For the elements investigated, and for the less energetic neutrons used, the potential scattering almost certainly exceeds πR^2. In Table 6 are also listed the total neutron cross sections σ_t at about 3 MeV., as reported by Goldsmith, Ibser and Feld (1947), and the value of πR^2 for the two nuclei.

The difference between σ_t and the potential scattering should represent the cross section for all inelastic processes. These include, in addition to the (np) and (nα) reactions and inelastic scattering, the neutron capture and (n2n) processes. However, fast neutron capture is improbable at the energies used, and only about 10% of the neutrons in the spectra used have energies exceeding the (n2n) threshold for F and Na. Accordingly, these two processes may be disregarded. If it is assumed that the average sticking probability for compound nucleus formation is unity, and the total inelastic cross section is therefore πR^2, then the values of $(\sigma_t - \pi R^2)$ in Table 6, column 6, must represent the potential scattering cross section, and the value of $[\pi R^2 - \sigma_{(np)} - \sigma_{(n\alpha)}]$ listed in the last column of Table 6 must represent $\sigma_{(nn)}$, the cross section for re-emission of a neutron from the compound nucleus. The difference in probability of the (nn), (np) and (nα) processes proceeding via the same compound nucleus is probably mainly connected with the different number of states available in the residual nuclei.

Table 5

Reaction	Q (MeV.)	Mass of product nucleus	Other determinations	Method	Ref.
^{19}F(np)^{19}O	$-3{\cdot}9 \pm 0{\cdot}7_5$	19·0095 ± 0·0007	19·00484 19·00935	(np) ion chamber β-energy	(*a*) (*b*), (*c*)
^{19}F(nα)^{16}N	−1·2 ± 0·9	16·0109 ± 0·0009	16·010 16·01110 16·00887 16·011	β-energy β-energy (np) ion chamber (nα) ion chamber	(*d*) (*e*) (*a*) (*f*)
^{23}Na(np)^{23}Ne	−3·6 ± 0·8	23·0018 ± 0·0008	23·0010 23·00213	β-energy (dp)	(*g*) (*h*)
^{23}Na(nα)^{20}F	−5·4 ± 0·3	20·0081 ± 0·0003	20·00654	(dp) Q-value	(*i*)

(*a*) Scherrer *et al.* (1941) ; (*b*) Huber *et al.* (1945) ; (*c*) Chang *et al.* (1937) ; (*d*) Somers and Scherr (1946) ; (*e*) Bleuler *et al.* (1945, 1947) ; (*f*) Harkins *et al.* (1935) ; (*g*) Pollard and Watson (1940) ; (*h*) Elder *et al.* (1947) ; (*i*) Bower and Burcham (1939).

Table 6

Element	$\sigma_{(np)}$	$\sigma_{(n\alpha)}$	σ_t	πR^2	$\sigma_t - \pi R^2$	$\sigma_{(nn)}$
F	0·12	0·19	1·5	0·50	1·0	0·19
Na	0·12	0·31	2·5	0·58	1·9	0·15

Units of 10^{-24} cm² are used in this Table.

APPENDIX

THE THEORETICAL EXCITATION FUNCTION

The method for reaction energy determination depends on the form of the excitation function. It was assumed that it had the form shown in Figure 3. From compound nucleus theory there is some justification for this. If the excitation of the compound nucleus is great enough, the levels will be overlapping, resonance effects will not appear and a statistical picture of the process should be valid (see, for example, Weisskopf and Ewing 1940). When a sodium or fluorine nucleus is hit by a neutron the excitation energy of the compound nucleus is approximately the neutron energy plus the binding energy of a neutron which in this case is about 7 Mev. For nuclei of atomic number about 10, resonances for neutron processes are not likely for excitations greater than about 10 Mev. Thus for neutron spectra whose energies are mainly less than 3 Mev., it is expected that resonances may occur and prevent one assuming a smooth excitation function. The resonances reported in the $^{14}N(np)^{14}C$ excitation function (Barschall and Battat 1946) and in the $^{9}Be(n\alpha)^{6}He$ excitation function (Allen *et al.* 1947) illustrate this. However if one uses only spectra such as B(dn) and Li(dn) in which most of the neutrons have energies above 4 Mev., it is clear that some simplified expression for the cross section at neutron energy E may be used, such as

$$\sigma_E = \pi R^2 \xi \Gamma_Q / \sum_{\text{all Q}} \Gamma, \qquad \ldots\ldots(i)$$

where R is the radius of the initial nucleus, ξ is the average sticking probability for all values of orbital momenta of incoming neutrons up to $2\pi R/\lambda$ and Γ_Q is the partial width averaged over the compound levels for disintegration by process Q. If $\lambda/2\pi R$ is small, ξ approaches unity, and this condition is nearly satisfied for neutrons above a few Mev. in energy. The partial width will be made up of the penetrability of the outgoing particle multiplied by the 'width without barrier' for the particular process. This last factor will depend, for fast out-going particles, mainly on the number of states available in the residual nucleus. In this experiment the main processes which will compete are (nn), (np), (nα) and (n2n). The (nn) process includes all scattering processes in which a compound nucleus is formed, but does not include the potential scattering. Since the last three processes are expected to have negative Q-values, the energy available for excitation of the residual nucleus is less in these cases than in the (nn) case and scattering is likely to predominate. If this is so then $\sum_{\text{all Q}} \Gamma \sim \Gamma_n$ and equation (i) may be rewritten:

$$\sigma_E = P_{qQ}(\pi R^2 \xi \gamma_Q / \Gamma_n), \qquad \ldots\ldots(ii)$$

since $\Gamma_Q = \gamma_Q P_{qQ}$, where γ_Q is the width without barrier for the process leading to nucleus Q and P_{qQ} is the penetrability factor for particle q leaving residual nucleus Q. Then if the minimum neutron energy is greater than a few Mev., the second factor in (ii) may be expected to vary slowly with incident neutron energy compared with the variation in P_{qQ}. In the Q-value determination we assume that it is constant and have denoted it by σ_0 in equation (8).

ACKNOWLEDGMENTS

The authors wish to thank Professor O. R. Frisch for his assistance in preparing this paper and in particular his advice on the theoretical analysis of the results, Dr. W. E. Burcham for his continued interest and advice throughout the experimental work, and Mr. W. Birthwistle for maintaining and running the high tension equipment.

One of us (J. V. Jelley) is indebted to the Department of Scientific and Industrial Research, and the other (E. B. Paul) to the National Research Council of Canada for financial assistance.

REFERENCES

Ageno, M., Amaldi, E., Bocciarelli, D., Cacciapuoti, B. N., and Trabacchi, G. C., 1941, *Phys. Rev.*, **60,** 67.

Allen, K. W., 1947, *Thesis*, Cambridge.

Allen, K. W., Burcham, W. E., and Wilkinson, D. H., 1947, *Nature, Lond.*, **159,** 473.

Amaldi, E., D'Agostino, O., Fermi, E., Pontecorvo, B., Rasetti, F., and Segrè, E., 1935, *Proc. Roy. Soc.* A, **149,** 552.

Barschall, H. H., and Battat, M. E., 1946, *Phys. Rev.*, **70,** 245.

Bethe, H. A., 1937, *Rev. Mod. Phys.*, **9,** 69.

Bjerge, T., and Westcott, C. H., 1934, *Nature, Lond.*, **134,** 286.

Bleuler, E., and Scherrer, P., Zünti, W., 1945, *Helv. Phys. Acta*, **18,** 262 ; 1947, *Ibid.*, **20,** 96, 445.

Bleuler, E., and Zünti, W., 1946, *Helv. Phys. Acta*, **19,** 375 ; 1947, *Ibid.*, **20,** 195.

Bower, J. C., and Burcham, W. E., 1939, *Proc. Roy. Soc.* A, **173,** 379.

Chang, W. Y., Goldhaber, M., and Sagane, R., 1937, *Nature, Lond.*, **139,** 962.

Curran, S. C., and Strothers, J. E., 1940, *Proc. Camb. Phil. Soc.*, **36,** 252.

Elder, F. K., Motz, H. T., and Davidson, P. W., 1947, *Phys. Rev.*, **71,** 917.

Fermi, E., Amaldi, E., D'Agostino, O., Rasetti, F., and Segrè, E., 1934, *Proc. Roy. Soc.* A, **146,** 483.

Fowler, W. A., Delsasso, L. A., and Lauritsen, C. C., 1936, *Phys. Rev.*, **49,** 561.

Goldsmith, H. H., Ibser, H. W., and Feld, B. T., 1947, *Rev. Mod. Phys.*, **19,** 259.

Harkins, W. D., Gans, D. M., and Newson, H. W., 1935, *Phys. Rev.*, **47,** 52.

Holloway, M. G., 1940, *Phys. Rev.*, **57,** 347.

Huber, O., Lienhard, O., Scherrer, P., and Wäffler, H., 1944, *Helv. Phys. Acta*, **17,** 139 ; 1945, *Ibid.*, **18,** 221.

Klema, E. D., and Hanson, A. O., 1948, *Phys. Rev.*, **73,** 106.

Mattauch, J., and Flügge, S., 1947, *Nuclear Physics Tables* (New York : Interscience).

Nahmias, M. E., and Walen, R. J., 1936, *C.R. Acad. Sci., Paris*, **203,** 71 ; 1937 a, *Ibid.*, **203,** 1149 ; 1937 b, *J. Phys. Radium*, **8,** 153.

Naidu, R., and Siday, R. E., 1936, *Proc. Phys. Soc.*, **48,** 332.

Polessitsky, A., 1937, *Phys. Z., U.S.S.R.*, **12,** 339.

Pollard, E., and Watson, W. W., 1940, *Phys. Rev.*, **58,** 12.

Powell, C. F., 1942, *Proc. Roy. Soc.* A, **181,** 344.

Richards, H. T., 1941, *Phys. Rev.*, **59,** 796.

Scherrer, P., Huber, P., and Rossel, J., 1941, *Helv. Phys. Acta*, **14,** 314, 618.

Somers, H. S., and Scherr, R., 1946, *Phys. Rev.*, **69,** 21.

Weisskopf, V. F., and Ewing, D. H., 1940, *Phys. Rev.*, **57,** 472.

Wilhelmy, E., 1937, *Z. Phys.*, **107,** 769.

Slow Neutron-induced Activities in Europium and Samarium

By J. M. HILL and L. R. SHEPHERD
Cavendish Laboratory, Cambridge

Communicated by E. S. Shire ; MS. received 7th July 1949

ABSTRACT. The activities produced by the neutron irradiation of europium and samarium have been investigated by means of a thin lens type β-ray spectrometer and by absorption and coincidence methods. The 9·2-hour activity in europium is due to the dual decay of ^{152}Eu by β^- emission and by K capture. The long period activity is due to both ^{152}Eu and ^{154}Eu, and again both β^- emission and K capture are present. This long period K capture is due to ^{152}Eu, and the β^- emission is possibly due to both ^{152}Eu and ^{154}Eu. The energies of the emitted radiations are discussed and possible decay schemes proposed.

The 47-hour activity induced in samarium is due to the β^- decay of ^{153} Sm, and measurement of the energies of the emitted radiations has been made.

I. EUROPIUM

§ 1. INTRODUCTION

The rare earth element europium has two stable isotopes, ^{151}Eu and ^{153}Eu, which are present in almost equal proportions. Irradiation by slow neutrons produces a strong activity of 9·2 hours half life-time in addition to activity of much longer life (6–8 years). These activities could be due to either ^{152}Eu or ^{154}Eu, which would be produced by neutron capture by the stable isotopes. The assignment of the activities to the respective isotopes has recently been made by Inghram and Hayden (1946, 1947), who report that the 9·2-hour activity is due to the isotope ^{152}Eu, and that both the isotopes ^{152}Eu and ^{154}Eu have long-period activities. ^{152}Eu thus exists in two isomeric states which are both unstable and decay with half life-times of 9·2 hours and 6–8 years respectively.

§ 2. THE 9·2-HOUR EUROPIUM

The β spectrum of the 9·2-hour activity has been investigated by Tyler (1939) who used a semi-circular type β-ray spectrometer. He found the upper energy limit of the β spectrum to be 1·88 Mev., and he also found two strong conversion electron groups at 72·7 kev. and 112·8 kev. The separation of these groups is 40·1 kev., which is significantly less than the difference of the K and L binding energy of gadolinium, the element that is produced by the β decay of europium. Further, the intensity of these groups is approximately the same, which is unusual if they result from the K and L conversion of a single γ ray. On this basis Tyler suggested that these two electron groups may be due to K conversion of two γ rays of 123 kev. and 163 kev.

Bothe (1946) has reported the existence of K capture in both the 9·2-hour activity and the long-period activity.

(i) *The β Spectrum*

In the experiments by the authors, sources of high specific activity were produced by the irradiation of spectrographically pure Eu_2O_3 in the experimental pile at the Atomic Energy Research Establishment. Several thin sources (*c.* 1 mg.cm^{-2}) mounted on 2 mg.cm^{-2} aluminium foil were investigated in a thin lens type β-ray spectrometer.

Figure 1 shows a typical β spectrum obtained in this manner, the number of particles $P(\eta)$ being plotted against the momentum η, measured in $\boldsymbol{m_0 c}$ units. The two strong conversion electron groups have peaks at $73{\cdot}5 \pm 0{\cdot}3$ kev. and $113{\cdot}5 \pm 0{\cdot}3$ kev. and a separation of $40{\cdot}0 \pm 0{\cdot}5$ kev. These figures are in agreement with Tyler's results and are again significantly less than the difference in the K and L binding energies in gadolinium. No evidence could be found for a peak at 155 kev., which would be expected from the L conversion of a γ ray of 163 kev.

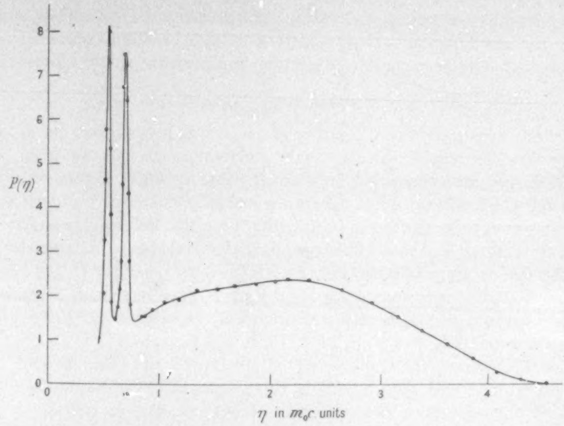

Figure 1.

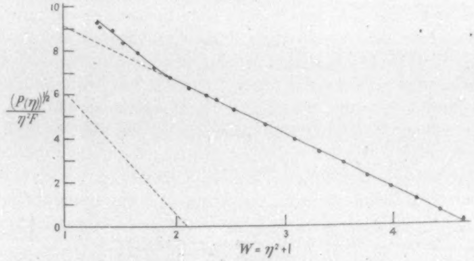

Figure 2.

Comparison of the areas under the peaks of the conversion lines, and under the continuum, enabled the intensities of the conversion lines to be estimated. Correction must, however, be made for the partial absorption of the counter window, and, when this is done, the number of conversion electrons, expressed as a percentage of the number of β particles, is found to be: $73{\cdot}5$ kev. electrons, 9%; $113{\cdot}5$ kev. electrons, $6{\cdot}5$%.

A Kurie plot of the continuum is shown in Figure 2. This indicates that the end-point of the spectrum is at $1{\cdot}880 \pm 0{\cdot}005$ MeV., which is again in excellent agreement with the value given by Tyler. The spectrum is of the Fermi allowed type down to energies of 0·5 MeV. ($W_0 = 2{\cdot}0\, m_0c^2$), but below this is a deviation which could be attributed to a partial spectrum with an end-point of 0·55 ± 0·02 MeV., and of intensity approximately 10% of the total. The evidence to support this hypothesis is, however, meagre, and a deviation from the theoretical Fermi allowed type of spectrum is not to be unexpected since the 9·2-hour activity lies between the first and second forbidden curves of the Sargent diagram.

The possibility of positron emission was investigated by means of a spiral filter in the spectrometer. No positrons could be detected, although this arrangement should be capable of detecting one positron in 10^4 electrons.

(ii) *The γ Radiation*

The γ radiation from the 9·2-hour europium was investigated in the spectrometer by measurement of the secondary electron spectrum produced. About 10 mg. of Eu_2O_3 was contained in a small brass cylinder (5 mm. in diameter, 5 mm. long) which was placed in the source holder. Silver or lead foils could be placed in front of this cylinder to investigate the photoelectrons produced by the γ radiation. Figure 3(*a*) shows the secondary electron spectrum from the capsule in the absence of any radiating foil, and Figure 3(*b*) the lower portion of the secondary electron spectrum with 11 mg.cm^{-2} of silver foil. These peaks correspond to the K and L photoelectrons from silver, ejected by a γ ray of 120 kev. No peak corresponding to a γ ray of 163 kev. was detected.

Figure 3 (*c*) shows the upper part of the spectrum from a lead radiator 110 mg.cm^{-2} thick, and Figure 3 (*d*) is this photoelectron distribution after the removal of the Compton background. These peaks are mainly K photoelectrons from the lead radiator ejected by γ rays of energies 0·94 ± 0·02 MeV., 0·82 ± 0·01 MeV., 0·69 ± 0·01 MeV., and ~0·41 MeV. The relative intensities of the 0·94 MeV., 0·82 MeV., and 0·69 MeV. γ rays have been estimated from the heights of the photoelectric peaks, and these ratios are approximately 4 : 6 : 1. The intensity of the 0·41 MeV. γ radiation is considerably less than the others.

The number of γ quanta emitted per β particle has been estimated by means of calibrated β and γ counters, the efficiencies of which were known, and it would seem that there is approximately one quantum of 0·94 MeV. or 0·82 MeV. per two β particles. If these γ rays were produced in the daughter nucleus gadolinium, it would be necessary to postulate a complex β spectrum. This is refuted by the Kurie plot, which indicates a simple spectrum over the energy range in question.

(iii) *Coincidence Experiments*

To obtain more information of the decay scheme of the 9·2-hour europium, and also to establish correlation between the various radiations emitted, a series of coincidence experiments has been carried out. In the first of these, a source was placed between a β counter and a γ counter and investigation was made of the variation of coincidence counting rate as a function of aluminium absorber thickness. This established that coincidences occurred between the γ rays and the conversion electrons, but not between the γ rays and the continuous β spectrum. This is additional evidence that the γ radiation is not associated with the β decay, but arises from some other mode of decay, i.e. K capture, or possibly an isomeric transition in the europium nucleus.

Investigation of γ–γ coincidences showed that coincidences exist and that they can be cut out by relatively small amounts of lead absorber. The absorption coefficient of these γ–γ coincidences corresponds to the absorption of a γ ray of approximately 0·13 MeV., and this is interpreted as indicating that the γ ray of

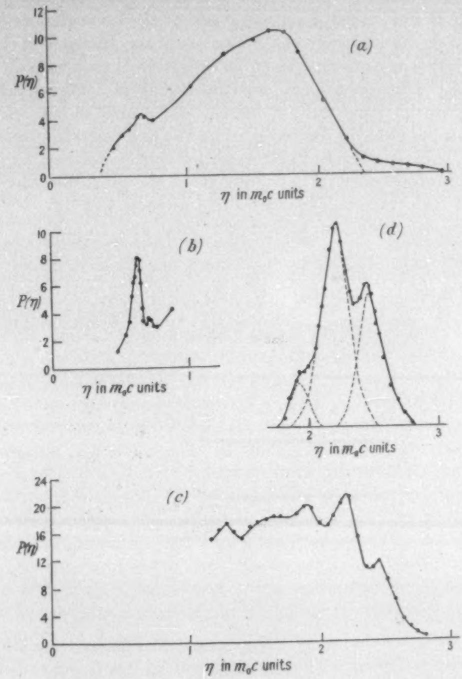

Figure 3.

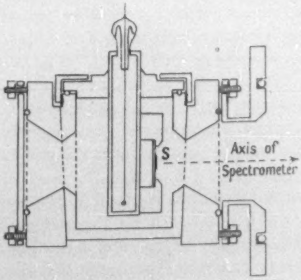

Figure 4.

0·12 Mev. is in cascade with one or both of the γ rays of 0·82 Mev. or 0·94 Mev. It also shows that the γ rays of 0·82 Mev. and 0·94 Mev. are not in cascade.

Confirmation of these results was obtained by investigating coincidences between the γ radiation and the β particles and conversion electrons focused in the β-ray spectrometer. A thick-walled γ counter was mounted in the source holder (Figure 4) and investigation was made of the coincidences between the γ radiation and the focused electrons. The quantum efficiency of this γ counter was found for different γ-ray energies by investigation of sources with well-known decay schemes. This experiment confirmed that no coincidences occurred between the β particles and the γ radiation, and it also showed that the same coincidence rate per electron was recorded on the two electron groups at 73 kev. and 113 kev. The coincidence rate per recorded conversion electron corresponds to the net quantum efficiency of the counter at the energy of the γ ray in question. The energy of the γ radiation found by this method was $0{\cdot}8 \pm 0.1$ Mev. This figure is in satisfactory agreement with the measured values of 0·82 Mev. and 0·94 Mev.

Investigation of coincidences between K X rays and the conversion groups at 73 kev. and 113 kev. demonstrated that these groups were K and L conversion groups of a single γ ray. An X-ray counter was mounted on the source end of the spectrometer, the X rays and γ rays being transmitted through a distrene window (Figure 5). This window was 1 cm. thick, this thickness being sufficient to stop all β particles and soft L X rays, while transmitting K X rays and γ rays with little attenuation. Using a source of ^{153}Sm, the decay of which is described in the second part of this paper, it was found that the X-ray coincidence rate per conversion electron, i.e. the probability of recording a K X ray after the ejection of a K conversion electron, was $0{\cdot}43 \pm 0{\cdot}03 \times 10^{-3}$. The X rays from the ^{153}Sm source are europium X rays, since they originate from the daughter nucleus after β^- emission. The X rays from the 9·2-hour europium are, as will be shown later, samarium X rays produced after K capture. Since europium and samarium are neighbouring elements, it may be assumed that the efficiency of detecting these X rays will be almost the same.

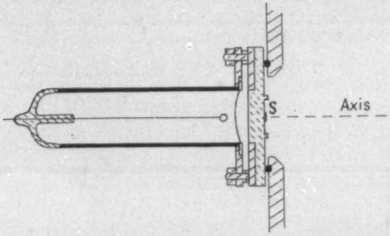

Figure 5.

With the 9·2-hour europium source the total X-ray plus γ-ray coincidence rate per conversion electron was $1{\cdot}5 \pm 0{\cdot}1 \times 10^{-3}$ in the case of the 73·5 kev. conversion electron group, and $1{\cdot}1 \pm 0{\cdot}1 \times 10^{-3}$ in the case of the 113·5 kev. electrons. It is known from the previous coincidence experiment that the γ-ray coincidence rate is the same for each of the two groups. The difference in total coincidence rate corresponds therefore to an additional K X-ray being in coincidence with the 73·5 kev. conversion electron group. This indicates that the 73·5 kev. and 113·5 kev. electron groups are respectively K and L conversion groups of a single γ ray.

(iv) *X-ray Measurements*

To confirm that the γ radiation, which is associated with the X rays emitted, is produced after K capture, the X rays were identified by the method of critical absorbers. If the X rays have an energy slightly higher than the K binding energy of the absorber, the absorber will have a strong absorption. On the other hand, if the energy is slightly lower than this, the X rays will not be able to eject any K photoelectrons and the absorption will be very much less. The K binding energy of cerium lies between the K_α radiation of samarium and that of europium; the neighbouring elements to cerium are lanthanum, on the low energy side, and praesodynium, on the higher energy side. We should expect therefore that if the X rays are from samarium, the mass absorption coefficient of the lanthanum would be high, and that of cerium and praesodynium low. On the other hand, if the X rays are from europium we should expect the mass absorption coefficient of lanthanum and cerium to be high and that of praesodynium to be low.

The elements lanthanum, cerium and praesodynium are, unfortunately, rather rare, particularly praesodynium, and it was only possible to obtain them in the form of salts. The experimental method employed therefore was to use them in solution, solutions of the nitrates of the three elements being made up to the same concentration. The amounts of these critical absorbers available were insufficient to resolve the absorption curves obtained into their constituent parts, and it was not possible therefore to give absolute values for the mass absorption coefficients. The curves did, however, demonstrate the absorption jump between cerium and praesodynium with X rays that were known to be europium X rays (^{153}Sm source), and also showed that with the X rays from the 9·2-hour europium the absorption jump occurred between lanthanum and cerium. This confirms that the X rays from the 9·2-hour europium are samarium X rays, and hence shows the existence of K capture.

§ 3. THE LONG-PERIOD EUROPIUM ACTIVITY

The long-period activity has been investigated in the same manner as that employed for the 9·2-hour activity.

(i) *The β and γ Spectra*

The source investigated was prepared by a six weeks' irradiation in the experimental pile at the Atomic Energy Research Establishment. The specific activity was, however, very much less than in the case of the 9·2-hour activity, and it was not possible to use the maximum resolution in the spectrometer. The β spectrum obtained is shown in Figure 6, and a Kurie plot is given in Figure 7. This indicates that the spectrum is complex, with a final end-point at 1·58 ± 0·01 Mev. The lower portion of the spectrum appears to consist of more than one component, but a complete analysis cannot be made with confidence. A tentative analysis indicated end-points at 0·86 Mev., 0·66 Mev. and 0·49 Mev.

The electron spectrum includes several groups of conversion electrons. The energies of these groups have recently been given by Shull (1948), who has used a high resolution spectrometer and obtained results to a higher degree of accuracy than could be achieved on our spectrometer. He has also examined the secondary electron spectrum from a lead radiator irradiated by the europium x rays and has identified radiation with energies of 243, 344, 442, 774, 959, 1082 and 1402 kev.

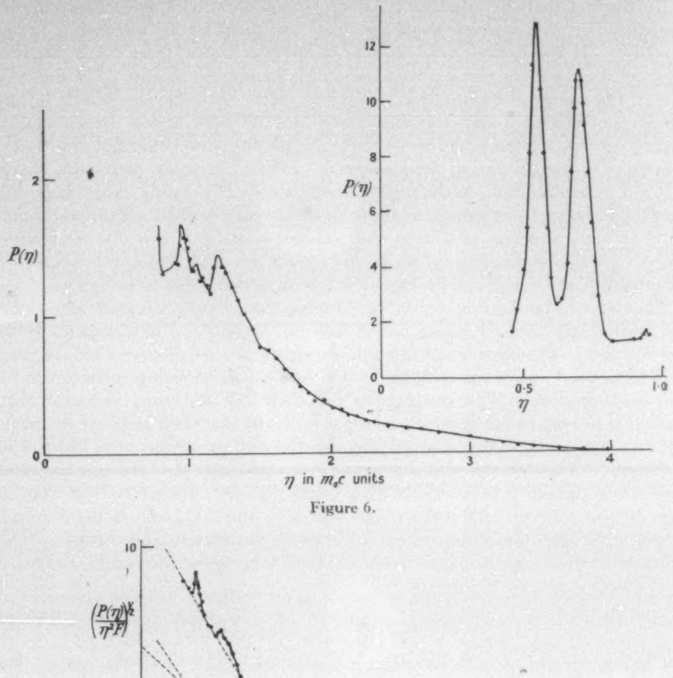

Figure 6.

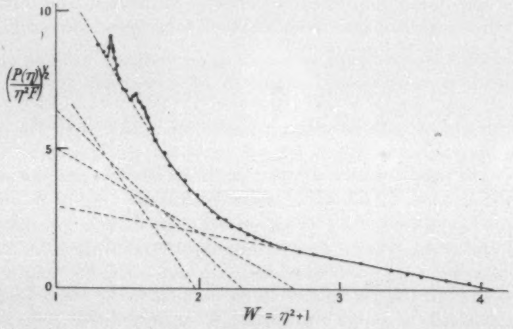

Figure 7.

The results we obtained are, within the limits of experimental error, in agreement with these figures. Two important results should, however, be mentioned, namely,

(i) the two strong conversion electron groups shown in Figure 6 are, within the limits of experimental error, of exactly the same energy and relative intensity as the two groups found in the 9·2-hour activity; and (ii) these conversion groups contain more electrons than the total number of β particles in the continuum. These are strong indications that the electron groups result from the decay of the long-period isomer of ^{152}Eu, and that the decay is by K capture and leads to the same excitation level in the samarium as in the case of the 9·2-hour activity.

No positron emission could be detected, but the existence of K capture was confirmed by critical absorption measurements on the X rays emitted.

(ii) *Coincidence Experiments*

Investigation of coincidences between X rays and the strong conversion electron groups demonstrated that these electron groups are due to K and L conversion of a γ ray produced after K capture. This experiment was similar to the equivalent investigation on the 9·2-hour activity except that with the long-period source it was possible to make a more detailed investigation. As indicated previously, coincidences were recorded by both γ rays and X rays. The coincidence rate due to the γ radiation was determined by absorbing the X rays in 270 mg.cm^{-2} of silver foil placed in front of the X-ray counter. This thickness of silver will reduce the X rays to about 0·05 of their initial intensity without materially reducing the γ radiation. The following coincidence rates per conversion electron were recorded:

(1) γ + X ray	(73·5 kev. line)	$1{\cdot}12 \pm 0{\cdot}05 \times 10^{-3}$
(2) γ + 0·05 X ray	(73·5 kev. line)	$0{\cdot}50 \pm 0{\cdot}05 \times 10^{-3}$
(3) γ + X ray	(113·5 kev. line)	$0{\cdot}84 \pm 0{\cdot}05 \times 10^{-3}$
(4) γ + 0·05 X ray	(113·5 kev. line)	$0{\cdot}53 \pm 0{\cdot}05 \times 10^{-3}$

From these figures the coincidence rates due to the X rays are $0{\cdot}65 \pm 0{\cdot}07 \times 10^{-3}$ in the case of the 73·5 kev. electrons, and $0{\cdot}33 \pm 0{\cdot}07 \times 10^{-3}$ in the case of the 113·5 kev. electrons. The ratio of these coincidence rates is $2{\cdot}0 \pm 0{\cdot}4$, and this shows that the 73·5 kev. electrons are in cascade with two K X rays and the 113·5 kev. electrons are in cascade with only one.

Investigation of coincidences between the γ radiation and these two conversion lines showed that the coincidence rate was the same in each case, and corresponded to the conversion electrons being in cascade with γ radiation of about 1 Mev. It was not possible to identify which of the various γ rays are in cascade with the conversion electrons. One possibility is the γ ray of 959 kev. This would be consistent with the coincidence measurements, and it should also be noted that the difference in energy between this γ ray and the γ ray of 1082 kev. corresponds exactly with the energy of the transition responsible for the conversion electrons. Another possibility is that the strong γ rays of 344 kev. and 744 kev. may themselves be in cascade and lead to the 0·12 Mev. excitation level.

Coincidences were also detected between the γ radiation and the low-energy component of the continuous β spectrum. The coincidence rate obtained indicated that these β particles are in cascade with γ radiation of total energy of approximately 1·3 Mev. No appreciable β–γ coincidence rate could be detected with that part of the β spectrum having energies greater than about 0·7 Mev. This indicates that the higher energy component of the β spectrum is not in cascade with any energetic γ radiation.

§4. CONCLUSIONS

The 9·2-hour ^{152}Eu decays by both β^- emission to ^{152}Gd and by K capture to ^{152}Sm, the probability of β emission being about double that of K capture. The β decay is predominantly to the ground state of ^{152}Gd, very little, if any, of the γ radiation being associated with this mode of decay. The decay by K capture leads to one or more excited states in ^{152}Sm and the γ radiation is emitted in the subsequent de-excitation of these states. The γ radiation of 0·120 Mev. almost certainly occurs in the final de-excitation to the ground state and is probably in cascade with the radiation of 0·82 Mev. This leads to the assumption of an excited state in ^{152}Sm with energy of 0·94 Mev., and the γ radiation of this energy may be emitted as an alternative mode of de-excitation of this state. The possibility that this γ radiation is also in cascade with the 0·120 Mev. level cannot however be excluded, as it has not been possible to measure the intensity of the 0·120 Mev. radiation with sufficient accuracy to distinguish between these possibilities.

The long-period activity in europium is due to both β^- emission and to K capture. The decay by K capture can be attributed to the isomer ^{152}Eu and leads to one or more excited levels in ^{152}Sm. The de-excitation of the ^{152}Sm nucleus is by way of the same 0·120 Mev. level as was observed in the case of the 9·2-hour activity. The other γ radiation in cascade with this level has a total energy of about 1 Mev. The decay by β emission could be attributed to either ^{152}Eu or to ^{154}Eu. The low-energy β spectrum is in cascade with γ radiation of approximately 1·3 Mev., while the high-energy spectrum is not associated with energetic γ radiation. It is difficult to fit these two spectra into a single decay scheme, and it would seem possible that both ^{152}Eu and ^{154} Eu contribute to this β^- activity.

II. SAMARIUM

Irradiation of samarium with slow neutrons produces a strong activity of 47 hours half life-time. Hayden and Inghram (1946) have shown that this activity is due to the isotope ^{153}Sm, and Bothe (1946), using absorption methods, has reported that the maximum energy of the β spectrum is 0·75 Mev. Cork *et al.* (1948) and Hill (1948) have recently reported conversion electron groups which correspond to γ radiation of 102 kev. and 67 kev.

(i) *The β Spectrum*

The β spectrum obtained in the β-ray spectrometer is shown in Figure 8. The conversion electron groups have energies of 53·1 ± 0·3 kev. and 93·3 ± 0·3 kev., and correspond to the conversion of a γ ray of 101·5 ± 0·3 kev. in the K and L shells of the daughter nucleus ^{153}Eu.

The window of the Geiger counter has stopping power equivalent to 15 mm. of air, and this will cause considerable absorption of the low-energy electrons. When correction is made for this absorption, it is estimated that the number of conversion electrons in the two groups is $45 \pm 5\%$ of the number of β particles in the continuum. The ratio of K conversion to L conversion is estimated as $5 \pm 0{\cdot}5 : 1$. These results may, however, be influenced by the self-absorption of the source which had a thickness of approximately 1 mg.cm^{-2}.

A Kurie plot of the continuum (Figure 9) indicates the presence of two spectra with maximum energies of 0·80 ± 0·01 Mev. and 0·68 ± 0·01 Mev. The difference in energies of these spectra corresponds, within the limits of experimental error, to the energy of the γ radiation emitted, and it is reasonable to assume that these two spectra correspond to transition to the ground state and to a 101·5 kev. excitation level in the daughter nucleus. It is estimated from the Kurie plot that the intensity of the low-energy spectrum is approximately double that of the other.

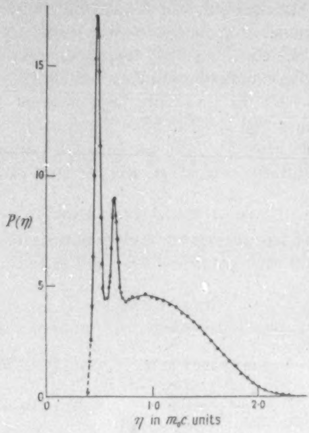

Figure 8.

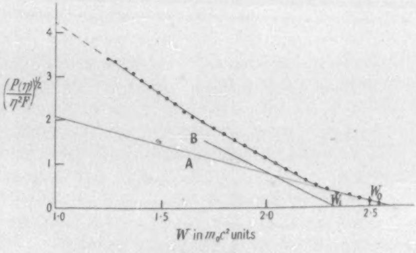

Figure 9.

(ii) *Coincidence Experiments*

Coincidences were detected between the γ radiation and the β particles and also between the conversion electrons and the β particles. This confirms that the γ radiation is emitted from the daughter nucleus europium.

Investigation of x-ray coincidences was also made in order to obtain an estimate of the number of K conversion electrons which is not influenced by the absorption of the counter window or the self-absorption of the source. With the spectrometer focused on the K conversion line, the coincidence rate per conversion electron gives the probability of detecting a K x ray after the ejection of a K conversion electron. With the spectrometer focused on the continuum, the coincidence rate per β particle, after correction for γ-ray coincidences, gives the probability of detecting a K x ray after the ejection of a β particle. The ratio of these coincidence rates gives therefore the probability that a β particle is in cascade with a K conversion electron, i.e. the probability that a K conversion electron is ejected after a β particle. This value was found to be $0{\cdot}5 \pm 0{\cdot}05$.

It has not been possible to determine the intensity of the unconverted γ radiation, but from the above results it is apparent that the internal conversion coefficient of the 101·5 kev. radiation must exceed 70%. The low energy of the γ radiation, together with the unusually high internal conversion coefficient, suggested the possibility that the 101·5 kev. level in the daughter nucleus may have a measurable half life-time. No such half life-time could, however, be detected with our equipment, which had a lower limit of 10^{-7} second.

ACKNOWLEDGMENTS

The authors would like to express their gratitude to Mr. E. S. Shire and Dr. J. V. Dunworth for their continued help and interest in this work.

REFERENCES

BOTHE, W., 1946, *Z. Naturforsch.*, **1,** 179.
CORK, J. M., *et al.*, 1948, *Phys. Rev.*, **74,** 240.
HAYDEN, R. J., and INGHRAM, M. G., 1946, *Phys. Rev.*, **70,** 89.
HILL, R. D., 1948, *Phys. Rev.*, **74,** 78.
INGHRAM, M. G., and HAYDEN, R. J., 1947, *Phys. Rev.*, **71,** 130.
SHULL, F. B., 1948, *Phys. Rev.*, **74,** 917.
TYLER, A. W., 1939, *Phys. Rev.*, **56,** 125.

Directional Measurements of the Diurnal Variation of Cosmic-Ray Intensity

By H. ELLIOT and D. W. N. DOLBEAR
Manchester University

Communicated by P. M. S. Blackett ; *MS. received 6th July* 1949

ABSTRACT. Measurements of the solar daily variation in cosmic-ray intensity have been made for a total of 360 days using two arrays of Geiger–Müller counters inclined at 45° to the vertical in the North and South directions. Both the diurnal and semi-diurnal variations are found to be significantly different for the two directions, and since the particles recorded by the two sets have passed through the same amount of atmosphere under similar conditions, it must be supposed that at least a part of the variation is due to causes which lie outside the earth's atmosphere.

It is found that both the amplitude and phase of the daily variation for the South-pointing recorder vary with season, whereas in the North direction the amplitude only shows any seasonal variation. The amplitude is greatest in summer in both directions.

The experimental results are compared with those of earlier workers and are discussed in relation to some of the interpretations of the daily variation which have been put forward. The difference between the variations in the two directions is interpreted as evidence for a non-isotropic distribution of the primary cosmic rays in space. A variation with sidereal and not with solar time would be expected under these conditions, but it is pointed out that the magnetic field of the sun may modify the direction of arrival of the primary rays at the earth so as to produce a resultant solar time variation.

§ 1. INTRODUCTION

Measurements of the solar daily variation in cosmic-ray intensity have been made by many observers using either ionization chambers or Geiger–Müller counters, and it is now well established that the variation has an amplitude of about 0·2% with the maximum intensity in the afternoon.

There is, as yet, no generally accepted explanation of the daily variation, although several different interpretations have been suggested. Jánossy (1937) pointed out that the solar magnetic field should produce a daily variation in the cosmic-ray intensity at the earth. This suggestion has been elaborated by Epstein (1938), by Vallarta and Godart (1939) and by Jánossy and Lockett (1941). Rossi showed in 1947 (private communication) that since the geomagnetic latitude effect increases with height, the amplitude of the daily variation must also increase with height if it is due to the solar magnetic field. He estimated that the difference between the day and night intensities should be about 10% at latitude 48·7° at 14,000 ft., which is not in accord with the observations of Hess and Graziadei (1936) on the Hafelekar. Their data show a daily variation with an amplitude of about 0·2%, which is similar to that at sea level.

Following a suggestion by Alfvén (1947), Kane, Shanley and Wheeler (1949) have shown, however, that the daily variation due to the solar magnetic field will be much smaller than that estimated by Rossi, owing to the scattering of primary radiation into periodic orbits by the earth's magnetic field. Vallarta and Godart's (1939) estimate of 0·2% for the daily variation at sea level would also be very much reduced by this effect. It appears, therefore, that whilst the solar magnetic field may be responsible for the latitude cut-off, it is unlikely to cause an appreciable variation in intensity over the day at sea level.

Duperier (1946), from the seasonal change in amplitude and phase of the daily variation, inferred the existence of both a solar and a sidereal component of the cosmic radiation and suggested that the solar daily variation is due to the emission of cosmic rays by the sun.

In order to distinguish between atmospheric effects and effects due to the magnetic field of the earth or of the sun, Alfvén and Malmfors (1943) measured the daily variation at different zenith angles. These measurements were made in Stockholm at 30° and 60° to the vertical in the North–South and East–West directions. Similar measurements were made by Kolhörster (1941) in Berlin.

A non-isotropic distribution in the radiation falling on the earth should appear as a difference between the daily variation in the two directions since the North and South-pointing counter telescopes sweep out different directions in space as the earth rotates. Since the rays have traversed the atmosphere under the same conditions for both the North and South directions, effects due to the daily pressure and temperature changes in the atmosphere are eliminated in the difference. The results obtained by Alfvén and Malmfors and by Kolhörster show that there is a marked difference between the diurnal variations in different directions, and Malmfors (1945) interprets this difference as being due to a non-isotropic distribution of the incident radiation. He concludes that the effect cannot be accounted for either by the heliomagnetic or geomagnetic fields.

Measurements of this kind have been made in Manchester in the North–South directions, and the results obtained, which are in qualitative agreement with those of Alfvén and Malmfors, are given below.

§ 1. APPARATUS

The cosmic-ray intensity recorder used in the present work consisted of two independent arrays of Geiger–Müller counters referred to as Recorder 1 and Recorder 2. Each array consisted of three trays with ten counters in each tray. The active area of each tray was 2,400 cm^2 and the trays were closely superimposed so that each array subtended a wide solid angle.

The counters were of the self-quenching copper-in-glass type with a tungsten wire anode, and were filled with argon and alcohol. Each counter was connected to a single-stroke multivibrator which quenched the initial discharge before it spread the full length of the wire, and also prevented the formation of multiple pulses (Elliot 1949). The use of these multivibrators considerably improved the stability of the recording set both by improving the voltage characteristics of the counters and by increasing their useful life-time.

The arrays were enclosed in metal boxes which also contained the E.H.T. supplies and the coincidence circuits. These boxes were mounted on a framework so that one was pointing South at 45° to the horizon and the other North. The framework could be turned about a vertical axis so that the directions of the recorders could be alternated. In this position the counting rate of each recorder was about 50,000 threefold coincidences per hour. The coincidence pulses were fed through a cathode follower to scaling units (one for each recording set) which scaled by 100 and the output from which worked electromechanical registers. These registers, together with a clock and an aneroid barometer, were mounted on a panel which was automatically photographed every fifteen minutes.

Figure 1 shows the effective polar diagram in the vertical plane of the two arrays, taking into account the variation of intensity with zenith angle, the sensitivity in a particular direction being defined as the product of the effective area by the intensity of the radiation in that direction. It will be seen that the direction of maximum sensitivity is at 65° to the horizontal. The polar diagram in the plane at 65° to the horizontal has a half-width of about 40°.

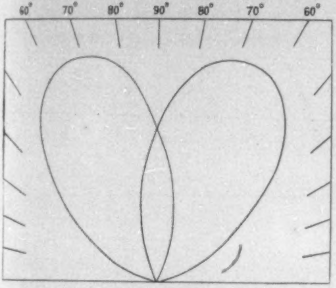

Figure 1. Polar diagram in the vertical plane for the two recording sets inclined at 45° to the vertical.

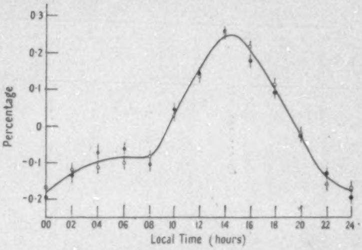

Figure 2. Daily variation measured by the two recorders, showing that there is no systematic difference between them. Each set has spent the same number of days pointing North and South.

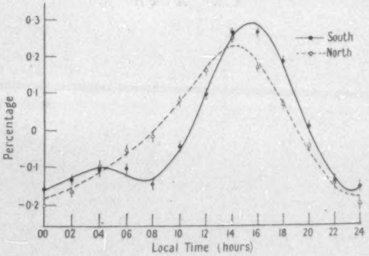

Figure 3. Daily variation in the North and in the South directions for 360 days.

§ 3. EXPERIMENTAL RESULTS

In order to eliminate any systematic difference which may have existed due to small differences in the geometry of the two arrays they were turned round at fortnightly intervals so that each pointed North and South alternately. Figure 2 shows the mean daily variation measured by the two recorders over a period of about 320 days, each recorder having spent very nearly the same number of days looking to the South as to the North. It is evident that there is no appreciable systematic difference between the data for the two sets.

Figure 3 shows the mean daily variation for the North and South directions for a total of 360 days. Figure 4 shows the difference curve obtained by subtracting the North variation from that for the South direction measured on the same days. In Figures 3 and 4 the curves drawn through the points are the sums of the first and second harmonics of best fit. The standard deviations shown for each point were calculated from the total number of particles counted during each two-hourly interval ($c.\ 4{\cdot}0 \times 10^7$).

Figure 5 shows the first harmonics for the North and South directions plotted on a harmonic dial. The radii of the standard deviation circles shown in all the harmonic dials have been determined from the scatter of the harmonic coefficients calculated for monthly groups of data.

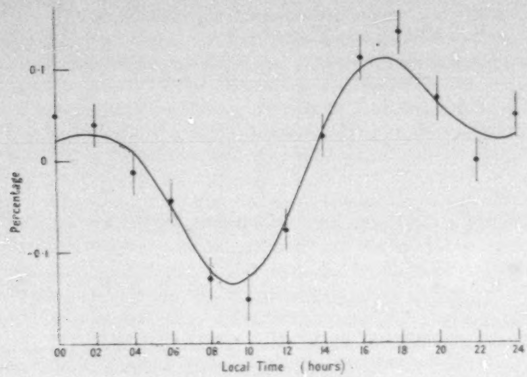

Figure 4. Difference curve obtained by subtracting the daily variation in the North direction from that for the South.

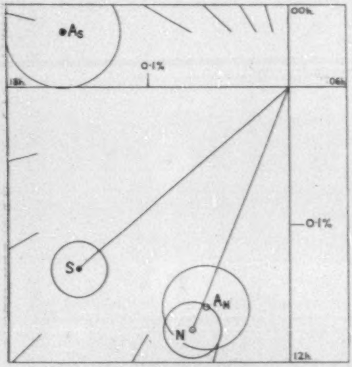

Figure 5. Solar time dial showing the first harmonics of the daily variation in Manchester for North (N) and South (S) and Stockholm for North (A_N) and South (A_S).

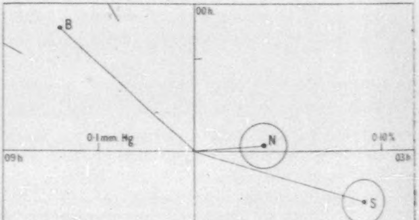

Figure 6. Solar time dial showing the second harmonics of the daily variation in cosmic-ray intensity for North and South together with the corresponding variation in atmospheric pressure.

Figure 6 shows the second harmonics for the North (N) and South (S) directions, together with the second harmonic, B, for the barometric pressure corresponding to the days used for N and S

Figures 5 and 6 show clearly that there is a marked difference between the two directions for both the first and second harmonics. No corrections for the diurnal change in atmospheric pressure or temperature have been applied to any of the above data.

Figure 7 shows the first harmonics for the data divided into groups according to season, spring being February, March and April; summer, May, June and July; and so on. Since the first harmonic of the daily pressure variation differed appreciably from group to group, these data have been corrected for pressure using a barometer coefficient of 2·68%/cm.Hg. This coefficient was determined independently by correlating atmospheric pressure with cosmic-ray intensity over a long period. The differences (S minus N) of the first harmonics for the seasons are plotted in Figure 8.

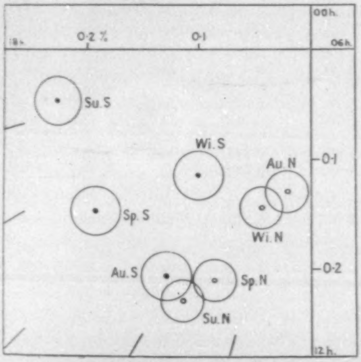

Figure 7. First harmonics for North and South grouped according to season.

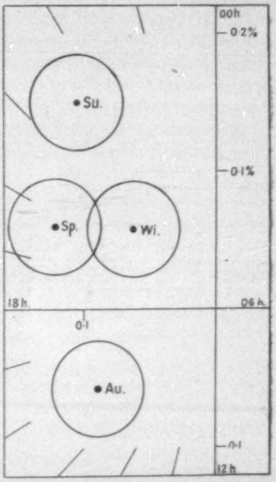

Figure 8. Seasonal variation of difference between the first harmonics for the North and South directions.

The Table gives the coefficients of the first and second harmonics of the various groups of data, which are expressed in the form

$$\left(a_1 \cos\frac{2\pi}{24}t + b_1 \sin\frac{2\pi}{24}t\right)\% \text{ for the first}$$

and

$$\left(a_2 \cos\frac{2\pi}{12}t + b_2 \sin\frac{2\pi}{12}t\right)\% \text{ for the second harmonic,}$$

where t is in hours. The rows numbered 1 give the harmonics uncorrected for diurnal and semi-diurnal pressure changes, while the rows numbered 2 are for the same data corrected for pressure.

§4. DISCUSSION OF RESULTS

It is of interest to compare the results obtained in Manchester with those of Alfvén and Malmfors (1943) in Stockholm for a zenith angle of 30°. Figure 5 shows their results for the North and South directions as A_N and A_S respectively. The radii of the standard deviation circles shown in the diagram have been estimated from the scatter of their harmonic coefficients. It will be seen that the amplitude and phase of the first harmonic for the North-pointing recorder in Stockholm is not significantly different from that found in Manchester, but the shift in phase of the first harmonic for the South-pointing recorder is not as great in Manchester as in Stockholm. Consequently, the difference curve shown in Figure 4, although similar in shape to that obtained in Stockholm, is of smaller amplitude. This may well be due to the larger solid angle covered by the recorders used here, which would be expected to smooth out the difference between North and South to some extent.

		SOUTH				NORTH			
		a_1	b_1	a_2	b_2	a_1	b_1	a_2	b_2
All data	1	−0·132	−0·150	−0·030	+0·089	−0·177	−0·070	−0·007	+0·042
	2	−0·135	−0·152	+0·004	+0·060	−0·171	−0·069	+0·031	+0·007
Spring	1	−0·123	−0·183	−0·026	+0·111	−0·177	−0·091	+0·029	+0·025
	2	−0·147	−0·194	+0·022	+0·087	−0·210	−0·087	+0·076	−0·004
Summer	1	−0·063	−0·237	−0·060	+0·072	−0·250	−0·128	−0·023	+0·037
	2	−0·047	−0·229	−0·029	+0·041	−0·229	−0·117	+0·011	+0·010
Autumn	1	−0·182	−0·115	−0·045	+0·081	−0·126	−0·005	−0·018	+0·055
	2	−0·206	−0·130	−0·008	+0·040	−0·129	−0·023	+0·020	+0·007
Winter	1	−0·134	−0·116	−0·011	+0·089	−0·173	−0·055	−0·002	+0·030
	2	−0·114	−0·101	+0·025	+0·062	−0·143	−0·045	+0·035	−0·003

It is not possible to compare the behaviour of the second harmonics since these are not given by Alfvén and Malmfors. There can be little doubt, however, that the difference between the second harmonics for North and South is real since it is at least four times the standard deviation. If, as is generally supposed, the bulk of the mesons is generated at a height of 16 km. above the surface of the earth, the difference in latitude of the regions of production covered by the two telescopes is about 0·1 degree, and it is unlikely that the amplitude of the atmospheric oscillations can change by a factor of two and half over such a small range of latitude. This difference therefore seems to preclude any interpretation of these second harmonics on the basis of atmospheric oscillations alone.

As shown in Figure 6, the second harmonics for both North and South have a maximum at approximately 03.30 hr. and are not exactly out of phase with the pressure vector, which has a maximum at 10.30 hr. This appears to be additional evidence that the second harmonics observed here are not due to atmospheric oscillations alone.

The difference curve (South minus North) of Figure 4 shows a remarkable similarity to the diurnal variation in the horizontal component of the earth's field in these latitudes, but it is doubtful whether this is of any significance. According to Vallarta and Godart (1939) the ionospheric current systems which cause the diurnal variation in the earth's magnetic field should be capable of producing a variation in cosmic-ray intensity near the equator but cannot affect the sea-level intensity at latitudes greater than 40°. In this connection, however, directional measurements at latitudes below 40° would be of value since the diurnal variation of H varies markedly with latitude.

Malmfors (1945) has interpreted the difference between the daily variation in the North and South directions as possibly due to a lack of isotropy of the primary rays outside the solar system. He points out that if the direction of anisotropy changes during the course of one year it would produce a diurnal variation with both solar and sidereal time, and he shows, by plotting his data according to sidereal time, that whilst an appreciable sidereal daily variation is present for the South data, that for the North-pointing recorder is very much less. This is the result which would be expected since the direction in which the South recorder is pointing changes as the earth rotates, whereas that for the North recorder does not.

Compton and Getting (1935) showed that if the primary cosmic rays originate outside the galaxy the effect of galactic rotation will be to produce a non-isotropic distribution of radiation and consequently a variation of intensity with sidereal time. A non-isotropic distribution is also to be expected if the primary cosmic rays are produced in the stars of the galaxy, because of the non-uniform distribution of these stars.

If the (S – N) difference is due to a non-isotropic distribution produced in either of these two ways, the (S – N) vectors shown in Figure 8 should rotate in an anticlockwise direction about the origin, making one complete rotation in a year. In addition, since the amplitude of the vectors should be the same for each season, there should be no resultant (S – N) vector when the data are averaged over a complete year. Since the (S – N) vectors do not show a cyclic arrangement about the origin, and there is a resultant vector for the whole year, the effect cannot be interpreted directly in terms of a sidereal time variation.

If, however, the effect of the magnetic field of the sun on a non-isotropic flux is taken into account, the time of maximum and the amplitude of the sidereal variation may be expected to vary with season, due to the deflecting action of the solar field. As the earth describes its orbit, the direction of maximum intensity will change relative to the direction of the sun, and therefore the effect of the sun's field on the sidereal component will change. As a result of this seasonal variation the sidereal daily variation will not average out over the year and a residual effect will remain which will appear as an apparent variation with solar time.

It should be possible to decide whether the difference between the daily variation in the two directions is due to an effect of this kind by measuring the solar daily variation in the East–West plane so that the two recorders sweep out the same directions, the West-pointing recorder following the East at a fixed time interval, depending on the angle between the direction of maximum sensitivity of the two recorders (see Figure 1).

Measurements in the East–West plane have been made by Alfvén and Malmfors (1943), but because of the comparatively short period of observation the statistical errors are too large to allow a satisfactory comparison to be made with their North–South data. Measurements in the East–West directions are at present being made in Manchester with the recording equipment described above.

If this interpretation of the South–North difference should prove to be correct it will, of course, still be necessary to postulate some additional mechanism to account for the solar daily variation observed on a recorder pointing along the axis of rotation of the earth.

§ 5. CONCLUSION

The experimental results of Alfvén and Malmfors (1943) on the dependence on direction of the first harmonic of the diurnal variation of cosmic-ray intensity are confirmed for the North and South directions, and it is found that the difference between the first harmonics for the two directions shows a variation with season. The second harmonic has a markedly different amplitude for the two directions, and the semi-diurnal variation cannot, therefore, be due to atmospheric oscillations as has been previously supposed.

It is tentatively suggested that the difference in the diurnal variation in the two directions may be due to a sidereal component of the primary rays whose direction and intensity are modified by the presence of a solar magnetic field.

ACKNOWLEDGMENTS

We are indebted to Professor P. M. S. Blackett for providing the facilities for this work and for many valuable discussions. We also wish to thank Professor A. Duperier and Professor L. Jánossy for suggesting the experiment.

Finally, we wish to express our gratitude to the Department of Scientific and Industrial Research for a grant covering the cost of the intensity recording equipment, which was built by Cinema-Television Ltd.

REFERENCES

Alfvén, H., 1947, *Phys. Rev.*, **72,** 88.
Alfvén, H., and Malmfors, K. G., 1943, *Ark. Mat. Astr. Fys.*, **29 A**, No. 24.
Compton, A. H., and Getting, I. A., 1935, *Phys. Rev.*, **47,** 817.
Duperier, A., 1946, *Nature, Lond.*, **158,** 196.
Elliot, H., 1949, *Proc. Phys. Soc.* A, **62,** 369.
Epstein, P. S., 1938, *Phys. Rev.*, **53,** 862.
Hess, V. F., and Graziadei, H. T., 1936, *Terr. Magn. Atmos. Elect.*, **41,** 9.
Jánossy, L., 1937, *Z. Phys.*, **104,** 430.
Jánossy, L., and Lockett, P., 1941, *Proc. Roy. Soc.* A, **178,** 52.
Kane, E. O., Shanley, T. J. B., and Wheeler, J. A., 1949, *Rev. Mod. Phys.*, **21,** 51.
Kolhörster, W., 1941, *Phys. Z.*, **42,** 55.
Malmfors, K. G., 1945, *Ark. Mat. Astr. Fys.*, **32 A**, No. 8.
Vallarta, M. S., and Godart, O., 1939, *Rev. Mod. Phys.*, **11,** 180.

Some Properties of Penetrating Cosmic-Ray Showers and Star Phenomena seen in the Cloud Chamber

By C. C. BUTLER, W. G. V. ROSSER and K. H. BARKER
The Physical Laboratories, The University, Manchester

Communicated by P. M. S. Blackett; MS. received 21st July 1949

ABSTRACT. Cloud-chamber photographs of cosmic-ray showers containing penetrating particles have been obtained at sea level. The spectrum of the penetrating particles has been measured and a study made of the interaction of the energetic particles in lead and in the gas of the cloud chamber. Conclusions about the nature of the penetrating particles are discussed; these show that about half the penetrating particles are protons and the remainder are probably π-mesons and mesons of heavier mass. Three heavy particles produced in stars are probably τ-mesons.

§ 1. INTRODUCTION

The Wilson cloud chamber has been employed by Fretter (1948, 1949), Rochester (1946), Rochester and Butler (1948 b), and other workers, in studies of the groups of penetrating particles which constitute a small fraction of cosmic-ray showers. Most of these particles are lightly ionizing, and for this reason only tentative conclusions about their nature have been reached. Rochester and Butler (1948 b) discussed the evidence that the penetrating showers contain fast protons and mesons. Their work has now been extended using a more complicated detection apparatus.

A large group of cosmic-ray showers photographed in a magnetic field has been examined, in particular those showers containing one or more particles which penetrate the 3·4 cm. lead plate in the chamber without multiplication. These showers are described as penetrating showers. In addition, a number of high-energy interactions in the lead plate have been studied. Mesons and protons are clearly produced in these showers which would probably be classified as penetrating showers if a chamber large enough to contain a second 3 cm. lead plate had been used. The particles produced in the lead plate are found to have a wide angular distribution and the events are referred to as 'stars'. The term 'penetrating shower' is used solely to describe showers produced above the cloud chamber with some particles which penetrate the lead plate. This distinction is necessary in a phenomenological discussion but does not imply that the high-energy stars are fundamentally different from the penetrating showers. There is good evidence that the stars are showers of penetrating particles.

The cloud-chamber photographs of penetrating showers and stars show complicated structures, and before any general conclusions can be reached they must be analysed into various types. This process is outlined for stars in § 4 and a selected set of showers is discussed in detail in § 5. These showers are also mainly stars and are the most valuable for analysis since the whole event is usually seen in the chamber, and so the geometrical factors are well known. As a result of the 'botanical' classification of the showers, a number of general measurements have been made which are now discussed.

§ 2. THE EXPERIMENTAL ARRANGEMENT

(i) *The Geiger Counter Sets*

Two series of photographs, designated R and B respectively, were obtained with slightly different geometrical arrangements of the lead transition material (Figures 1 and 2). In both of these arrangements two counter sets are employed which can trigger the chamber independently. One set of counters, P, is the P-set arrangement first used by Jánossy and Rochester (1942), who demonstrated that it was rigidly selective for penetrating showers since at least two penetrating particles are required for operation. The second set, M, is a simple shower detector possessing no special selectivity for any particular type of shower; thus only a selection from the photographs obtained which satisfy certain criteria (§ 3) is included in the analysis of the penetrating showers. All the photographs obtained with the P-set are significant in such an analysis, and operation of this set was shown on the photographic record by the flash of a small indicator lamp. The simultaneous use of a selective and a non-selective counter arrangement yields a higher rate of rare events, such as penetrating showers at sea level, provided that the average waiting period is appreciably longer than the dead time of the chamber. Under these circumstances the two arrangements are acting substantially independently (Wilson 1948).

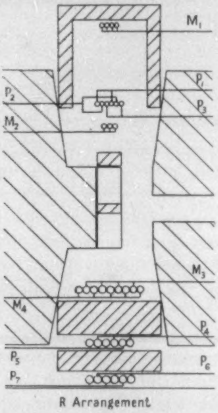

Figure 1.

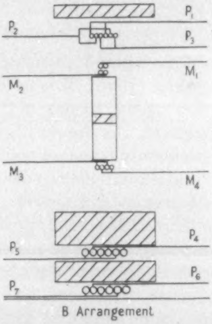

Figure 2.

The cloud chamber was covered with 10 cm. of lead in the R series; this was divided into two portions, 5 cm. immediately over the chamber and 5 cm. as transition material above all the counters. A transition layer of 5 cm. of lead was used alone for the B series. The R arrangement was replaced by the B arrangement in order to produce some of the penetrating showers as close to the cloud chamber as possible. In this way it was hoped to learn something of the angular distribution of the penetrating particles, but as yet insufficient data have been accumulated.

(ii) *The Cloud Chamber and Magnetic Field*

The cloud chamber described by Rochester and Butler (1948 a) was operated in a magnetic field of approximately 7,500 gauss. It was illuminated by two Siemens S.F.4 discharge tubes, each dissipating 400 joules per discharge. The flash was delayed 70 msec. after the completion of the chamber expansion to allow the drops to reach a size suitable for photography. Kodak R55 or Ilford 5G91, both orthochromatic recording films, were found to be the most suitable.

A pair of Leitz Hektor wide-angle lenses of aperture f/6·3 and focal lengths 2·8 cm. were used to obtain stereoscopic photographs of the chamber. These lenses give excellent depth of focus when used at a magnification of one-ninth, are free from curvature distortion, and enable the whole chamber to be photographed. The Hektor lenses replaced the Taylor, Taylor and Hobson corrected lenses used in the previous work.

(iii) *The Accuracy of Energy Measurements*

The curvature compensator devised by Blackett (1937) was employed for curvature measurements. The chamber is fitted with a metal piston of diameter 25 cm.; this is covered with black velvet to provide a suitable background for the tracks. Only tracks with the piston as background are suitable for measurement, as appreciable distortion often occurs at its edges. A minimum track length of 6 cm. is acceptable for measurement. The maximum detectable momentum as defined by Blackett (1937) was found to be $8\cdot0 \times 10^9$ ev/c. from measurements made on 75 meson tracks obtained in zero magnetic field. To reduce distortion to a minimum the temperature of the chamber and its surroundings is maintained constant to 1° c. over a period of 12 hours. Even under these conditions slight distortion in the neighbourhood of the plate is often found, but it can usually be disregarded.

§ 3. ANALYSIS OF SHOWERS

The number of showers is shown in Table 1. They consist of cascade showers, knock-on showers and those containing penetrating particles. Most of these photographs were obtained with the M arrangement.

Table 1

Series	No. of photographs	Running time* (hr.)	No. of showers >4 tracks	>9 tracks
R	4774	834	309	128
B	849	143	178	106

* Corrected for resetting time.

The counting rate of the M-set was 5·8 c. per hr. in both the R and B series. The solid angle of the M-set was approximately the same in the two series and was chosen to give a reasonable rate.

The number of showers obtained with the two arrangements is given in columns 4 and 5 of Table 1. The majority of these showers are knock-on phenomena and electron cascades from the atmosphere which penetrate the 5 or 10 cm. lead shields. The rate of these events is much higher in the B series than in the R series. This must be due to the use of only a single transition layer of 5 cm. of lead in the B series, whilst two layers of 5 cm. each were used in the R series. Geometrical factors must also have influenced the rates of the electron cascades of various sizes recorded by the two arrangements.

The P-set is efficient for recording penetrating showers, and the majority of these events were obtained in this way. The P-set was in operation for 529 hours and 43 photographs were obtained; thus the rate of the P-set was 0·081 c. per hour. It was not in use during the whole of the R and B series. The 43 photographs can all be considered as parts of penetrating showers. The chamber did not cover the whole solid angle of the P-set so that some tracks will have been missed.

An additional number of penetrating showers, which triggered only the M-set, were obtained. Photographs showing at least two particles penetrating the lead plate, and accompanied by either heavily ionizing particles or a cascade component or both, are included in the analysis as penetrating showers. A less complex event must be rejected owing to the difficulty of distinguishing it from a knock-on shower or from a random coincidence of two mesons. The number of penetrating showers thus selected from the photographs obtained with the M-set was eleven in the R series and three in the B series. As each of these showers contains two or more penetrating particles, the value of using both the selective and the non-selective counter arrangements is amply demonstrated. Thus 57 penetrating showers have been analysed and the measurements on the penetrating particles are given in §6.

§4. "STAR" PHENOMENA SEEN IN THE CHAMBER

Altogether 23 star-like showers have been observed during 1,000 hours of running time. These can be divided into (i) recognizable stars from the lead immediately above the chamber which usually contain heavily ionizing-particles, (ii) star phenomena in the lead plate, and (iii) stars in the gas of the cloud chamber. Usually these events are distinguished from cascade showers by the presence of heavily ionizing particles or penetrating particles and by the wide-angular distribution of the particles.

(i) *Star-like Showers produced immediately above the Cloud Chamber*

There are nine showers in this class, all in the R series, when 5 cm. of lead was in contact with the top wall of the cloud chamber. Soft component and heavily ionizing particles only are found in two of these stars; the remainder are all penetrating showers, but four have at least one heavily ionizing particle. Shower A, Plate I, is a high-energy star event produced in lead immediately above the cloud chamber, and will be described in detail in §5.

In the B series three penetrating showers were produced in the transition material; they can probably be classed as star events, and all have an electronic component.

(ii) *Stars produced in the* 3·4 *cm. Lead Plate*

A total of ten star-like events has been observed in the lead plate; these are classified as follows:

(*a*) *Low energy stars.* There are only two stars in this category; one contains two protons and the other four protons. These events are similar to those discussed by Rochester and Butler (1948 a) and found so frequently in photographic emulsions.

(*b*) *Stars associated with penetrating showers.* Three showers can be described as secondary events in penetrating showers, and they demonstrate the cascade formation of stars in penetrating showers first reported by Fretter and Hazen (1946). The three showers are reproduced in Plate II, E, F and G. Shower L, Plate IV, is probably a penetrating shower with associated stars in the plate and gas.

(*c*) *High-energy interactions in the lead plate produced by single ionizing particles.* There are four showers in this category; they are similar to those in section (*b*) but appear to be primary events, as in each case the star-producing particle is unaccompanied. Showers H, I and J of Plate III are examples of this type of event and are discussed in detail in § 5.

(iii) *Stars observed in the Gas of the Cloud Chamber*

Four stars in the gas have been observed in the present experiments and, in addition, one in a penetrating shower with 25 cm. of lead above the chamber. One of the stars is non-contemporary, and is of little interest. A second star is clearly associated with a penetrating shower but was obtained without the field, when calibration tracks were being photographed. The remaining stars are shown in Plate III, shower K, and Plate IV, showers L and M, and are described in detail in § 5 as they show unusual features and are associated with shower phenomena.

§ 5. DESCRIPTION AND DISCUSSION OF SELECTED PHOTOGRAPHS

The different types of events found in high-energy showers have been described in outline in § 4, and some examples are now discussed in detail.

In all cases the magnetic field was about 7,500 gauss, and in such a direction that a downward-moving positive particle is deviated to the left.

Plate I is composed of four penetrating showers which are of conventional type, and are in fact similar to showers A and B described by Rochester and Butler (1948 b).

Shower A, Plate I (R series, M-set).

This shower was produced in the lead immediately above the cloud chamber and is a typical high-energy event in which seven penetrating particles (tracks 1 to 7) are seen in the chamber. The momenta are in the range $(1\text{–}2) \times 10^9$ ev/c. and six are positive and one negative. There are at least three electrons with momenta approximately 10^8 ev/c. in the top of the chamber, where there is also a lightly ionizing particle with momentum approximately 10^9 ev/c. which may be an electron which produces some of the electrons below the plate.

Shower B, Plate I (R series, M-set).

This is a locally produced shower of unusual type because the three penetrating particles, 1, 2 and 3, are all negative with momenta approximately 8×10^8 ev/c. These tracks are associated with tracks 4 and 5. Track 4 is positive with momentum $8{\cdot}6 \times 10^8$ ev/c. and estimated ionization 3–4 minimum. A proton of this momentum would have an ionization of 1·6 minimum, but a deuteron would give 3·8 minimum. The range in lead of a deuteron of this ionization is 3·3 cm. and so such a particle should be absorbed in the plate, as is observed. Track 5 is too faint to be measured. In addition to the penetrating particles there is an electronic component below the plate which seems to be photon-induced and is of low energy.

Shower C, Plate I (B series, M-set).

This shower is a complex event of the same general type as shower A but the origin is indefinite. It may have been formed in the transition material or else in the atmosphere above the cloud chamber. There are at least four penetrating particles (tracks 1, 2, 4 and 5) with measured momenta between 10^9 ev/c. and 5×10^9 ev/c., of which three are positive and one negative. The electronic component is very complex as there appear to be several energetic cascades below the plate initiated by high-energy electrons and photons. Particle 3 of measured momentum $6{\cdot}0 \times 10^9$ ev/c. is of particular interest as it initiates a narrow-angle star in the plate. The star consists of at least four tracks, the outside ones being tracks 6 and 7. These particles have measured momenta 3×10^9 ev/c. and 6×10^9 ev/c. respectively and the angle between them is 1·5°. Between tracks 6 and 7 there are at least two others with momenta approximately 10^9 ev/c. It is very unlikely that this event is an electron cascade, as the angle between the tracks is larger than would be expected for such high energies, and there are no obviously associated electrons of lower energy. Owing to the confusion in the neighbourhood of this star it is not possible to examine it in greater detail. This event appears to be an example of a very narrow-angle shower of high energy, but it is associated with a complex event. Above the plate the photograph is reminiscent of a high-density air shower; indeed, the event may have been associated with an extensive shower.

Shower D, Plate I (R series, P-set).

This shower consists of three positive penetrating particles only, but the origin is indefinite as the tracks do not reproject back to a point. Tracks 2 and 3 have momenta $9{\cdot}0 \times 10^8$ ev/c. and $2{\cdot}0 \times 10^9$ ev/c. respectively Track 1 is scattered through 12° in the plate and has a momentum of $1{\cdot}5 \times 10^9$ ev/c. below the plate; above the plate, however, the track is too faint to be measured. This is one of the anomalous scatterings described in § 8.

Plate II shows star phenomena associated with penetrating showers.

Shower E, Plate II (R series, P-set).

This shower is an example of a star in the plate in what must have been part of a penetrating shower as the P-set was operated. The star in the plate is associated with a negative penetrating particle (track 1) of momentum $2{\cdot}0 \times 10^9$ ev/c. Track 2 initiates the shower in the plate: its momentum cannot be measured accurately but it is probably greater than 10^9 ev/c. Track 5 is a proton of momentum $5{\cdot}5 \times 10^8$ ev/c. and estimated ionization 3 minimum. Track 6 is probably a proton of momentum 4×10^8 ev/c., but the ionization cannot easily be estimated as the track is on the edge of the light beam. At least two lightly ionizing tracks are produced; track 3 is positive with momentum $3{\cdot}5 \times 10^8$ ev/c. and so cannot be a proton, and track 4 is faint and unmeasurable. Above the plate there are several electrons with momenta between 10^7 and 10^8 ev/c. This star contains only a few visible particles but, owing to its position in the chamber, several particles may have been projected out of the light beam and so are not recorded.

Shower F, Plate II (R series, M-set).

A positive penetrating particle (track 1) of momentum $2{\cdot}8 \times 10^9$ ev/c. accompanies a star-producing particle (track 2), which is negative but too faint to measure accurately. The angle between them is 0·4° and they probably meet in the top transition material. Thus track 2 penetrates at least 5 cm. of lead with very little scattering before being seen in the chamber and yet it interacts in the plate. It is thus very unlikely to be an electron. Examination of Table 2, in which the momenta and angles of emission of the star particles are listed, shows that the star is not an electron cascade.

Table 2

Track No.	Sign and momentum ($\times 10^8$ ev/c.)	Projected angle with respect to track 2 (deg.)
3	+ 3·2	11·2
4	+ 1·0	8·1
5	+10·0	1·4
6	+ 0·56	—
7	− 0·52	—
8	− 1·4	19·6
9	−15·0	26·4
10	+ 1·5	59·4

Tracks 9 and 10 make large angles with track 2 and appear to have traversed at least 1 cm. of lead without forming secondary showers; it is thus very unlikely that they are electrons. The shower does contain electrons, for example, tracks 6 and 7 and possibly tracks 3, 4 and 8, but it cannot be concluded that these electrons originate in the star. As the star is formed 1 cm. from the bottom of the lead plate we can conclude that the electronic component is produced within this distance. Tracks 3, 4, 8 and 10 could be π-mesons but cannot be of proton mass. This star may have been a simple event consisting of two or three particles but with an associated electronic component.

Shower G, Plate II (P-set).

This photograph is a further example of a star associated with a penetrating shower and was obtained with the P-set subsequent to series B using a transition layer of 25 cm. of lead. There are two penetrating particles; track 3 is too short for accurate measurement and track 2 is positive with momentum $1{\cdot}5 \times 10^9$ ev/c. Track 1 produces a star in the plate, but slight distortion and heavy background above the plate prevent reliable measurement of its momentum. The analysis of the star is contained in Table 3.

Table 3

Track No.	4	5	6	7	8
Sign	—	—	+	+	+
Momentum ($\times 10^8$ ev/c.)	1·6	—	4·1	3·6	1·7
Projected angle with track 1 (deg.)	30·5	17·3	6·8	25·9	31·8
Angle with plane of photograph (deg.)	0	40	0	12	25

Particles 7 and 8 are particularly interesting as they are heavily ionizing, and this fact, in conjunction with the angle of emission of tracks 5 and 6, serves to show that the interaction in the plate is not an electron cascade despite the obvious low-energy electronic component. Immediately below the plate tracks 7 and 8 are 3·7 cm. from the front of the chamber (9 cm. deep). At the bottom of the chamber they are 5·0 cm. and 6·6 cm. respectively from the front. Thus most of track 8 is in the main light beam. Particle 7 is positive with momentum $3{\cdot}6 \times 10^8$ ev/c. and estimated ionization 4–5 minimum. The calculated ionization for a proton is 4·7 minimum. Particle 8 is positive with momentum $(1\cdot7 \pm 0\cdot2) \times 10^8$ ev/c. The estimated ionization is 5 to 7 minimum, which gives a mass of $900\,m_e$ to $1140\,m_e$. The expected ionization for a proton of this momentum is 15 minimum and that for a π-meson 1·2 minimum. The track is free from visible distortion and the ionization may be compared with that of track 7. The ionizations appear to differ only a little but the momenta determinations are very different. As the two tracks are in close proximity and are of the same sign, any gas distortion should affect both tracks.

For particle 8 an average value for the mass of $950\,m_e$ can be used to calculate the effect of random gas scattering. Using Williams' formula, the error in the curvature is 2%; this error cannot change the interpretation, and we conclude tentatively that the mass of the particle is $(1000 \pm 200)\,m_e$.

Associated with the star are nine recognizable electron tracks with momenta in the range $(0\cdot5\text{–}2\cdot0) \times 10^7$ ev/c. These can be separated into two distinct groups and appear to constitute two small cascades, one on each side of the star. Their average directions make angles of 50° and 35° with the incident particle. Before these tracks appeared in the chamber, multiplication of the cascades in the lead plate may have occurred, and so it is not possible to decide whether the electrons or photons originated in the star itself. This is the only photograph in which very direct association between a star and the electron component can be seen.

Plate III, showers H, I and J, are star phenomena initiated by unaccompanied ionizing particles.

Shower H, Plate III (R series, M-set).

A cone of lightly ionizing particles with an angular spread of 90° is produced by particle 1, but as the event is close to the edge of the chamber it is not possible to make accurate measurements; the difficulty is enhanced by the presence of distortion in the neighbourhood of the plate. Most of the tracks have momenta approximately 10^9 ev/c., so that the event is definitely not an electron cascade. The incident track cannot be measured accurately owing to its short length over the piston. A back-scattered particle 2 is produced which appears to originate at the centre of the star, 2·3 cm. below the top of the lead plate. Its momentum is $5\cdot6 \times 10^7$ ev/c. and the sign negative if the particle travelled upwards. The estimated ionization is 5 minimum. For this momentum a π-meson would be 5·0 minimum and a μ-meson 2·8 minimum; hence the particle can be identified as a meson, but we cannot differentiate experimentally between π- and μ-mesons.

Shower I, Plate III (R series, M-set).

This is a similar, but simpler, photograph to H. An incident positive particle 1, with measured momentum $4\cdot0 \times 10^9$ ev/c., which is almost in the vertical plane, produced tracks 2, 3, 4, 5 and 6 in the plate. Track 2 is positive if travelling upwards, has momentum $1\cdot4 \times 10^8$ ev/c., and is inclined at an angle of 142° to the direction of 1. This track appears to be almost lightly ionizing and may be a π-meson or a μ-meson. It traverses 2 cm. of lead without producing secondaries, as would almost certainly be the case if it left the star as an electron. Track 6 is positive, momentum $1\cdot1 \times 10^9$ ev/c., and is at an angle of 32° with 1. Track 5 is an electron of momentum $1\cdot2 \times 10^7$ ev/c.; track 4 is positive with momentum $8\cdot2 \times 10^8$ ev/c. and inclined at 0·9° to 1. In addition, there is a faint track 3 which is too short for measurement.

PROC. PHYS. SOC. VOL. 63, PT. 2—A (C. C. BUTLER, W. G. V. ROSSER AND K. H. BARKER)

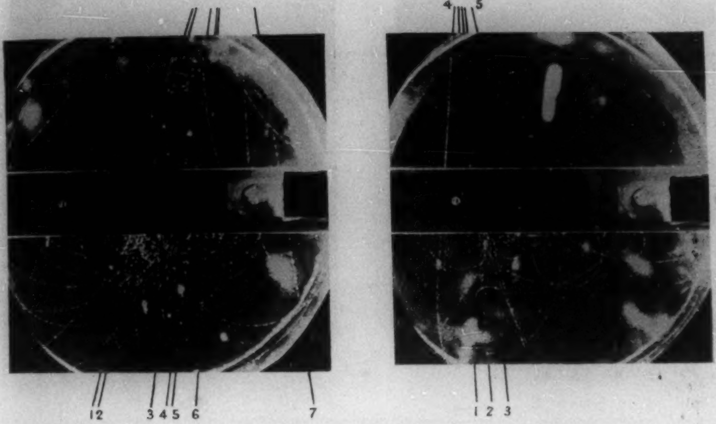
1 2
3 4 5 6
7
4
5
1 2 3

Shower A

Shower B

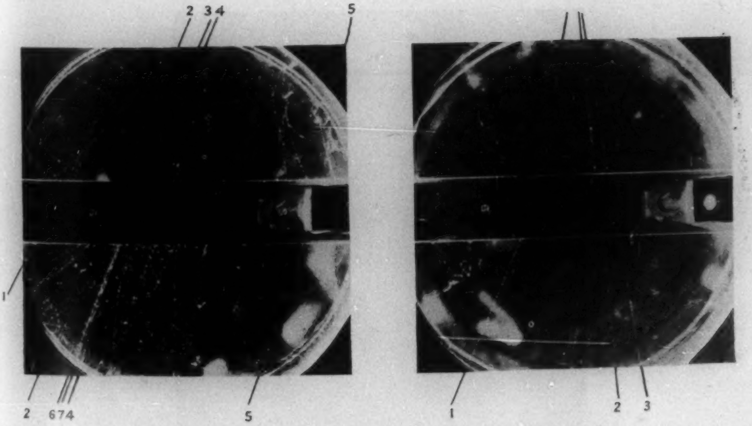
2 3 4
5
1
2
6 7 4
5
1
2
3

Shower C

Shower D

Plate I.

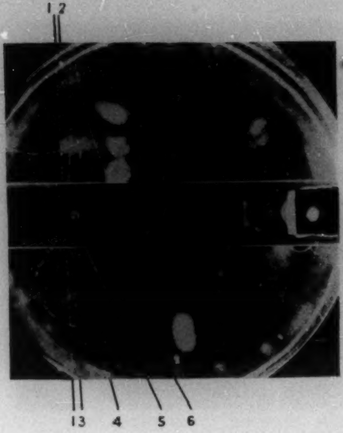

Shower E

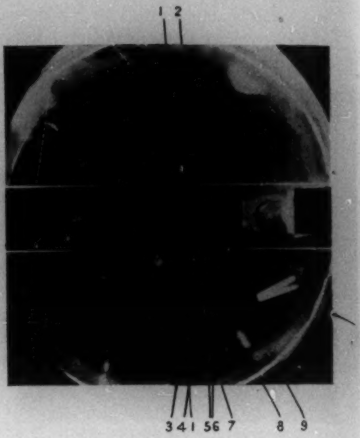
1 2
3 4 1
5 6
7
8
9

Shower F

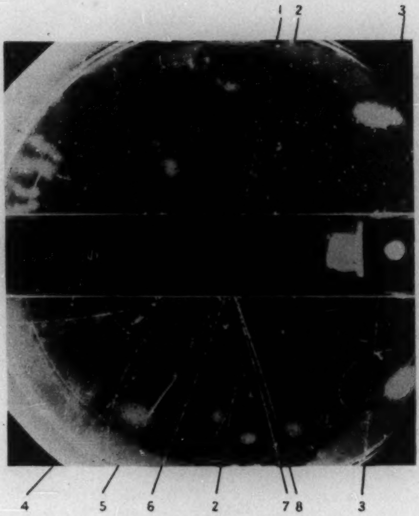
1 2
3
4
5
6
2
7 8
3

Shower G

Plate II

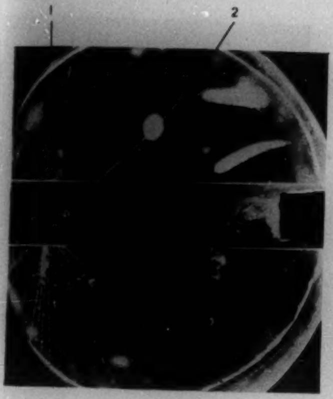

Shower H

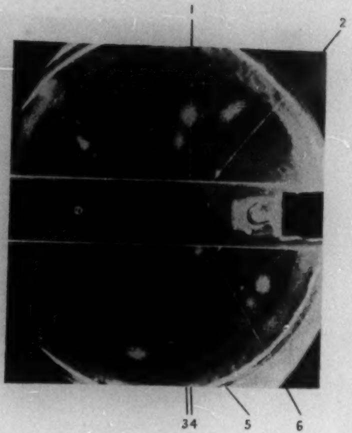

Shower I

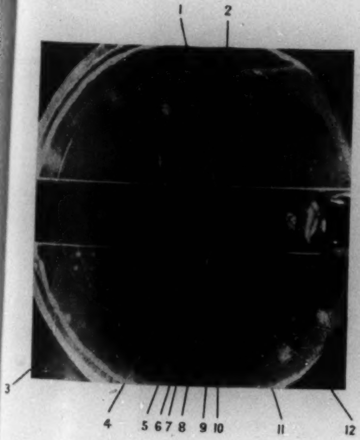
1
2
3
4
5
6
7
8
9
10
11
12

Shower J

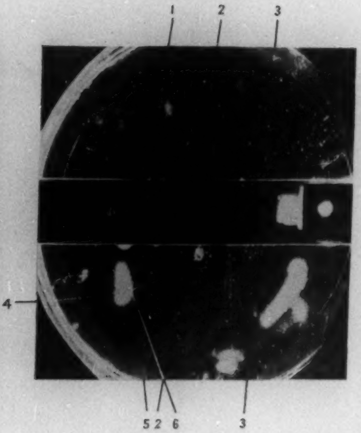

Shower K

Plate III.

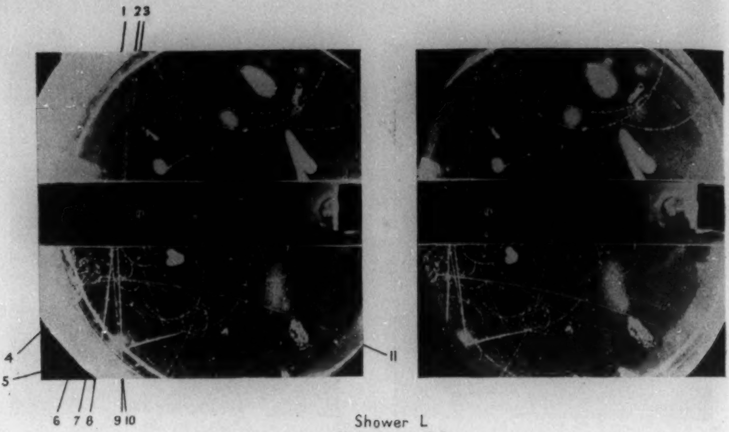
1
2
3
4
5
6
7
8
9
10
11

Shower L
Stereoscopic Pair

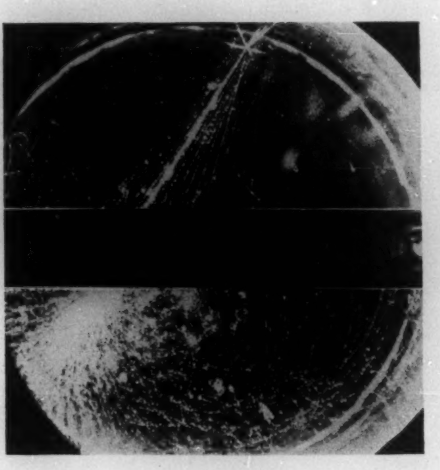

Shower M

PLATE IV.

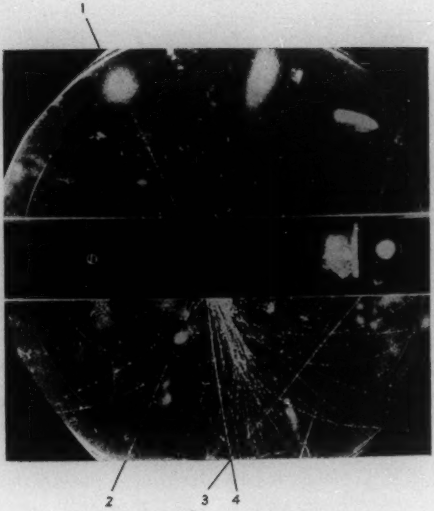

Shower N

PLATE V.

Shower J, Plate III (R series, M-set).

Particle 2 is positive with a measured momentum of $5{\cdot}0 \times 10^9$ ev/c. and initiates a star of at least 18 particles, the majority of which are not electrons. Details of the particles produced are given in Table 4.

Table 4

Track	Sign	Momentum ($\times 10^8$ ev/c.)	Projected angle with track 1 (deg.)	Ionization ($\times$ minimum)	Particle identification
3	+	17·0	49·7		
4	+	4·3	25·0	3	Proton
5	+	5·7	17·1	2	Proton
6	+	1·7	12·7		Not proton
7	+	1·7	10·7		Not proton
8	+	15·0	6·6		
9	+	11·0	0·6		
10	+	31·0	2·7		
11	+	8·4	20·2		
12	−	6·7	38·2		

The total angular spread of the shower is 90° and, owing to the high-energy tracks produced, it cannot be an electron cascade. At least seven identifiable electrons with momenta around 10^7 ev/c. are associated with the shower. There is some evidence of a back-scattered proton (track 1) but, as it entered the piston, only a short length is available for measurement, and a reliable estimate of ionization cannot be made. Track 3 is of particular interest as it is of high momentum and makes an angle of 50° with 1. Since most of the particles are not electrons and their momenta are such that they are capable of penetrating several centimetres of lead, we consider the event shows the collision of a primary proton with the formation of a penetrating shower.

Plate III, shower K, and Plate IV, showers L and M, show star phenomena in the gas of the cloud chamber which are associated with showers.

Shower K, Plate III (P-set).

This photograph shows a penetrating shower formed in 25 cm. of lead and detected by the P-set. Tracks 1, 2 and 3 are penetrating particles; track 1 is negative, 2 and 3 are positive. Track 1 is very faint below the plate, but reprojection shows that it is a penetrating particle and the momentum is $5{\cdot}8 \times 10^8$ ev/c.; as it is lightly ionizing it cannot be of proton mass. Below the plate this particle forms a star in the gas with five visible prongs. The origin of this star is partly obscured by a non-contemporary α-particle due to radioactive contamination and, unfortunately, the star-producing particle (track 1) is very faint near the star.

This star is at the back of the chamber; several of the particles are on the edge of the light beam and some enter the piston. Track 4 is short but heavily ionizing and is most probably a proton. Track 6 is positive with measured momentum $6{\cdot}1 \times 10^8$ ev/c. and the estimated ionization is 10 minimum. A proton with the measured momentum would be 2·6 minimum but a deuteron would be 6·7 minimum, thus the particle is probably a deuteron. Track 5 is positive with momentum $6{\cdot}3 \times 10^7$ ev/c. and estimated ionization 5–6 minimum. A π-meson with this momentum would be 4 minimum, and so the particle could well be a π-meson but hardly a μ-meson, which would be 2·5 minimum. Thus the star is produced by a negative penetrating particle which interacted with an argon or oxygen nucleus in the gas 2 cm. below the plate. The incident particle may be a negative π-meson.

Shower L, Plate IV (R series, M-set).

This shower is a complicated event since the section seen in the chamber shows two stars. Track 3, which is negative and of momentum $2{\cdot}0 \times 10^9$ ev/c., initiates a star in the plate from which two positive tracks, 8 and 9, with momenta $1{\cdot}7 \times 10^8$ ev/c. and $3{\cdot}2 \times 10^8$ ev/c. respectively, are identifiable as protons. At least five lightly ionizing particles are also produced but, owing to their shortness, measurements are not possible. Track 5 is a slow proton which may have originated in a low-energy star formed in the piston. Track 1 may be a penetrating particle, but the confusion below the plate prevents a definite interpretation, so that this photograph cannot be identified as a penetrating shower, although it seems likely to be part of such a shower. The photograph is thus similar in type to showers E, F and G.

Below the lead plate a small star is formed in the gas 7·1 cm. from the front of the chamber which is 9 cm. deep. This star consists of three prongs, one of which is very short, as the particle travelled into the piston. Track 4 is too short for measurement, but track 11 can be measured accurately and is positive, with momentum $(1{\cdot}1 \pm 0{\cdot}1) \times 10^8$ ev/c. The track is at the back of the chamber and on the edge of the main light beam, but is definitely heavily ionizing. Examination under the microscope shows that the track, although sharp, is almost continuous, and a lower limit to the value of the ionization is 6 minimum. It is more difficult to assess a maximum value, but owing to the sharpness of the track this maximum is not likely to be more than 10 minimum. When the ionization exceeds 10 minimum tracks appear broader than normal, which is not so for this track. The estimated mass corresponding to 6 minimum is 650 m_e and that corresponding to 10 minimum 900 m_e. For the particle to be a proton the ionization would have to be as high as 36 minimum.

A π-meson of momentum $1{\cdot}1 \times 10^8$ ev/c. would have an ionization of 2 minimum, and as this is not the case we can be confident that the mass is greater than 300 m_e. Thus we conclude that the particle must have a mass in the range 650 m_e to 900 m_e. It is necessary to consider the error in the measured curvature due to random scattering. Using Williams' formula and assuming a mass of 800 m_e for the particle, the error in curvature is 4·4%. If the particle is to be a proton the momentum must be at least $3{\cdot}0 \times 10^8$ ev/c., but it is most unlikely that an abnormally high scattering error could increase the momentum by a factor of 3. On the lower momentum side the particle would have had to be as low as 5×10^7 ev/c. to be a meson. Thus scattering cannot appreciably change the observed curvature and we conclude, again tentatively, that the particle is a meson of mass (800 ± 200) m_e. This star is initiated by a non-ionizing particle possibly produced in the star in the plate. This photograph is a further example of the successive production of particles other than electrons.

Shower M, Plate IV (R series, M-set).

This shower is an unusual cascade shower; excluding the star in the gas, the total measured momentum of the 36 tracks above the plate is 10^{10} ev/c. Of these 36 tracks, 19 have momenta greater than 10^8 ev/c. and eight momenta greater than 5×10^8 ev/c. The thick core is made up, in part, of a heavily ionizing track from the star. It is not possible to determine how many other ionizing tracks are in the core. Inspection of the photograph shows that if the main shower is an electron cascade, then it must be in its early stages of development above the lead plate and may reach its maximum below the lead plate. The shower falls obliquely on the lead plate and so the effective thickness becomes 4 cm. or eight cascade units.

The measurements indicate that the incident energy must be at least 2×10^{10} ev., and assuming this as a minimum value, and also that the point of production of the shower is a few cascade lengths in lead above the top of the chamber, then it is possible to calculate the number of particles expected above and below the lead plate. Higher values of the initial energy can be considered, and in each case the number of tracks above and below the plate can be calculated using the cascade tables compiled by Jánossy (1948). The results for a number of initial conditions are given in Table 5.

Table 5

Assumed incident energy (ev.)	2×10^{10}	10^{11}	10^{12}
No. of particles under two cascade units ($x=2$)	36	50	120
No. of particles with $x=4$	136	240	1117
No. of particles N ($P > 10^8$ ev/c.) for $x=2$	10	16	80
No. of particles N ($P > 10^8$ ev/c.) for $x=4$	10	63	300
No. of particles N ($P > 5 \times 10^8$ ev/c.) for $x=2$	—	10	40
No. of particles N ($P > 5 \times 10^8$ ev/c.) for $x=4$	—	10	80
No. of particles at shower maximum	200	500	8000
No. of particles under $x=2+8$ units	120	400	8000

If we assume the incident energy to be as low as 2×10^{10} ev. then 36 particles should appear in the top of the chamber if the shower starts two cascade lengths in lead above the chamber wall. This agrees well with the number observed, but only 120 particles should appear below the plate under $(2+8)$ cascade units. It is estimated that there are approximately 500 particles below the plate. Examination of the table shows that an incident energy of 10^{11} ev., with the cascade starting two cascade lengths in lead above the top wall of the chamber, fits all the observations very well. Under these initial conditions ten electrons in the top of the chamber are expected with energies greater than 5×10^8 ev. Eight such electrons are found, and so it is concluded that there are not many additional electrons of high energy in the core which are obscured by the star particle.

It is not possible to compare the angular distribution of the particle above the plate with shower theory because the number of particles in the core is uncertain and also the spread due to the magnetic field introduces very large corrections which are difficult to determine. The photograph is without doubt a cascade shower which may have been produced by a knock-on electron or by collision radiation from a very energetic meson.

The star in the gas occurs in the core of the shower; there are at least nine prongs, one of which follows the direction of the core of the cascade. One star particle can be measured and is identified as a proton with momentum $4{\cdot}7 \times 10^8$ ev/c. Two lightly ionizing particles originate from the star but, unfortunately, they are out of the light beam and are too faint for measurement.

The star is likely to arise from the disintegration of a gas atom, probably of argon, and phenomenologically it is not possible to decide if a charged particle, a photon or a neutral particle produced it. The excitation energy must be at least 5×10^8 ev. Above the plate only ten electrons with momenta greater than 5×10^8 ev/c. are expected and so the number of photons with energy greater than 5×10^8 ev. will not be much greater than ten. The collision length for such photons must be smaller than 100 gm/cm², so that one star is expected in a minimum length of 5,000 cm. of gas (density 0·002 gm/cm²). The maximum track length in the top of the chamber is 10 cm., so that the maximum probability of observing a photon-induced star associated with the cascade is 1 in 500. Thus it seems that the disintegration is unlikely to be due to a photon.

From the work of Tongiorgi (1948) it is known that a neutron flux occurs in air-showers which are presumably electron cascades. Thus the star may have been produced by a neutron, but this is also a very unlikely event as the collision length must again be of the order of 100 gm/cm².

Shower N, Plate V.

This shower has recently been obtained under a transition layer of 20 cm. of paraffin wax and is similar in type to shower G, Plate II. Track 1, with measured momentum 5×10^9 ev/c., initiates a star in the plate. The event occurred in the middle of the chamber. This star has a considerable electronic component but there are several high-energy tracks which must originate in the star. For example, track 2 is positive with momentum $2{\cdot}0 \times 10^9$ ev/c. and is at 45° to track 1.

A negative, heavily-ionizing particle (track 4) is produced in the star. The momentum is $(1{\cdot}7 \pm 0{\cdot}2) \times 10^8$ ev/c. and the estimated ionization is in the range 4 to 6 minimum. These observations give a mass for the particle within the range $800\, m_e$ to $1020\, m_e$. If the track is that of a negative meson it would be at minimum ionization. The ionization of track 4 can be compared with that of the electrons and fast particles in the shower, and there can be no doubt that it is heavily ionizing. A proton of $1{\cdot}7 \times 10^8$ ev/c. would be 15 minimum and can be excluded. The error in the curvature due to random gas scattering is approximately 2% for a particle of mass $900\, m_e$ and momentum $1{\cdot}7 \times 10^8$ ev/c. Careful considerations lead us to the view that the particle must have been of heavier mass than a π-meson and yet lighter than a proton.

Track 3 is also of interest; its measured momentum is $9{\cdot}5 \times 10^8$ ev/c. and estimated ionization 3 to 5 minimum. These observations give a mass range of $3520\, m_e$ to $5140\, m_e$. It is difficult to assess the accuracy in the momentum measurement as the track is inclined at a steep angle to the vertical and is towards the edge of the chamber, but the error may have an extreme value of 50%. Thus it cannot be excluded that the particle may have been a proton from a secondary star below the chamber; it is positive if travelling upwards.

§6. THE DIFFERENTIAL MOMENTUM SPECTRUM OF THE STAR PARTICLES

A total of 71 penetrating particles has been observed in 57 showers and 67 are suitable for measurement, although most of them can only be measured in one half of the chamber. There are 52 positive and 15 negative particles; this large positive excess confirms the result obtained previously by Rochester and Butler (1948 b). The most probable interpretation of these data is that about half of the penetrating particles are protons, and evidence exists to support this conclusion. The differential momentum spectrum of all the particles is given in row 2 of Table 6.

The use of a lead plate in the chamber to examine the penetration of shower particles necessarily imposes a bias on the measured spectrum of penetrating particles; a proton requires a minimum momentum of $5{\cdot}7 \times 10^8$ ev/c. and a π-meson $2{\cdot}3 \times 10^8$ ev/c. to penetrate the plate. Thus shower particles with energies in the chamber below about 200 Mev. are not included in this analysis. Of the penetrating particles four can be identified as protons since a proton begins to ionize heavily below a momentum of $6{\cdot}5 \times 10^8$ ev/c. A further nine particles in this low momentum range which do not ionize above the minimum value are probably π-mesons. It is reasonable to assume that the negative particles are mesons, and the total number of identified mesons is shown in row 3 of Table 6. The number of identified protons is shown in row 4 of Table 6.

Table 6

Momentum range ($\times 10^8$ ev/c.)	1–5	5–10	10–20	20–30	30–∞
Total number of particles	9	22	18	14	4
No. of mesons identified	5	7	6	—	2
No. of protons identified	—	4	—	—	—

It is of interest to determine the average energy carried by the penetrating particles in a penetrating shower which is a P-set event. This requires a knowledge of the mean energy of the penetrating particles and of the average multiplicity of such a shower.

In order to obtain a value for the average energy per shower particle it is assumed that half the particles are protons and half mesons. If the negative particles are identified as mesons it is reasonable to double the number of negative particles in each range of the differential momentum spectrum to obtain the total contribution due to mesons. The mean energy of the mesons is found to be of the order of 8×10^8 ev. and that of the protons of the order of 9×10^8 ev.

Forty-three photographs of penetrating showers were obtained using the P-set. The numbers of photographs with 0, 1, 2, 3, 4 penetrating particles were 20, 16, 4, 2 and 1 respectively.

Owing to the different dispositions of the lead in the R and B series it is not possible to make a reliable estimate of the average number of penetrating particles in a shower from these data. From other evidence, which will be published in due course, we estimate that the average multiplicity is five ionizing penetrating particles per steradian; this may be a minimum value.

We thus conclude that the average energy required to trigger the P-set is about 7×10^9 ev. This estimate neglects the lower energy particles and assumes that the high-energy particles are confined within unit solid angle.

Three events, showers H, I and J, have been described in § 5 which were identified as showers of hard particles probably due to primary protons. Showers E, F, G, L and N are secondary showers or stars. The momentum spectrum of the emitted particles not obviously electronic in nature in all these events is shown in Table 7.

Table 7

Momentum range ($\times 10^8$ ev/c.)	<1	1–5	5–10	10–20	>20
No. of particles	1	17	5	6	2

A positive excess of 5 to 1 is found which may indicate a rather smaller proportion of mesons in these showers. The spectrum appears to have a maximum at approximately 3×10^8 ev/c., considerably lower than the value of 10^9 ev/c. found for the particles penetrating the plate. Of the 17 particles within the range $(1\text{–}5) \times 10^8$ ev/c., five are protons, nine are positive and three negative; several of the latter group of particles are identifiable as mesons. It is possible that some of the particles are electrons, and we cannot attach much weight to the positive bias found within this group. The average multiplicity of lightly ionizing particles emitted from stars in the plate is of the order of five per event.

§7. THE ANGULAR DISTRIBUTION OF THE STAR PARTICLES

A number of stars formed in the lead plate have been described in §5, and inspection of the photographs reveals that the events are not primarily electron cascades. Shower J is of particular interest as it is an example of a high-energy star probably similar in type to the showers of lightly ionizing particles observed by Powell and others (Brown, Camerini *et al.* 1949) in photographic emulsions. The large positive excess and the existence of two identifiable protons in this shower suggest the presence of a considerable number of protons. Furthermore, the assumption of a non-ionizing component of comparable intensity, probably neutronic, is necessary to explain the lack of balance of the resolved momentum perpendicular to the direction of the incident particle. The momenta of particles in this shower which may be protons correspond to values of β ranging from 0·4 to 0·95. An examination of Table 4 shows further that there is no obvious correlation between momentum and angle of emission.

A study of the average projected angle made with the incident particle for 25 tracks contained in 8-star showers gives a value of 31°. Fretter (1949) has also examined the production of penetrating showers in lead in a cloud chamber and obtains an average projected angle of 18·6° for the penetrating particles. The discrepancy probably indicates that the present data are concerned mainly with rather less energetic interactions than those analysed by Fretter. However, any comparison is necessarily inadequate since the rate of production of penetrating showers in the 3 cm. lead plate at sea level is very slow.

The lightly ionizing star particles with momenta greater than 6×10^8 ev/c. in these showers are fairly evenly distributed about the direction of the primary particles in the angular range 10–60°. The range 70–110° is in general inaccessible to observation owing to the size of the lead plate, and any lightly ionizing particles emitted in this range will rarely appear in the chamber. All the stars formed in the plate are found to have an associated electronic component. Owing to their occurrence deep within the lead plate, it is not possible to conclude that the electronic component originates directly in the star but only that it is produced very close to the point of formation. This implies the spontaneous decay of an emitted particle, probably neutral, with a very short life-time of the order of 10^{-10} sec.

In the R and B series no evidence was found for the existence of exclusively narrow-angle penetrating showers in the chamber. This type of shower has been found by previous workers, e.g. Rochester (1946), Rochester and Butler (1948b), but in every case the shower was produced above the apparatus under conditions in which all the particles inclined at 20° to the initiating particle would not be seen in the chamber. Fretter has not reported the presence of highly collimated showers in his work at an altitude of 3,000 m.

§8. ANOMALOUS SCATTERING OF PENETRATING PARTICLES AND INTERACTIONS IN THE LEAD PLATE ASSOCIATED WITH PENETRATING SHOWERS

The scattering of the penetrating particles in the 3·4 cm. lead plate has been examined and four cases of scattering, much in excess of that predicted by Williams' formula, have been found. It is probable that one or two additional cases of abnormal scattering occurred almost exactly towards or away from the camera. These are very difficult to detect if the available track length is less than 5 cm.; on such tracks, angles towards or away from the camera of less than 10° cannot be measured accurately by reprojection. The four cases of heavy scattering approximately in the plane of the photographs are analysed in Table 8.

Table 8

Track No.	1	2	3	4
Sign	+	+	+	+
Momentum above plate ($\times 10^8$ ev/c.)	6·5	7·0	–	10·0
Momentum below plate ($\times 10^8$ ev/c.)	3·4	1·8	15·0	11·0
Observed scattering (deg.)	51·2	74·1	12·2	6·6
Probable scattering (Williams' formula) (deg.)	2·9	2·8	1·5	1·9

Particles 1 and 2 are at minimum ionization below the plate and, therefore, cannot be protons but could well be positive π-mesons. Assuming that the penetrating particles are all the same, one abnormal scattering occurs per 60 cm. of track in lead.

Of the four cases of heavy scattering observed, two involve a considerable reduction in momentum of the particle and so it is most likely that a star was formed, but the short-range particles do not become visible owing to the thickness of the lead plate. In view of the possibility of star formation at the point of the anomalous scattering, it is unwise to separate the heavy scatterings from those interactions seen in the plate which are accompanied by penetrating particles. In the present work only three such interactions have been observed. Thus approximately 75 penetrating particles have been seen traversing 250 cm. of lead, and accompanied by seven abnormal scatterings or secondary interactions. This indicates one such event per 35 cm. of lead.

We can compare this result with that of Fretter (1949), who employed a chamber fitted with 16 lead plates each 0·5 inch thick. If the suggestion that stars are often formed when energetic particles are deflected through large angles is correct, then we should expect few scatterings without accompanying stars in Fretter's work owing to the thinness of his plates. This is in fact the case, as he finds only 12 scatterings of greater than 15° in 58 metres of track in lead. He finds, in addition, 78 interactions of other types. Thus one scatter or interaction occurs per 70 cm. of track in lead.

Fretter's criterion for an abnormal scatter may be unduly severe. He was not able to measure momenta and will thus have omitted scatterings of 10–15° made by particles of over 10^9 ev/c. Moreover, owing to the short track length between the plates, scatterings towards or away from the camera must be difficult to determine. Thus the interaction length of 70 cm. of lead is likely to be a maximum value.

Similarly, it can be argued from the present data that the value of 35 cm. of lead for the mean path of the shower particles, or collision length, is a maximum value. A number of anomalous scatterings in the forward or backward directions will be missed and possibly a few particles may be catastrophically absorbed, as described by Rochester and Butler (1948 b), and omitted from the analysis, as it is often difficult to ensure that the particle, if present, would be visible below the plate.

§ 9. HEAVILY IONIZING PARTICLES IN ALL TYPES OF SHOWERS

A considerable number of heavily ionizing particles have been found and many identified as shown in Table 9.

Table 9

	No. of showers containing heavy particles	Total No. of heavy tracks	Protons	Mesons	Unmeasurable tracks
R	47	65	42	11	12
B	15	19	11	2	6

We find that of the 53 protons observed in all types of showers only six are associated with cascade showers. Of the remainder, eleven occur in penetrating showers and 36 in star-like phenomena or as odd tracks which may well be prongs of low-energy stars formed in the plate, piston or walls of the chamber. Cocconi, Cocconi-Tongiorgi and Greisen (1949) have found a large number of low-energy neutrons associated with penetrating showers. These may be correlated with the soft protons in penetrating showers. Since the ratio of the mass of the π-meson to that of the μ-meson is known to be 1·33 (Serber 1948) it is not possible in our experiment to distinguish between these mesons using the momentum measurements and visual estimates of ionization.

§ 10. THE EVIDENCE FOR τ-MESONS

Three photographs, showers G, L and N, show heavily ionizing particles produced in the chamber which cannot be identified as protons or π-mesons. Tentative conclusions about the masses of these particles were reached in § 5. The essential data are summarized in Table 10.

Table 10

(1)	(2)	(3)	(4)	(5)	(6)	(7)
G (8)	+	$1{\cdot}7 \pm 0{\cdot}2$	5–7	900–1140	15	1·2
L (11)	+	$1{\cdot}1 \pm 0{\cdot}1$	6–10	650–900	36	2·0
N (4)	−	$1{\cdot}7 \pm 0{\cdot}2$	4–6	800–1020	15	1·2

(1) Shower and track number; (2) Sign; (3) Momentum ($\times 10^8$ ev/c.); (4) Estimated ionization range ($\times$ minimum); (5) Mass range (m_e); (6) Ionization for proton ($\times$ minimum); (7) Ionization for π-meson ($\times$ minimum).

Since the measured momentum in each case is only a small fraction of the maximum detectable momentum the influence of chamber distortions on the accuracy of measurements is negligible. The most important uncertainties involved in the momentum determinations are those introduced by multiple scattering in the gas and by the non-uniformity of the magnetic field. The errors quoted in Table 10 represent extreme values.

As the mean magnification of the camera lenses is only 1/9·5, any features of a track susceptible to quantitative investigation are rapidly obscured as the ionization increases and only visual estimates are possible. A heavily ionizing track can be recognized by comparison with minimum ionization tracks formed in the same region of the chamber where condensation conditions will be reasonably uniform. A track of ionization 2 minimum is just detected as heavy on visual inspection. To facilitate an estimate of the probable range of $I/I_{\min}$ certain qualitative characteristics of the track are examined under a low-power microscope. The length and frequency of definite gaps in a track decrease progressively up to an ionization of about 10 minimum. At this stage a track becomes continuous, and any further increase of ionization results only in an appreciable broadening. These observations are based on an examination of a large number of proton tracks. An estimate of ionization based on the overall blackness of a track is unreliable as this is influenced by such factors as the degree of condensation, the variation of illumination in the chamber and the prevailing background conditions. In the present experiment the illumination is very uniform in the central region of the chamber but decreases appreciably at distances of about 1·5 cm. from the back and front of the chamber.

Shower G has a proton of comparable ionization close to the heavy meson track, and this helps in the determination of the ionization range. We can exclude the possibility of the particle being a π-meson, and it seems unlikely that it is as heavily ionizing as 15 minimum, which is required for a proton (column (6), Table 10).

The unusual particle in shower L is produced in a star in the gas. The momentum measurement is particularly accurate, but the event is somewhat out of the main light beam. A minimum value for the ionization can be fixed with certainty (i.e. 6 minimum), but it is more difficult to decide on an upper limit. The track appears almost continuous but is sharp, and so the ionization is very unlikely to be as high as 36 minimum, which is required for a proton. Thus the lower limit of the mass given in column (5) of Table 10 is probably too low, and we cannot definitely exclude a much higher value than 900 m_e, although we consider that this is unlikely.

Shower N is of particular interest as the particle is negative and is undoubtedly produced in the lead plate. Again the momentum measurement is good, and as the particle is heavily ionizing we can exclude the possibility of its being a π-meson. This photograph is the most convincing evidence presented for the existence of a particle of mass 900 m_e.

The three tracks have momenta within the range $(1\text{–}2) \times 10^8$ ev/c.; only in this narrow range can we hope to identify particles of mass intermediate between the π-meson and the proton. If these particles are τ-mesons it is interesting to consider the frequency of their production. The present data do not permit such an estimate, as showers G and N were obtained subsequent to the R and B series. This recent work has not been fully analysed, but the three events occurred in a total of 200 penetrating showers. In a later publication we hope to discuss the frequency of τ-mesons in relation to the number of identifiable π-mesons produced in stars.

The total track length of the three particles in the chamber is approximately 30 cm., and as no decay occurs we conclude that the life-time is probably longer than 10^{-9} sec.

Rochester and Butler (1947) observed two events each of which was interpreted as the spontaneous decay of a τ-meson in the gas. No further example of this phenomenon has been found although more than 100 penetrating particles have been observed to traverse the chamber. Other evidence for τ-mesons has been obtained by Powell and his colleagues (Brown, Camerini *et al.* 1949), Leprince-Ringuet and Lhéretier (1946), and Alicanyan and his colleagues (1948).

§ 11. DISCUSSION

The behaviour of the particles in locally produced penetrating showers has been observed in the 3·4 cm. lead plate, and an interaction length of 35 cm. deduced from the number of scatterings and interactions. We cannot be sure that these showers are exclusively local events; a small number may have been associated with extensive showers. Fretter has determined the interaction length to be 70 cm. of lead, whilst Lovati and his colleagues (1949) find 30 cm. of lead. It is likely that Fretter's value is a maximum and that the experimental data available are not inconsistent with the conclusion that the collision length of the fast shower particles for secondary interactions is approximately 160 gm/cm^2 in lead. Cocconi (1949 a, b) has found a collision length of 160 gm/cm^2 for the formation of penetrating showers in lead at sea level, presumably by nucleons. The geometrical area of the lead nucleus corresponds to a collision length of 170 gm/cm^2 or an interaction length of 15 cm. of lead. This is likely to represent the maximum interaction for fast nucleons with lead nuclei and should hold for the protons produced in penetrating showers. However, the observed interaction length for the shower particles is 30 cm. of lead. These particles consist of protons and mesons; it is therefore certain that mesons must be less reactive than the protons provided that the value of 15 cm. for the interaction length of protons is correct.

A small number of penetrating showers were observed to be formed in the lead plate. The angular distribution of the fast particles has been examined in conjunction with momenta measurements. Before any significant conclusion can be made it is important to know the nature of each particle in order that its velocity may be determined. In showers of this type we cannot unambiguously identify the mesons, and so it is not possible to examine their distribution in the centre-of-mass system of the colliding nucleons. Many theories assume this distribution to be isotropic. The protons must be recoils or originate in secondary processes; thus they are unlikely to be isotropic in the centre-of-mass system of the colliding nucleons. Collimated groups of lightly ionizing particles are frequently observed in stars produced in photographic emulsions. If these stars originate in silver or bromine nuclei an appreciable fraction of the lightly ionizing particles may be protons—a suggestion which should be considered when making Lorentz transformations on this type of star.

Owing to the present difficulties in meson theories it is not possible to compare the experimental results with theory in detail. We cannot distinguish between the multiple production of mesons in a single collision as suggested by Heisenberg (1949) and Lewis, Oppenheimer and Wouthuysen (1948) and the plural process first suggested by Hamilton, Heitler and Peng (1943) and extended subsequently by Jánossy (1943) and by Heitler and Walsh (1945).

Heisenberg (1949) gives formulae for the angular spread and average energy of the mesons produced as the result of a collision between a fast nucleon and a hydrogen nucleus. The present data cannot be compared directly with these formulae. For example, shower J is presumably the result of the collision of a fast proton with a nucleon or nucleons in a lead nucleus. The particles produced may be scattered within the nucleus and secondary processes may occur. Heisenberg points out that these processes will tend to widen the angular distribution and possibly increase the multiplicity. Furthermore, we cannot separate the mesons from the protons in shower J with certainty.

The maximum intensity of the mesons among the penetrating particles in penetrating showers appears to be at approximately 8×10^8 ev. and the average multiplicity five ionizing particles. Heisenberg calculates the maximum intensity of the energy spectrum of the mesons to be $65n$ MeV., where n is the average number of mesons both neutral and charged. He estimates that the number of charged particles is $2n/3$. The observed multiplicity includes protons, and it is difficult to assess the value of n to be used in Heisenberg's formula. A value of $n = 4$ seems reasonable; this leads to the prediction that the maximum intensity of the particles is at $2{\cdot}5 \times 10^8$ ev., a value which appears to be too low. This argument, however, depends on the average total multiplicity of the showers, which is not known accurately.

Stars originating in the gas of the cloud chamber have been found in showers K, L and M. Shower K is certainly, and shower L probably, a penetrating shower, but shower M is a cascade, and the difficulties in explaining the origin of the associated star in the gas have already been discussed. An additional star has been observed, associated with a penetrating shower, when the magnet was not in use. Thus, out of 59 penetrating showers, three show stars in the gas, one of which could be due to a negative π-meson. The 59 penetrating showers contain approximately 75 penetrating particles. In addition we may expect, at most, some 75 neutrons of comparable energy to pass through the chamber. Most of these 150 particles will have momenta greater than 5×10^8 ev/c. and probably possess sufficient energy to produce stars. Since the average path length is 15 cm. the total path length is approximately 2,000 cm. The density of the gas in the chamber is approximately $0{\cdot}002$ gm/cm^3, so that the mass of material traversed is of the order of 4 grammes. We can assume that the cross section for interaction of the particles in the gas corresponds to the nuclear cross section, i.e. approximately 100 gm/cm^2. Then the number of stars on the 59 photographs would not be more than 1/25. In fact we have found three stars produced by charged or neutral particles.

The discrepancy can be interpreted in three possible ways: (*a*) The events may be due to a statistical fluctuation and so not likely to be found again in a similar sample of showers. (*b*) Particles exist which at a momentum of 10^9 ev/c. have a cross section for interaction larger than the nuclear cross section. (*c*) The showers contain a much higher flux of energetic neutral particles or radiation than has been assumed. We may comment as follows on these hypotheses. The first is possible assuming a large fluctuation; the second is theoretically very improbable. The last is perhaps the most plausible and deserves further quantitative investigation, both in relation to the energetic neutron flux in showers and to the probability of a considerable number of neutral mesons with high nuclear interaction being emitted together with protons and charged mesons in penetrating showers.

§ 12. CONCLUSIONS

The general conclusions that have been reached are:

(i) The classification of penetrating showers and stars into their various categories is very important and is necessary before general results can be obtained. High-energy stars produced in the lead plate are the most valuable for detailed study as the momenta and angular distributions of the particles can be found.

(ii) The spectrum of the penetrating particles produced above the chamber shows a strong bias towards positive particles. We consider that half the particles are protons. An attempt has been made to estimate the spectrum of the protons and that of the mesons. The average energy of the protons is of the order of 9×10^8 ev. and the maximum of the meson spectrum is at 8×10^8 ev.

(iii) An estimate has been made of the average energy required to trigger the P-set. The value, which is likely to be a minimum, is of the order of 7×10^9 ev.

(iv) The collision length of the radiation produced in penetrating showers is found to be 35 cm. of lead.

(v) A wide-angular distribution is found for the fast particles produced in the lead plate. The lead plate introduces a forbidden region, but for momenta greater than 5×10^8 ev/c. a wide range of angles seems possible for any particular momentum range.

(vi) All the star phenomena produced in the lead plate have an associated electronic component. Owing to the thickness of the lead plate it is not possible to decide experimentally if the electrons originate in the stars or are produced as secondary events.

(vii) Three unusual heavily ionizing tracks have been observed. They appear from star phenomena, and assessment of their momenta and ionization indicates that they are probably mesons of mass $1000\, m_e$. As yet no estimate of the frequency of these events can be made.

ACKNOWLEDGMENTS

It is with pleasure that we express our thanks to Professor P. M. S. Blackett for the excellent laboratory facilities he has given us and for the close interest he has taken in our experiments. We are grateful for helpful advice from Dr. G. D. Rochester and Dr. J. G. Wilson and for discussions on meson production with Dr. J. Hamilton.

REFERENCES

ALICANYAN, A. I., ALIKHANOV, A. I., and VAISENBERG, A., 1948, *J. Phys. USSR.*, **18,** 301.

BLACKETT, P. M. S., 1937, *Proc. Roy. Soc.* A, **159,** 1.

BROWN, R., CAMERINI, U., FOWLER, P. H., MUIRHEAD, H., POWELL, C. F., and RITSON, D. M., 1949, *Nature, Lond.*, **163,** 47, 82.

COCCONI, G., 1949 a, *Phys. Rev.*, **75,** 1074; 1949 b, *Ibid.*, **76,** 984.

COCCONI, G., COCCONI-TONGIORGI, V., and GREISEN, K., 1949, *Phys. Rev.*, **74,** 1867.

FRETTER, W. B., 1948, *Phys. Rev.*, **73,** 41; 1949, *Ibid.*, **76,** 511.

FRETTER, W. B., and HAZEN, W. F., 1946, *Phys. Rev.*, **70,** 230.

HAMILTON, J., HEITLER, W., and PENG, H. W., 1943, *Phys. Rev.*, **64,** 78.

HEISENBERG, W., 1949, *Nature, Lond.*, **164,** 65.

HEITLER, W., and WALSH, P., 1945, *Rev. Mod. Phys.*, **17,** 252.

JÁNOSSY, L., 1943, *Phys. Rev.*, **64,** 345; 1948, *Cosmic Rays* (Oxford: University Press).

JÁNOSSY, L., and ROCHESTER, G. D., 1942, *Nature, Lond.*, **150,** 633.

LEPRINCE-RINGUET, L., and LHÉRITIER, M., 1946, *J. Phys. Radium*, **7,** 66, 69.

LEWIS, H. W., OPPENHEIMER, J. R., and WOUTHUYSEN, S. A., 1948, *Phys. Rev.*, **73,** 127.

LOVATI, A., MURA, A., SALVINI, G., and TAGLIAFERRI, G., 1949, *Nuovo Cim.*, **6,** 207.

ROCHESTER, G. D., 1946, *Proc. Roy. Soc.* A, **187,** 464.

ROCHESTER, G. D., and BUTLER, C. C., 1947, *Nature, Lond.*, **160,** 855; 1948 a, *Proc. Phys. Soc.*, **61,** 307; 1948 b, *Ibid.*, **61,** 535.

SERBER, R., 1948, *Report of Solvay Conference*.

TONGIORGI, V., 1948, *Phys. Rev.*, **73,** 923.

WILSON, J. G., 1948, *Science Prog.*, **142,** 226.

Experiments on the Nature of Penetrating Events in Extensive Air Showers

By B. CHOWDHURI *
University of Manchester

Communicated by P. M. S. Blackett; MS. received 18th July 1949

ABSTRACT. The discharges, in coincidence with extensive showers, of individual counters of a group placed in a cavity under 15 cm. lead have been studied with particular reference to the number of these counters simultaneously discharged in a single event. It is shown that the observed multiplicity of discharge is not consistent with operation by particles, each discharging one counter only, distributed at random in the extensive shower falling on the apparatus. The multiplicity is also inconsistent with that expected for low energy photons at the extreme range of normal cascades, and with that arising from the secondary electrons of a reasonable μ-meson spectrum. Entry of energy into the shielded cavity is shown to take place over an area much smaller than the total area of the cavity, but the mechanism then leading to the observed multiplicity has not been identified.

§ 1. INTRODUCTION

We have shown in a previous publication (Chowdhuri 1948) that the density of penetrating events, recorded by a tray of six Geiger counters connected in parallel under 15 cm. lead, associated with extensive air showers, is proportional to the total particle density in the region of the shower at the apparatus.

The average probability of a single ionizing shower particle being associated with a subsequent penetrating count was found to be $0{\cdot}020 \pm 0{\cdot}002$, and almost independent of shower density over the whole range of densities which were important with this experimental arrangement.

It was observed in agreement with other workers (Broadbent and Jánossy 1947, Mura, Salvini and Tagliaferri 1947) that no significant change of the rate for penetrating events took place when part of the shielding material (lead) was replaced by iron of equal thickness in the units of cascade theory.

The experiment has now been extended so that the discharges of individual counters in the shielded layer are distinguished and recorded on the accompanying cloud chamber photograph. In this way information has been obtained concerning the nature of the events arising under 15 cm. of lead when extensive showers fall upon the apparatus.

§ 2. EXPERIMENTAL ARRANGEMENT

Extensive showers were selected by coincidence between three unshielded Geiger counters each of area 200 cm^2 and arranged along the sides of a horizontal equilateral triangle of side 120 cm. The cloud chamber, with an effective area of collection of about 70 cm^2, was placed 40 cm. below the centre of the triangle of counters. The shielded counter array was placed about 1 m. from the selecting array, and consisted of six counters each of area 120 cm^2. The discharge of each shielded counter in coincidence with the threefold array was recorded in the

---

* Now at Tata Institute of Fundamental Research, Bombay.

corresponding cloud chamber photograph by the illumination of one of six indicator lamps each of which corresponded to a particular counter. The resolving time of this system was 25 μsec.

Two arrangements of the shielded counter array were used:

A. The six counters were placed horizontally in a single cavity in the lead shield, with 15 cm. lead above the counters and 8 cm. lead at the sides and below the counter (Figure 1 (*a*)).

B. The counters were placed in two layers, with three counters spaced 1 cm. apart in each layer and the layers spaced vertically about 15 cm apart. The array was again covered with 15 cm. lead and was shielded on the remaining sides by 8 cm. lead. Measurements were made with and without 10 cm. lead in the cavity between the two counter layers (Figure 1 (*b*)). When the lead was not in position the total material between the two counter layers was two thin iron sheets of thickness 1·5 cm. each.

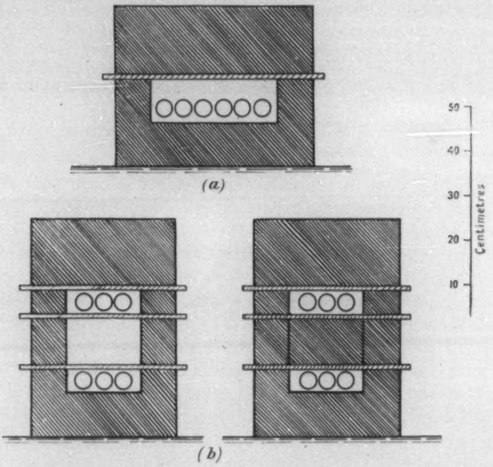

Figure 1. Array of six independently recorded shielded counters: (*a*) arrangement A; (*b*) arrangement B, with and without additional internal lead screen.

§ 3. RESULTS

Arrangement A.

In Table 1 is shown the relationship between the number of counters in the shielded array discharged and the number of ionizing shower particles in the accompanying cloud chamber photograph.

Arrangement B.

In Table 2 the multiplicity of discharge of shielded counters and their position (upper or lower layer) is summarized in terms of the number of tracks in the cloud chamber photograph.

Table 1

Multiplicity of Discharge of Shielded Counters : Arrangement A.
Observed events referred to number of tracks in cloud chamber

Tracks	Number of counters discharged						
	0	1	2	3	4	5	6
0	276	19	7	1	0	0	1
1	98	16	6	1	1	3	2
2	26	5	2	0	0	0	0
3	8	0	3	0	0	1	0
4	5	3	0	0	1	0	0
5	4	0	1	0	0	0	0
>5	1	4	1	0	1	1	1

Column headed Tracks gives number of tracks in cloud chamber photographs. Total number of shower counts = 514 in 171 hours, of which 81 counts are with penetrating events.

Table 2

Multiplicity of Discharge of Shielded Counters: Arrangement B.
Observed events referred to number of tracks in cloud chamber

Tracks	Upper	Lower							
		No lead				With lead			
		0	1	2	3	0	1	2	3
0–5	0	281	14	1	2	297	8	1	0
	1	14	6	1	1	13	4	1	1
	2	2	1	1	0	0	1	0	0
	3	2	1	1	2	2	1	0	1
>5	0	5	3	0	0	7	0	0	0
	1	1	0	0	1	1	0	0	0
	2	0	0	0	1	0	0	0	1
	3	0	0	0	1	0	0	1	0

Tracks : number of tracks in cloud chamber photographs.
Upper : number of upper counters discharged.
Lower : number of lower counters discharged.

§ 4. SECONDARY NATURE OF MULTIPLICITY

In the experiments with arrangement A we first observe that a qualitative difference of behaviour is to be expected between incident showers of high and low density. If, on average, one penetrating event takes place at the shielded layers for every 50 incident ionizing particles, then when less than 50 particles fall on the shielded layers it is unlikely that more than one penetrating event, whatever its nature, will occur. On the other hand, in dense showers, when many more than 50 particles fall in the shielded layer, more than one unit penetrating event may well occur.

If we assume that a penetrating event can discharge only one counter of the shielded layer (this would be the case if one incident shower particle in 50 were a μ-meson and if, for the moment, we ignore the detection of knock-on electrons), the probability for m shielded counters to be discharged by a shower showing n tracks on the cloud chamber photograph will be, following Chowdhuri (1948),

$$C(m,n)=A\int_0^\infty (1-e^{-2x})^3 e^{-0\cdot 7x}\frac{(0\cdot 7x)^n}{n!}(1-e^{-ks_1x})^m e^{-ks_1x(6-m)}\frac{dx}{x^{\gamma+1}},$$

where s_1 is the area of a single shielded counter in units of 100 cm² ($\sim 1\cdot 2$); $k=0\cdot 023$; $\gamma=1\cdot 5$. The actual numbers of occasions in our experiment on which shielded counters would be expected to be discharged are compared with the observed numbers in Table 3. The Table is divided in two parts, $n=0$–5 and $n>5$, corresponding to the conditions discussed in the first paragraph of this section.

Table 3

Observed Multiplicity of Discharge of Shielded Counters.
Compared with values calculated on the assumption that a single penetrating particle can discharge one counter only

No. of tracks (n) in cloud chamber	No. of shielded counters (m) discharged 1	2	3	4	5	6
$n=0$–5						
Observed cases	43	19	2	2	4	3
Calculated cases	64	8	1·4	0·16	0·015	0·0005
Probability of fluctuation	—	1/2500	1/5	1/100	$1/10^8$	$1/10^9$
$n>5$						
Observed cases	4	1	0	1	1	1
Calculated cases	3	2·3	1·4	0·7	0·4	0·4

Thus, when the density of an incident shower is so low that only one penetrating event is to be expected over the area of the shielded tray, the observed multiplicity of discharge of the shielded counter is not consistent with the assumption that a penetrating event can discharge only one of the shielded counters. On 12% of the occasions four or more counters were discharged, which on this assumption should occur only in 0·3% of penetrating events. The behaviour of the denser showers, $n>5$, is of less interest, but is consistent with the occurrence of more than one unit event of the kind responsible for the observed results with $n=0$–5.

This result must be reconciled with results, contradictory at first sight, obtained by Cocconi and Greisen (1948) and later by Greisen and Treat (1948), who looked for multiplicity in unit penetrating events without success. The essential difference between the arrangement used by these workers and our own lies in the fact that while we enclose a set of shielded counters in a single cavity, Greisen and his co-workers enclose the individual shielded counters in separate cavities with 6 cm. lead between the counters. We must suppose that the nature of the particles responsible for multiplicity in a single penetrating event does not allow these to pass through the separating lead barriers. This conclusion is strongly supported by experiments of Maze *et al.* (1949) who have shown coincidences between two shielded counters under 20 cm. lead in a single cavity, operated by an unshielded extensive shower array, to be reduced by 40% if an 0·8 cm. lead absorber is placed between the counters. It appears that many of the multiple discharges of shielded counters are therefore due to very soft particles.

§5. RANGE OF A SINGLE CASCADE SHOWER

In a recent paper Greisen (1949) has drawn attention to a feature in the final degeneration of a cascade shower which had hitherto been overlooked. At this stage of a cascade many photons will be present at energies of the order 3 MEV., and these, while discarded for the purposes of cascade development, are near the absorption minimum for photons in lead and hence have considerable range. They will suffer Compton collisions, and if the Compton electron is formed inside a counter, the presence of these photons will be detected. Greisen estimates that for atmospheric showers at sea level rather more than 15 cm. of lead is required if a considerable fraction of the discharges of a shielded counter array are not to be produced in this way.

It is necessary to consider if any large part of the multiplicity which we are discussing could be attributed to these events. If we assume, following Cocconi, Tongiorgi and Greisen (1949), that about $\frac{1}{8}$ of the penetrating events under 15 cm. lead arise from low energy photons at the end of range of cascade shower development, and with Greisen (1949) that the detection efficiency for these photons is of the order 0·02, then in our group of less dense showers (Table 3, 0–5 particles visible in the cloud chamber) there should, apart from fluctuations, never be more than about ten low energy photons entering our shielded cavity, and very frequently many fewer. It is immediately clear that the chance of a twofold count in the shielded layer will be less than 10% of that for single counts arising by this mechanism and the chance of threefold counts less than 1%. Hence the contribution to our total numbers of multiple counts cannot be more than about 1% of double counts and a negligible number of counts of higher multiplicity.

Experimental support for this conclusion is given by our results with arrangement B. Here, for showers of low density (five or less particles in the cloud chamber) the proportion of multiple discharges of the lower counter layer (Table 2) is reduced only from 9/31 with 15 cm. lead over this counter layer (intermediate lead block not in position) to 4/18 with 25 cm. lead (intermediate block in position). Under no condition would we expect the soft photon flux to be of comparable magnitude under 15 cm. and 25 cm. lead. Indeed, Cocconi and others have found experimentally that the effect due to soft photons is negligible beyond 20 cm. lead.

We therefore conclude that the main contributions to the secondary multiplicity in penetrating events does not, even under only 15 cm. lead, arise from the Compton electrons from soft shower photons. One may also expect an important contribution from the side showers to these measurements as the sides are shielded by only 8 cm. lead, but we think this effect is negligible, because it is shown from the measurements of various workers (for example Deutschmann 1947), as well as by our own, which will be given elsewhere, that substantially all showers at sea level are in the angular range 0–30° from the zenith.

§6. KNOCK-ON ELECTRONS FROM μ-MESONS

It is necessary to consider the extent to which the multiple effects we have observed might arise, if the penetrating particles were in fact μ-mesons of external origin, from the knock-on electrons produced in the lead shield and in the counter walls.

According to Jánossy's measurement (1942) the average probability of production of single knock-on secondaries by sea-level mesons is about 2%, while the observed percentage of cases in which at least two counters are discharged simultaneously is about 40% (Table 3).

Further relevant evidence concerning this process is contained in the results of cloud chamber experiments by Wilson (1938) and Nasser and Hazen (1946) (see also Wilson 1948). Nasser and Hazen show that the percentage of electrons which accompany the sea-level meson beam is about 6% for all electrons with energy greater than about 1 MEV., and Wilson shows that almost the whole of the electrons with greater energy than 10 MEV. may be attributed to mesons of energy greater than 3×10^9 ev. It is evident that any knock-on electrons capable of penetrating our counter walls (2 mm. glass) will have rectilinear trajectories in air and that all knock-on electrons will come from a very small area on the lower surface of the absorber at the point where the meson emerges. Hence we would expect less than 6% of counter discharges in addition to the first discharge in each count, whereas actually we observed about 80%. One might expect a greater percentage of knock-on electrons on the assumption that the meson component in extensive showers is much harder than the average meson beam at sea level. Then, however, the counters concerned would tend to be those adjacent to that discharged by the meson. There is no evidence of grouping of counters where two or three out of six were discharged. In Table 4 are analysed the 20 events in which two counters only of the shielded tray (arrangement A) were discharged. The actual distribution of discharged counters is compared with that to be expected if the distribution is random.

Table 4

Separation of Discharged Counters in Shielded Layer when Two Counters only are discharged.

Number of undischarged counters between the discharged counters	0	1	2	3	4
Observed events	7	7	4	1	1
Expected number from random selection of counters	6·6	5·4	4·0	2·6	1·9

Thus, while the assumption that the meson component is much harder than the total meson beam at sea level might allow an appreciable increase in the number of knock-on electrons to be expected, it seems quite incapable of explaining the large multiplicities observed and also the counter groupings involved in this work. Mitra and Rosser (1949) have observed certain particles in air showers which they consider to be penetrating particles of origin external to their apparatus. These particles are of momentum approximately 10^9 ev/c. and so are certainly not hard compared with the average sea-level meson spectrum: indeed, the few particles observed are softer than the average.

It is therefore concluded that the multiplicity observed in our measurements is not explained by the knock-on electrons accompanying μ-mesons, if these are assumed to form the penetrating events in extensive showers.

§7. DISCUSSION AND CONCLUSION

The points made in the previous sections are summarized as follows:

(i) The observed events leading to the multiple discharge of shielded counters when the density of the incident beam on the shielding material is less than 50 ionizing particles over the shielded area cannot be accounted for in terms of independent penetrating events. Thus most probably the discharges of more than one counter simultaneously are initiated by groups of particles produced in the local shielding material.

(ii) The mechanism proposed by Greisen, in which penetrating counts arise from the Compton electrons of photons in the most degenerate stage of cascade development, does not explain the multiple discharges observed in a counter array in a single cavity under a thick lead shield.

(iii) The knock-on electrons from fast particles with the momentum distribution of the normal meson beam would make only a small contribution. The few existing measurements on incident penetrating particles in showers suggest that the particles are of lower average momentum than the normal meson beam. Even if fast particles of an extremely high average momentum were present, the geometrical grouping of discharged counters in multiple operation is not that to be expected from an increased total number of knock-on electrons.

(iv) The distinction between observations of multiple discharges among shielded counters when these are and are not contained in a single cavity, and in particular the result of Daudin in which the effect of dividing a single cavity with a lead screen is examined, indicates that the inward flux of energy into a screened cavity under lead takes place over a restricted area and that effects may then be found at remote parts of the cavity.

If the inward flux of energy into the shielded cavity takes place at a point, then the simultaneous discharge of several counters inside that cavity, under the condition when the shower density is so low that the probability of random association is negligible, is most unlikely to be caused by a group of penetrating particles formed in one event as in the case of local penetrating showers.

It seems, therefore, plausible to regard the penetrating particles in extensive showers as single particles capable of producing large numbers of secondaries in the local shielding material, which are the immediate agency for discharging the shielded counters. This conclusion of ours agrees well with the 'hypothesis A' suggested by Broadbent and Jánossy (1948), where penetrating particles are supposed to come from the air above capable of discharging the shielded counter set by means of a triple knock-on shower. But it has been shown from all existing measurements that the probability of production of knock-on secondaries by μ-mesons is too small to account for our result.

Thus, if the above conclusion is valid, it is not easy to associate the required behaviour of the penetrating particles carrying energy into the shielded cavity with the known behaviour of ordinary μ-mesons. We have not distinguished, however, between the operation of known mechanisms for new particles of appropriate properties and the occurrence of some hitherto unexplored process taking place for familiar particles.

ACKNOWLEDGMENTS

I wish here to record my sincere thanks to Professor P. M. S. Blackett for all encouragements and facilities he has given for conducting this experiment.

I am also greatly indebted to Professor L. Jánossy and Dr. J. G. Wilson for many useful suggestions and discussions during the progress of the work. I acknowledge the help given me by Mr. B. G. Owen in making the electronic equipment.

REFERENCES

BROADBENT, D., and JÁNOSSY, L., 1947, *Proc. Roy. Soc.* A, **190,** 497; 1948, *Ibid.*, **192,** 364.
CHOWDHURI, B., 1948, *Nature, Lond.*, **161,** 680.
COCCONI, G., and GREISEN, K., 1948, *Phys. Rev.*, **74,** 62.
COCCONI, G., TONGIORGI, V., and GREISEN, K., 1949, *Phys. Rev.*, **75,** 1063.
DEUTSCHMANN, M., 1947, *Z. Naturforsch.*, **2a,** 61.
GREISEN, K., 1949, *Phys. Rev.*, **75,** 1071.
GREISEN, K., and TREAT, J. E., 1948, *Phys. Rev.*, **74,** 414.
JÁNOSSY, L., 1942, *Proc. Roy. Soc.* A, **179,** 362.
MAZE, R., FREÔN, A., DAUDIN, J., and AUGER, P., 1949, *Rev. Mod. Phys.*, **21,** 14.
MITRA, S., and ROSSER, W. G. V., 1949, *Proc. Phys. Soc.* A, **62,** 364.
MURA, A., SALVINI, G., and TAGLIAFERRI, G., 1947, *Nature, Lond.*, **119,** 368.
NASSER, S., and HAZEN, W. E., 1946, *Phys. Rev.*, **69,** 298.
WILSON, J. G., 1938, *Nature, Lond.*, **142,** 73; 1948, *Phys. Rev.*, **73,** 525.

LETTERS TO THE EDITOR

Observation of (γ, T), (γ, D) and (γ, np) Reactions in Boron

Boron-loaded Ilford nuclear research emulsions have been irradiated by a continuous spectrum of gamma-rays, of peak energy 24 Mev., from the Atomic Energy Research Establishment synchrotron. In addition to the expected alpha-particle stars arising from the reactions $^{12}\mathrm{C} \rightarrow 3\,{}^{4}\mathrm{He}$ (Hänni, Telegdi and Zünti 1948*) and $^{16}\mathrm{O} \rightarrow 4\,{}^{4}\mathrm{He}$ (Goward, Titterton and Wilkins 1949), stars have been observed which are consistent with the reactions

$$^{11}\mathrm{B} = {}^{3}\mathrm{H} + 2\,{}^{4}\mathrm{He} - 11{\cdot}1\ \text{Mev.,} \qquad \ldots\ldots\ (1)$$

$$^{10}\mathrm{B} = {}^{2}\mathrm{H} + 2\,{}^{4}\mathrm{He} - 5{\cdot}8\ \text{Mev.} \qquad \ldots\ldots\ (2)$$

Figures 1 (*a*) and 1 (*b*) show examples of ' boron stars ' of this nature. The events are identifiable by examining the momentum balance of the particles forming each star, a procedure which gives ready differentiation from ' carbon stars ' and which, in most cases, enables the events to be assigned to either reaction (1) or reaction (2). For some stars, however (about 30% in the present experiments), containing a short deuteron or triton track, this assignation cannot be made with certainty. Some other three-particle stars have been observed which will not give a balanced momentum for any reasonable assumed masses of the observed particles. This may be due to the emission of unobservable neutrons and, of ten such stars which have been observed, at least four are consistent with the reaction

$$^{10}\mathrm{B} = \mathrm{n} + \mathrm{p} + 2\,{}^{4}\mathrm{He} - 8{\cdot}0\ \text{Mev.} \qquad \ldots\ldots\ (3)$$

Possible competing reactions are $^{10}\mathrm{B}(\gamma, \mathrm{p})^{9}\mathrm{Be}$, $^{11}\mathrm{B}(\gamma, \mathrm{p})^{10}\mathrm{Be}$, $^{10}\mathrm{B}(\gamma, \mathrm{n})^{9}\mathrm{B}$, $^{11}\mathrm{B}(\gamma, \mathrm{n})^{10}\mathrm{B}$, which have thresholds at 6·5, 11·3, 8·3 and 11·4 Mev. respectively, and, in addition, there may be (γ, α) reactions. Where these reactions lead to emission of a single charged particle they are indistinguishable from the background of single tracks due to (γ, p) and (γ, α) processes in other elements contained in the emulsion.

The energy release in the reactions may be deduced from measurement of each star, and therefore, by assuming the threshold from the known mass values, the incident gamma-ray energy may be determined. An independent check of the correctness of the identification of the stars is thus obtained, since the upper limit of the energy released should be equal to

---

* Results will also be published shortly by Goward, Telegdi and Wilkins.

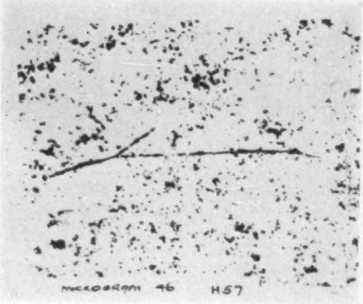
MICROGRAPH 46
H57

Figure 1 (*a*). Disintegration $^{11}B(\gamma, T)2\,^{4}He$.
Observer : Miss K. B. Treacy.

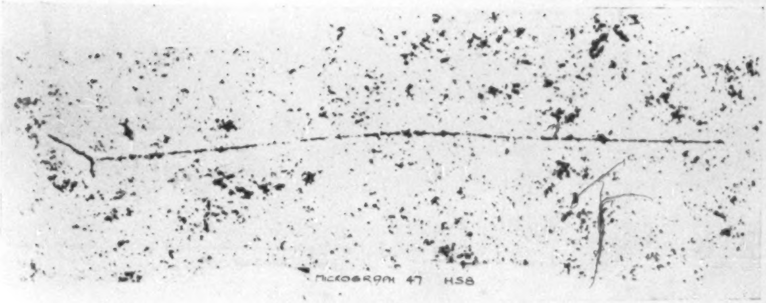
MICROGRAPH 47
H58

Figure 1 (*b*). Disintegration $^{10}B(\gamma, D)2\,^{4}He$.
Observer : Mrs. A. M. Brown.

the difference between 24 MeV. and the calculated threshold. The usefulness of this check is apparent from the histogram of Figure 2 (*a*) which shows the total energy released in stars assigned to reaction (1). Stars assigned to reaction (2) are fewer in number and give a less conclusive result, as shown in Figure 2 (*b*). The number of events examined is, as yet, insufficient to give an accurate indication of the cross sections of the reactions, but they appear (from intensity measurements with a thick-walled ion chamber) to be of the order of 10^{-28} cm^2, the reaction (2) cross section being comparable with that for reaction (1).

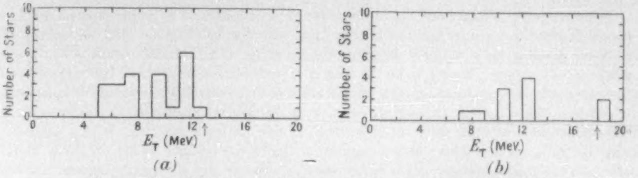

(*a*) (*b*)

Figure 2 (*a*). Total energy released, E_T, in ^{11}B (γ, T) 2 ^{4}He stars.

Figure 2 (*b*). Total energy released, E_T, in ^{10}B (γ, D) 2 ^{4}He stars.

Arrows on the E_T scales indicate the gamma-ray spectral limit (uncertain to $\pm 0{\cdot}5$ MeV.).

The mechanism of the reactions, and the intermediary products formed, may be determined in principle by calculating the excited levels of possible intermediary nuclei, such as ^{8}Be or ^{7}Li, which would give the observed particles. A consistent level-structure should be obtained for the correct assignation of the intermediary nucleus. With the present statistics the only certain assignation which can be made is that reactions (1) and (2) involve, in about 30–40% of the events, the 3 MeV. excited level of ^{8}Be. Other events involve ^{8}Be levels up to 10 MeV., unless some other intermediary nuclei are concerned.

Atomic Energy Research Establishment,
Harwell, Didcot, Berks.
30th November 1949.

F. K. Goward.
E. W. Titterton.
J. J. Wilkins.

Goward, F. K., Titterton, E. W., and Wilkins, J. J., 1949, *Proc. Phys. Soc.* A, **62**, 460.
Hänni, H., Telegdi, V. L., and Zünti, W., 1948, *Helv. Phys. Acta*, **21**, 203.

Conductivity of Thin Films

In a letter to the editor, R. Weale (1949) attempts to show that collisions with the boundaries can cause the temperature coefficient of resistance of a thin metallic film to become negative at low temperatures. This conclusion is arrived at following a treatment of the terms for resistivity and mean free path in a manner which seems to the writer to be unjustifiable.

The procedure in the letter appears to the writer to be in error in two respects; firstly the integration for the effective mean free path in a thin film has been over simplified, and secondly the variation of mean free path in the bulk metal with temperature is made to follow a different law from that of the variation of conductivity, this being done arbitrarily and without explanation. It is this second feature which in Weale's argument allows the temperature coefficient of resistance of a thin film to become zero or negative at low temperature. In a metal, however, the conductivity σ is proportional to the mean free path l_0, and moreover it is the variation of the latter with temperature which determines the variation of the conductivity. When this is the case, the size and shape of the sample cannot affect the sign of the temperature coefficient of resistance, and anomalous effects of the type referred to cannot arise simply as a result of the thickness of a film, or its temperature. This has already been shown in detail by Appleyard (1937) and Lovell (1936).

With regard to the integration, a preferred method for determining the mean free path in a film with thickness D small compared with l_0 was used by Lovell (1936) and quoted later by Appleyard (Appleyard 1937). Lovell assumed that the collisions with the boundaries were inelastic. The mean free path in a thin layer of metal became $l'=D[1+\ln(l_0/D)]$. It follows, and it was explicitly deduced by Appleyard, that metallic films however thin should still have a positive temperature coefficient. This was confirmed in Lovell's work on caesium, with films of thickness less than 50 A., deposited in very good vacuum on clean surfaces at low temperature. This conclusion applies equally for the case $l'=l_0/[1+k(l_0/D)]$, which is of the form employed by Weale, if σ is proportional to l_0, as it would be in a truly metallic film.

Negative temperature coefficients are however encountered in experimental work, and we will proceed to consider features of thin films which might explain this behaviour. It is of course possible for σ to fail to be proportional to l_0, in a material which is not properly metallic. This is well known to be the case in a semiconductor, where the number of free electrons (or holes) can increase with temperature over a considerable range of temperature. In addition, there may be in such substances an ' impurity scattering ', which varies with temperature in a manner different from that of the lattice scattering, which governs the behaviour of l_0. Films which have a negative temperature coefficient are probably therefore semiconductors, not metals. This could arise (*a*) due to the solution of gas in the crystal lattice, or (*b*) to its occlusion at crystal surfaces and boundaries, or (*c*) in certain cases it could arise in the absence of gas, as indicated below. Exceptional vacuum conditions and care in processing are needed to avoid such gas. When it is present in the lattice, the normal semiconductor theories would apply, while adsorbed layers of gas on crystal boundaries may ' trap ' electrons from the crystals, lowering the free electron concentration, or they can themselves be the seat of conductivity (Schwarz 1949). In cases (*a*) or (*b*) the temperature coefficient of resistance might well change from negative at low temperatures to positive at higher ones. In such cases however the laws relating resistivity and mean free path with temperature would not have the form employed by Weale, and moreover the temperature coefficient would be a function of the state of the material in the layer, and not primarily of its thickness. That is to say, in cases (*a*) and (*b*) it is not the dependence of l' on D which determines the temperature coefficient, but only the composition of the layer. This may in fact depend in a secondary way on D, in that whereas a very thin film may be severely gas-contaminated, continued deposition of a film under maintained conditions may give a lower gas content in the layers deposited later, due to ' gettering ' of some of the gas by the earlier layers or due to the gradual purification of the source of the layers, e.g. the sample under evaporation (Anderson 1949).

It may be noted here that at one time there was a theory that metallic films were amorphous, with negative temperature coefficient of resistance, below a certain transition temperature, above which they were metallic. The writer suggested then (Wright 1937) that the effects were due to gas in the film, which was verified by Fukuroi (1938).

The possibility (*c*) of semiconductor behaviour in very thin layers of pure metals does perhaps exist however, and such behaviour would vary with thickness. Thus when alkali metal atoms are brought together with metallic spacing, every atom provides one valence electron and one energy level which can accommodate two electrons. The structure should therefore always be metallic, as observed by Lovell. With the alkaline earth metals, however, each atom provides one level, and two electrons, so that the band of levels formed in a structure with metallic spacing will be filled, and the structure will be an insulator unless this band overlaps a higher band of levels. In a three-dimensional alkaline earth metal, such overlap does occur, and the structure is metallic, but there is evidence that the overlap is not great in some cases, especially Ca and Be, and that it depends on the existence of three dimensional symmetry. With such metals therefore it is at least possible that very thin two dimensional films should have semiconducting and even insulating properties at low temperature. Clearly this behaviour would be markedly dependent on D. In the case of trivalent metals, the behaviour should again be metallic in all geometries, but no simple general deductions appear to the writer to be possible concerning the metals with higher valency. It may be noted that in the case of molybdenum, de Boer and Kraak (1936) proposed that pure thin films are semiconductors, but this was a suggestion of a possibility, rather than a particular study of molybdenum. They found experimentally, as others have found since with other metals, that a thickness could be chosen at which the temperature coefficient was zero. Again however this is not due to the dependence of l' on D, but, if not to gas, to the dependence of the zone structure of the metal on its thickness. The above argument might well apply to bismuth, where, as in some of the alkaline earth metals, there is very little overlap between the conduction band and the highest filled band, so that again thin films, even when gas free, might be semiconductors.

The writer hopes that this correspondence will be noticed by those who are expert in the theory of solids, who will comment on the possibilities envisaged under section (*c*). Unless these suggestions receive support from detailed theory, the writer is inclined to regard factors (*a*) and (*b*) as the important ones in practice.

Research Staff of the M. O. Valve Co. Ltd.
at the Research Laboratories of the
General Electric Company Ltd.,
Wembley, Middx.
22nd November 1949.

D. A. WRIGHT.

ANDERSON, P. A., 1949, *Phys. Rev.*, **76**, 388.
APPLEYARD, E. T. S., 1937, *Proc. Phys. Soc.*, **49**, Extra Part, 118.
DE BOER, J. H., and KRAAK, H. H., 1936, *Res. Trav. Chim. Pays-Bas*, **55**, 941.
FUKOROI, T., 1938, *Sci. Pap. Inst. Phys. Chem. Res., Tokyo*, **34**, 333.
LOVELL, A. C. B., 1936, *Proc. Roy. Soc.* A, **157**, 511.
SCHWARZ, E., 1949, *Proc. Phys. Soc.* A, **62**, 530.
WEALE, R. A., 1949, *Proc. Phys. Soc.* A, **62**, 135.
WRIGHT, D. A., 1937, *Nature, Lond.*, **140**, 107.

The writer would like to express his thanks to Mr. Wright for his many valuable comments. Lovell's expression, quoted in the above letter, represents the limiting value for small thicknesses of an expression of which Planck's formula (1914) gives the limit for large thicknesses. Lovell's expression is derived on the assumption that all electron paths originate on either of the two film boundaries : but this can apply only at very small values of D/l. It is evident that otherwise the film resistivity would be equal to the bulk resistivity already at $D=l$, which is quite unlikely. Choosing this expression thus cannot be a matter of preference. In any case, Fuchs (1938) has developed a rigid theory, and the writer (1949) has given a simple expression which seems to be quite satisfactory for most purposes : for very small values of D/l this expression becomes similar to Lovell's, for large ones it can be identified with Planck's.

As far as the temperature coefficient of the resistivity of thin films is concerned, Swann (1914) was the first seriously to attempt an explanation of the zero and negative values. In the light of modern ideas his theory does not seem to be acceptable as it stands. The present writer assumed that the resistivity could be represented by $\rho=\rho_0(a+\alpha T)$, and the mean free path by $l=l_0/\alpha T$, where ρ_0, l_0, α and a are constants (the suffix zero referring to 0° c.), and T is the absolute temperature. Mr. Wright objects to the omission of the term a in the second instance. It is easily seen that this is one way of indicating that the metal in question is turning into a semiconductor (cf. van Itterbeek and De Greve 1949). Thus

$$l\rho=l_0\rho_0\left(1+\frac{a}{\alpha T}\right)=\frac{\boldsymbol{m}}{\boldsymbol{e}^2N_0\Big/\left(1+\frac{a}{\alpha T}\right)}\simeq\frac{\boldsymbol{m}}{\boldsymbol{e}^2N_0\exp\left(-\frac{a}{\alpha T}\right)};\qquad \frac{a}{\alpha T}\ll 1.$$

N, $\boldsymbol{e}$ and $\boldsymbol{m}$ are the usual electronic constants. This is a possible description of what happens to some metals when they are in the form of thin films, and may perhaps be connected with Mr. Wright's case (*c*).

R. A. WEALE.

FUCHS, K., 1938, *Proc. Camb. Phil. Soc.*, **34**, 100.
VAN ITTERBEEK, A., and DE GREVE, L., 1949, *Physica*, **15**, 80.
PLANCK, W., 1914, *Phys. Z., Lpz.*, **49**, 531.
SWANN, E., 1914, *Phil. Mag.*, **28**, 467.
WEALE, R. A., 1949, *Proc. Phys. Soc.* A, **62**, 135, 661.

The Photoconductivity of Bismuth Sulphide and Bismuth Telluride

The search for an infra-red photoconductive detector of high sensitivity has engendered considerable interest in lead telluride and similar materials. Recent American work has suggested that bismuth sulphide and bismuth selenide may be photosensitive to wavelengths as long as 7 microns, and a patent application made (Fink and Mackay 1946). However, the patentees admit that their cells are less sensitive than a thermocouple in their working range. Probably the most surprising feature of this patent is the claim that Bi_2S_3 has the same spectral response as Bi_2Se_3. This, together with the low sensitivity of the cells, suggests that possibly the effect is due to scattering of short wavelength radiation in the monochromator used to examine the cells, or alternatively a bolometric effect.

The writers have separately and independently made Bi_2S_3 and Bi_2Te_3 photoconductive and photovoltaic layers of considerable sensitivity by vacuum evaporation. The results obtained are in very reasonable agreement in view of the differences in original material employed and do not confirm the suggestion of sensitivity to 7 microns.

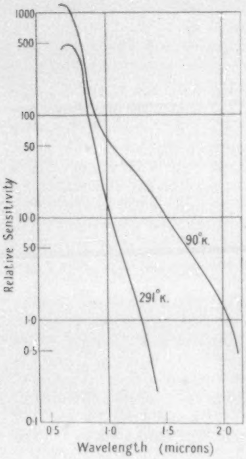

Figure 1. Photoconductivity spectrum of bismuth sulphide at 291° K. and 90° K.

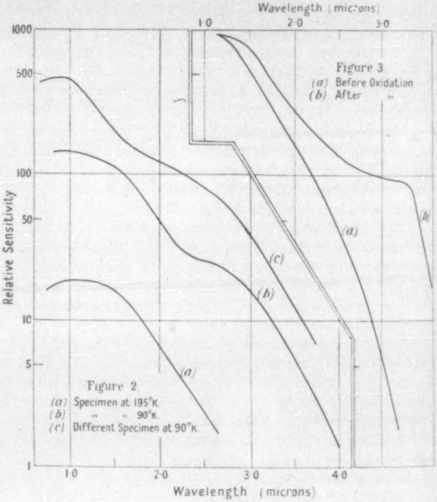

Figures 2 & 3. Photoconductivity of bismuth telluride.

The spectral response of a typical Bi_2S_3 layer is shown in Figure 1. At room temperature the sensitivity at 1·4 μ is more than 1,000 times less than the maximum value, but at 90° K. the sensitivity extends to longer wavelengths. Typical spectral response curves of Bi_2Te_3 are shown in Figure 2. This material is not sufficiently sensitive at room temperature for measurements to be made, but measurements at solid CO_2 temperature indicate that it also shows sensitivity at longer wavelengths on cooling. In this respect Bi_2S_3 and Bi_2Te_3 are like PbS and PbTe (Moss 1947).

It will be seen that the spectral response of Bi_2Te_3 consists of two peaks. Experiments show that the second peak is due to oxygen treatment (Figure 3). Similar results have been reported for PbTe. It would appear that oxygen impurity centres produce a new photoconductive absorption band centred about 2·8 microns.

It was found that a photovoltaic Bi_2Te_3 cell has an almost identical spectral response to those shown in Figure 2, this again being similar to the case of PbTe and its associated compounds.

The specific resistances of Bi_2Te_3 layers are about 1 ohm cm., and thermoelectric power measurements indicate positive hole conduction.

We conclude therefore that Fink and Mackay (1946) are mistaken in their assessment of Bi_2S_3, Bi_2Se_3 and Bi_2Te_3 as photodetectors of long wavelength radiation. Our measurements indicate that the bismuth compounds behave in an analogous way to compounds of the lead series, but are inferior to these.

The work described was carried out at the Telecommunications Research Establishment (A.F.G.) and at the laboratory of Colloid Science, University of Cambridge (T.S.M.). Our thanks are due to the Chief Scientist, Ministry of Supply and to the Controller of H.M. Stationery Office for permission to publish this note.

Physics Department, A. F. GIBSON.
Telecommunications Research Establishment,
Ministry of Supply.

Department of Colloid Science, T. S. MOSS.
University of Cambridge.

31st October 1949.

FINK, C. G., and MACKAY, J. S., 1946, U.S. Patent No. 2,406,139.
MOSS, T. S., 1947, *Nature, Lond.*, **159**, 476.

Validity of Two-dimensional Design of Synchrotron Pole-Faces

A synchrotron pole-face design aims primarily at producing a field between the magnet poles such that, using cylindrical polar coordinates,

$$-(r/H_z)(\partial H_z/\partial r)=n, \qquad \ldots\ldots (1)$$

where H_z is the axial field component and $n \simeq 0{\cdot}7$. Goward and Wilkins (1948) have discussed the validity of design methods which neglect the cylindrical symmetry of the problem and employ a two-dimensional approximation. Their discussion was based on the comparison between (*a*) two-dimensional electrolytic tank measurements (Peierls 1946) and (*b*) magnetic measurements on actual synchrotron magnets. For a large 300 MEV. sychrotron magnet, of 125 cm. orbit radius, no significant discrepancies between measurements of *n* by methods (*a*) and (*b*) were observable. For the magnet of a 30 MEV. synchrotron of 10 cm. orbit radius, however, the results of Figure 1, Curves I and II, were obtained, representing discrepancies which, although not serious in their effect, were considered too great to be due purely to experimental error. These discrepancies were consequently attributed to the inherent error of a two-dimensional method, which would be expected to be more serious for the small magnet.

In a recent note, Robinson (1949) has pointed out that the *n* law of a synchrotron magnet field may be accurately calculated by a relaxational process (Fox 1947), taking full account of cylindrical symmetry. By carrying out similar calculations on a two-dimensional basis it becomes possible to ascertain with more certainty the source of the above-mentioned *n* value discrepancies. Figure 1, Curve III, represents *n* values calculated from three-dimensional (cylindrically symmetrical) equations. The superposed points are *n* values calculated in the same way from two-dimensional equations. Comparison of these points and curves now shows various interesting features.

In the first place the two sets of calculated *n* values agree remarkably closely, in fact to within the errors of the calculations. Hence it appears that even less inherent error is involved in a two-dimensional design than was suggested by Goward and Wilkins (1948), at least in this particular case. To test this further, a similar two-dimensional calculation was made on the basis of the particular pole-face discussed by Robinson (1949), who gives the appropriate three-dimensional solution. Here again, quite good agreement is obtained, as shown in Figure 2.

Secondly the discrepancy between Curves II and III of Figure 1 is well outside the estimated experimental error, and is probably due to the known poor quality of the magnet used, which was an early development model. Infinite permeability magnet iron is, of course, assumed for design purposes. Using a much better magnet, Robinson (1949) observed less discrepancy.

Thirdly it is worthy of note that the electrolytic tank result, Figure 1, Curve I, represents an adequate experimental accuracy. Moreover, the more difficult measurements on the 300 Mev. magnet, mentioned above, show that appreciably greater accuracy is obtainable when required (for a given accuracy in $(\partial H_z/\partial r)$, equation (1) shows that the n value errors are proportional to the orbit radius). With reasonable care, the Peierls (1946) form of electrolytic tank is thus a sufficiently accurate design tool, giving rapidity of test and adjustment and ready allowance for the effects of betatron core and exciting coils on the field law.

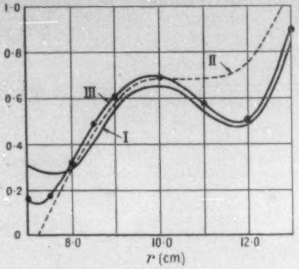

Figure 1. Comparison between measured and calculated 'n' values for a 30 Mev. synchroton magnet.

Curve I : Two-dimensional electrolytic tank measurements.
Curve II : Magnetic measurements on the magnet.
Curve III : Three-dimensional calculated values.
Dots ● : Two-dimensional calculated values.

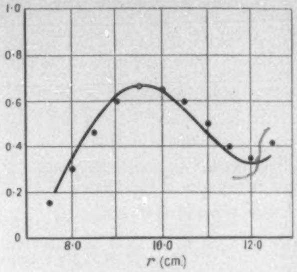

Figure 2. Comparison between two- and three-dimensional calculations of the 'n' law of a 30 Mev. synchrotron magnet.

Curve : Three-dimensional values.
Dots ● : Two-dimensional values.

The author is indebted to Miss K. Wyllie, of the Atomic Energy Research Establishment, for assistance with the relaxational calculations mentioned in this note.

A.E.R.E. Division,
Telecommunications Research Establishment,
Malvern.
3rd October 1949.

J. J. Wilkins.

Fox, L., 1947, *Proc. Roy. Soc.* A, **190,** 31.
Goward, F. K., and Wilkins, J. J., 1948, *Proc. Phys. Soc.*, **61,** 580.
Peierls, R. E., 1946, *Nature, Lond.*, **158,** 831.
Robinson, C., 1949, *Proc. Phys. Soc.* A, **62,** 592.

Properties of Superflow in Liquid Helium II

It is well known that when two volumes of liquid helium II are connected by a capillary or by the film, any difference in pressure or temperature will result in a peculiar type of mass transport which has been called ' superflow '. So far our information about this flow is based on observations made in the bulk liquid at the *ends* of the capillary link and practically nothing is known about the pressure and temperature *inside* the latter. The only experiment of this type (Daunt and Mendelssohn 1946) has revealed the remarkable fact that when the film flows with sub-critical velocity the pressure gradient in it is zero. Similar experiments, corresponding essentially to current–potential measurements in an electrical conductor, have now been carried out in capillary slits and the results are summarized in this note.

Of a number of arrangements used, that shown in Figure 1 has proved particularly useful. A glass tube ends in a polished flange which is opposed by an optically flat plate. An annular groove is cut into the flange and is connected at one place to a narrow side tube. By adjusting the position of the apparatus in the helium bath, B, liquid can be made to flow in and out of the central tube, C, through the slit while the pressure in the latter is indicated by the level in the side tube, S. The width of the slit was estimated to be approximately 2×10^{-4} cm. and the ratio of resistances to ordinary flow between CS and SB as 4·5 : 1.

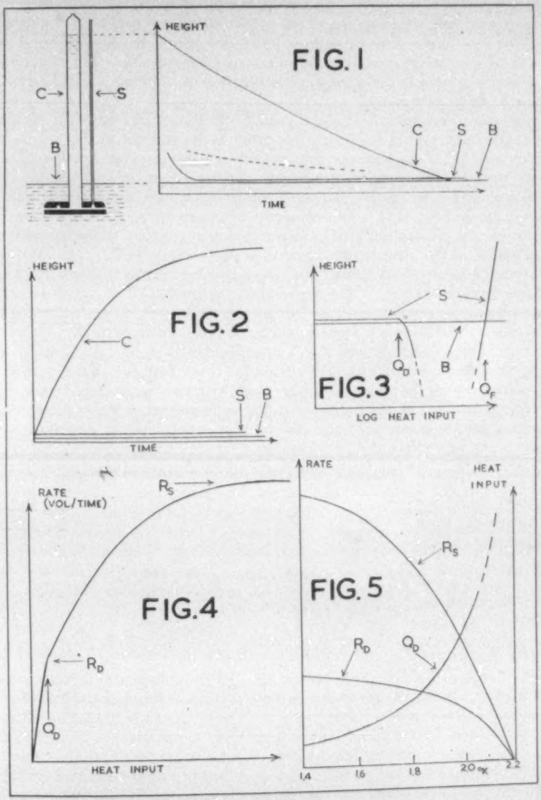

The flow in and out of C under gravity (Figure 1) was found to be largely pressure independent. In all experiments the level in S settled rapidly at a height of 0·15 cm. (due to surface tension) above B and stayed there, showing that *no* appreciable pressure gradient exists in the slit SB. If there had been a gradient in the slit corresponding to the pressure difference between C and B, S should have followed the dotted curve.

For the subsequent experiments a heating coil was inserted in C, and C and S were closed at the top. The effect of a small constant heat input is shown in Figure 2. Owing to the thermo-mechanical effect, the level in C rises gradually to a final value. However, the level in S remains practically unchanged, showing that the temperature difference between C and B does *not* produce a temperature gradient in the slit.

It was to be expected that, as the heat input is increased the level in S, too, should eventually rise, and this does indeed occur (Figure 3). However, well before this rise (at the heat input Q_F) takes place, the level in S drops, taking up equilibrium positions *below* the level in B. The critical heat input Q_D corresponding to this depression rises with rising temperature.

The rate of flow into C at a given temperature is plotted against the heat input in Figure 4. The rates are taken from the tangents at the origin of C/time curves of the type shown in Figure 2. The rate shows first an almost linear rise which is followed by a kink in the curve and a more gradual increase to a definite saturation rate R_S. The rate R_D at the heat input Q_D corresponds with fair accuracy to the position of the kink while the rate belonging to Q_F is the saturation rate R_S.

The temperature dependence of R_S, R_D and Q_D is shown in Figure 5. It is significant that the flow rate under gravity is of the same order as R_D and not as R_S.

Since the position of the annular gap in our apparatus is arbitrary and since other arrangements have yielded identical results, we conclude that below a certain critical flow velocity no appreciable gradient of pressure or temperature exists in a narrow slit connecting two volumes of liquid helium II. In conformity with our views (Mendelssohn 1945) there thus seems to exist a discontinuity of pressure and temperature at the narrowest place in the capillary which, in the present apparatus, is at its entrance at C. The experiments also show that beyond a certain (saturation) rate, increased heat input will not result in a higher flow of helium through the slit. The remarkable depression effect has also been observed with the two other arrangements used in this investigation and it does not seem possible to explain it as due to the Bernoulli force or to the vapour pressure in S. We are therefore inclined to regard the depression effect as a new phenomenon in liquid helium II. While it is clearly premature to venture an explanation for this effect, we gain the impression that it may be associated with the ' normal ' rather than with the ' superfluid ' part of the liquid. One of us (Mendelssohn 1945) has suggested that at high heat currents there should exist a flow under its osmotic pressure of the normal component in the direction of the lower temperature. The new effect and perhaps also a curious observation by Allen and Reekie (1939) may possibly be connected with this postulated diffusion of the ' normal ' component.

Clarendon Laboratory,
Oxford.
9th January 1950.

R. Bowers.
K. Mendelssohn.

Allen, J. F., and Reekie, J., 1939, *Nature, Lond.*, **144**, 475.
Daunt, J. G., and Mendelssohn, K., 1946, *Nature, Lond.*, **157**, 839.
Mendelssohn, K., 1945, *Proc. Phys. Soc.*, **57**, 371.

REVIEWS OF BOOKS

Atomic Energy Year Book, edited by J. Tutin. Pp. xx+237. 1st Edition. (London: Temple Press, 1949.) 21*s*.

Few would quarrel with the statement of the publishers on the dust cover of this book that the development of atomic energy "calls for the closest possible integration of industry and science and especially of a keen awareness, on both sides, of mutual interests, problems and achievements". To this end this year book aims at providing information for the industrialist and technician on atomic energy matters.

Many of its features are excellent and will undoubtedly assist in furthering the aims of the book. After first describing the history of the development of nuclear physics, chapters are devoted to a discussion of atomic energy reactors, and the problems facing the pile designer are set out in a concise but informative way. The following chapters deal with the production of radioactive tracers in the pile, the economics of atomic power production and a discussion of the possibility of ship propulsion using atomic power.

The book then passes to a more detailed study of developments completed and projected, in many countries, including a particularly full account of the applications that are being made of radioactive isotopes in medical research. Although much of this information is interesting, a good deal of it is repetitive and could have been condensed more appropriately into a table.

The least satisfactory chapter in the book deals with the "research frontiers" of modern atomic physics. It is a pity because such a fascinating picture could have been presented under this heading. As it is the treatment is not well balanced and undue prominence is sometimes given to the conjectures of the author of the chapter.

Changes in the arrangement of the subject-matter could be made with advantage and the principles governing selection of the material in some of the tables is not always clear. In fact a good deal more work will have to be done on the book before it contains sufficiently comprehensive material presented in sufficiently concise a form to justify its title.

Nevertheless the book contains much valuable information not previously collected in a concise form, including a helpful section on safety precautions to be followed in the handling and shipment of radioactive materials, and tables of radioactive isotopes available from the U.S.A. Atomic Energy Commission and from the Atomic Energy Research Establishment, Harwell, together with an account of the procedures to be followed to obtain these.

It is attractively produced with a considerable number of photographs, including an interesting "portrait gallery" of prominent atomic scientists, and its publication at this stage serves a useful purpose.

E. H. S. BURHOP.

Nuclear Forces, by L. Rosenfeld. Vol. II. Pp. 187–543. 1st Edition. (Amsterdam: North-Holland Publishing Co., 1948). No price.

In this second and concluding volume containing Parts III and IV Professor Rosenfeld completes his monumental and invaluable task of reviewing the present state of knowledge of the properties of atomic nuclei and of their interpretation in terms of forces between the constituent nucleons. The task of writing a book of this kind has deterred other less valiant authors. This is not surprising in view of the present unstable state of nuclear theory and the enormous outpouring of experimental and theoretical papers on the subject. Many of these, as the author laments, are incoherent, using the term in its technical sense, though with full awareness that it may also be an appropriate adjective in the literary sense. These difficulties only make it all the more necessary to have available a comprehensive survey of the present position of the subject. Every research worker in nuclear physics is therefore deeply indebted to Professor Rosenfeld.

The second volume contains the remaining Chapters IX–XVII, three Appendices, Addenda and Corrigenda, an Author and Subject Index, a Table of the Properties of Atomic Nuclei and a series of graphs illustrating these properties.

Chapters IX–XIV form the contents of Part III which is devoted to a description of the attempts made to describe the properties of nuclei more complex than the deuteron in terms of central forces between individual nucleons. Although such attempts have achieved qualitative success in several directions it is disappointing that no satisfactory method has been found for dealing quantitatively with a system of more than four nucleons. All the methods which have been tried are described adequately under the Chapter headings—Survey of nuclear models, Nuclear multiplets, Saturation properties of nuclear forces, Properties of heavy nuclei, Collective nuclear models and Properties of light nuclei.

Part IV is concerned with the discussion of non-central and of non-static forces. The discovery of the quadrupole moment of the deuteron by Rabi, Zacharias and Ramsey showed that the neutron–proton interaction cannot be purely central, thereby introducing a very considerable complication into nuclear theory. Chapter XV deals with general types of non-central and non-static nuclear forces and the remaining two chapters with applications to two-nucleon systems and to heavier nuclei respectively.

The three appendices are concerned with allowed β-transitions, electromagnetic properties of nuclei and the strong coupling theory of nuclear forces.

In addition the author has endeavoured to keep the work as up to date as possible by including short accounts of recent developments such as the discovery of the μ-meson and the evidence afforded from the study of the scattering of high energy neutrons by protons.

The table of atomic nuclei is a classification in terms of mass number, the most suitable classification from a theoretical viewpoint. For each nucleus, as far as possible, the binding energies are given and for the unstable nuclei, the half-lifetimes, the type of decay and the energy of the emitted radiation. The labour involved in preparing this valuable table must have been immense—over 4 pages of references are given for the material contained therein.

The concluding figures illustrate the mass-defect curve, the variation with mass and atomic number of the binding energy of the ‘ last ’ nucleon, the ‘ Euler diagram ’ showing lines of isotopes and isotones, binding energy surfaces, the distribution of β-stable nuclei and of the stable and unstable nuclei in general.

The reliable information contained within this book is so great that no serious worker in theoretical nuclear physics can afford to be without at least ready access to a copy. On the other hand its formidable comprehensiveness necessarily makes it less suitable for the physicist or mathematician who wishes to learn something of nuclear physics without proposing to undertake serious research on the subject. It is a pity that the difficulty of the book for such readers and also for the comparatively inexperienced research worker is enhanced by the rather cumbersome notation, particularly unfamiliar and forbidding to the British mathematician and physicist.

In spite of such minor criticisms the book is a *tour de force* of unique value to nuclear physicists and it is to be hoped that the author will find time to publish addenda from time to time which will go far to maintain the book up to date. H. S. W. MASSEY.

CONTENTS FOR SECTION B

PAGE

Dr. J. B. BIRKS. The Properties of Ferromagnetic Compounds at Centimetre Wavelengths . . . 65
Dr. L. JACOB. The Field in an Electron–Optical Immersion Objective . . . 75
Miss M. GILBERT. Colour Perception in Parafoveal Vision . . . 83
Dr. D. BROMLEY and Dr. R. H. HERZ. Quantum Efficiency in Photographic X-ray Exposures . . . 90
Mr. B. H. BRIGGS, Mr. G. J. PHILLIPS and Mr. D. H. SHINN. The Analysis of Observations on Spaced Receivers of the Fading of Radio Signals . . . 106
M. R. BUREAU. Les renforcements brusques des ondes très longues . . . 122
Dr. R. RIVAULT. Diffusion des échos au voisinage des fréquences critiques de F 2 . 126
Mr. D. R. BATES and Mr. M. J. SEATON. Theoretical Considerations Regarding the Formation of the Ionized Layers . . . 129
Physical Society Conference at Cambridge—Abstracts . . . 141
Reviews of Books . . . 151
Contents for Section A . . . 154
Abstracts for Section A . . . 155

ABSTRACTS FOR SECTION B

The Properties of Ferromagnetic Compounds at Centimetre Wavelengths, by J. B. Birks.

ABSTRACT. The magnetic and dielectric properties of γ-ferric oxide, magnetite, Mn–Zn ferrite and Ni–Zn ferrite have been measured at wavelengths from 60 cm. to 1·23 cm. The pronounced magnetic dispersion and absorption which occur are attributed to the decay ot the rotational magnetization, due to Larmor spin resonance in the internal anisotropy field H_N. The theoretical relation $H_N=2K/M$, where K is the anisotropy coefficient, and M the saturation intensity, agrees satisfactorily with the observations, and $|K|$ has been derived for each material. An inverse relationship between H_N and the initial susceptibility is shown to account quantitatively for the magnetic resonance observed in high-permeability materials at much lower frequencies.

The Field in an Electron–Optical Immersion Objective, by L. Jacob.

ABSTRACT. The electrolytic tank method was developed to record rapidly the potential variations which occur in the field of the immersion objective in the absence of space charge. The axial distribution over the region explored was found to conform with a law of the form $V=Ae^{kz}$. Here A is a voltage scale factor while k is a geometrical scale factor. The experimental results appear to show that for constant black-out voltage the gradient at the cathode remains constant over part of the range explored, independent of geometry. The ratio of accelerator to modulator voltage for zero gradient at the cathode varies inversely as the square of the hole diameter. A determination of the emitting area of the cathode was also made from the field plots.

Colour Perception in Parafoveal Vision, by M. Gilbert.

ABSTRACT. Quantitative studies of extra-foveal colour vision are inherently difficult owing to the poor discrimination and rapid adaptation found in the parafoveal and peripheral areas of the retina. Measurements of the luminosity, colour mixture and hue discrimination curves have been made by a single observer using a field subtending 1° 20′ and located at 2° and 4° from the fovea. The results suggest that for high retinal illumination parafoveal colour vision does not differ in essential characteristics from foveal colour vision, but at low illuminations colour perception becomes reduced to a type of dichromatic vision similar to the tritanopic form of defective colour vision and to that reported for small-field foveal vision.

Quantum Efficiency in Photographic X-ray Exposures, by D. Bromley and R. H. Herz.

ABSTRACT. The grain yield per absorbed quantum has been evaluated experimentally for four different photographic emulsions over a wavelength range of 1·2–0·01 A., i.e. from very soft x rays to gamma rays emitted from radium. The tests were carried out with both heterogeneous and monochromatic x rays. A grain yield of 1·0 per absorbed quantum appears to hold within a range of wavelengths of 1·2–0·37 A. (10 kv.–33 kv.). From 0·37 A. to short wavelengths (gamma rays) an increase of grain yield linear with quantum energy is obtained. At a wavelength of 0·0123 A. (1,000 kv.) about 80 grains are rendered developable per quantum absorbed. The rate of increase of grain yield with quantum energy is different for different emulsions. For a slow and fine-grain chloro-bromide emulsion the grain yield was found to be less than unity for wavelengths below 0·12 A. (i.e. 100 kv.). The results are consistent with the hypothesis that grains are made developable not only by the direct action of x rays but also by secondary electrons produced by the x rays. These are effective only when they are energetic enough to reach grains in the neighbourhood of that absorbing the original x-ray quantum.

The Analysis of Observations on Spaced Receivers of the Fading of Radio Signals, by B. H. Briggs, G. J. Phillips and D. H. Shinn.

ABSTRACT. The fading of a radio wave once reflected from an irregular ionosphere is discussed in terms of the variable diffraction pattern produced at the ground. It is pointed out that fading may arise either by a drift of the diffraction pattern past a receiver, or by irregular variations in the pattern, or by both mechanisms together. It is shown how, from observations at three receiving points, it is possible to deduce the rate at which the pattern is changing and the velocity with which it drifts over the ground. This velocity is of interest as it may be related to the wind velocity at ionospheric heights in the atmosphere, but the relation of the diffraction pattern to the irregular ionosphere which produces it is not discussed in detail.

Les renforcements brusques des ondes très longues, par R. Bureau.

ABSTRACT. During the last twenty years, enhancements of the mean level of atmospherics, on 11 km. wavelength, have been associated with some other phenomena such as simultaneous fade-outs of the field intensity of stations on decametric wavelengths, perturbations of terrestrial magnetism or Wolf numbers relative to solar activity.

More recently a search has been made for occasions on which the association between the different phenomena is not so close. It has been found that the usual fade-out on short waves does not occur in the same manner on all stations recorded; sometimes, indeed, an enhancement of short duration takes place at the beginning of the expected fade-out. This enhancement is probably due to the reception of a radioelectric radiation from the sun.

The author gives some examples of such phenomena which can be used for a better forecasting of radioelectric disturbance due to abnormal solar activity.

Diffusion des échos au voisinage des fréquences critiques de F 2, par R. Rivault.

ABSTRACT. From the study of ionospheric data recorded at Poitiers (46° N.) it appears that two sorts of scattered echoes take place in the neighbourhood of F2 critical frequencies.

The first one seems to be produced by the multiplication of magneto-ionic components. This scattering ends with ground sunrise; it exists during both quiet and perturbed ionospheric conditions; it is far more frequent and stronger when the nights are longer. Its existence seems to be connected with nocturnal thermal and convective disorder.

The second sort of scattering is mainly recorded during the second part of the night, after F2 penetration, at a virtual height of about 800 to 1,200 km. The sharp lower boundary of these reflections, which disappears a few moments after sunrise, leads to the postulation of an ionospheric G region, whose existence has been often discussed. This sort of scattering is connected with magnetically disturbed conditions and, chiefly, with meteoritic periods.

Theoretical Considerations Regarding the Formation of the Ionized Layers, by D. R. Bates and M. J. Seaton.

ABSTRACT. The detailed mechanisms involved in the formation of the E, F_1, F_2 and D layers by solar ultra-violet radiation are discussed. Use is made of the results of some recent calculations on the continuous absorption cross section of atomic oxygen and nitrogen, and of the evidence on the ionic composition of the layers that is provided by the analysis of the emission spectrum of the upper atmosphere during twilight. The uncertainties existing at present are emphasized.